INVESTIGATION OF MICROMECHANICAL PROPERTIES AND STRAIN SENSING BEHAVIOR OF ELECTRICALLY CONDUCTING AND PIEZORESISTIVE FLEXIBLE COPOLYESTER/CARBON NANOTUBES NANOCOMPOSITES

A THESIS SUBMITTED TO THE
CENTRAL DEPARTMENT OF CHEMISTRY
INSTITUTE OF SCIENCE AND TECHNOLOGY
TRIBHUVAN UNIVERSITY
NEPAL

FOR THE AWARD OF
DOCTOR OF PHILOSOPHY
IN CHEMISTRY

BY

KEDAR NATH DHAKAL
DECEMBER 2022

INVESTIGATION OF MICROMECHANICAL PROPERTIES AND STRAIN SENSING BEHAVIOR OF ELECTRICALLY CONDUCTING AND PIEZORESISTIVE FLEXIBLE COPOLYESTER/CARBON NANOTUBES NANOCOMPOSITES

A THESIS SUBMITTED TO THE
CENTRAL DEPARTMENT OF CHEMISTRY
INSTITUTE OF SCIENCE AND TECHNOLOGY
TRIBHUVAN UNIVERSITY
NEPAL

FOR THE AWARD OF
DOCTOR OF PHILOSOPHY
IN CHEMISTRY

BY

KEDAR NATH DHAKAL
DECEMBER 2022

DECLARATION

Thesis entitled **"Investigation of Micromechanical Properties and Strain Sensing Behavior of Electrically Conducting and Piezoresistive Flexible Copolyester/Carbon Nanotubes Nanocomposites"** which is being submitted to the Central Department of Chemistry, Institute of Science and Technology (IOST), Tribhuvan University, Nepal for the award of the degree of Doctor of Philosophy (Ph.D.), is a research work carried out by me under the supervision of Prof. Dr. Rameshwar Adhikari of Central Department of Chemistry, Tribhuvan University and co-supervised by Dr. Jürgen Pionteck, Senior Scientist of Leibniz-Institut für Polymerforschung (IPF) Dresden e.V., Germany.

This research is original and has not been submitted earlier in part or full in this or any other form to any university or institute, here or elsewhere, for the award of any degree.

<div align="right">

....
Kedar Nath Dhakal

</div>

RECOMMENDATION

This is to recommend that **Kedar Nath Dhakal** has carried out research entitled **"Investigation of Micromechanical Properties and Strain Sensing Behavior of Electrically Conducting and Piezoresistive Flexible Copolyester/Carbon Nanotubes Nanocomposites"** for the award of Doctor of Philosophy (Ph.D.) in **Chemistry** under our supervision. To our knowledge, this work has not been submitted for any other degree.

He has fulfilled all the requirements laid down by the Institute of Science and Technology (IOST), Tribhuvan University, Kirtipur, Kathmandu for the submission of the thesis for the award of Ph.D. degree.

Prof. Dr. Rameshwar Adhikari

Supervisor

Central Department of Chemistry

Tribhuvan University

Kirtipur, Kathmandu, Nepal

Dr. Jürgen Pionteck

Senior Scientist

Co-Supervisor

Leibniz-Institut für Polymerforschung (IPF) Dresden e.V.

Germany

(April 2023)

LETTER OF APPROVAL

On the recommendation of **Prof. Dr. Rameshwar Adhikari and Dr. Jürgen Pionteck**, this Ph. D. thesis submitted by **Kedar Nath Dhakal,** entitled "**Investigation of Micromechanical Properties and Strain Sensing Behavior of Electrically Conducting and Piezoresistive Flexible Copolyester/Carbon Nanotubes Nanocomposites"** is forwarded by Central Department Research Committee (CDRC) to the Dean, IOST, T.U..

Dr. Jagadeesh Bhattarai

Professor

Head

Central Department of Chemistry

Tribhuvan University

Kirtipur, Kathmandu

Nepal

ACKNOWLEDGEMENTS

Kedar Nath Dhakal

Central Department of Chemistry

Tribhuvan University, Kirtipur, Kathmandu, Nepal

December 2022

ABSTRACT

Various concentration of multiwalled carbon nanotubes (MWCNT) as conductive filler was incorporated into poly(butylene adipate-*co*-terephthalate) (PBAT), a flexible biodegradable copolyester by melt-mixing followed by compression moulding. Deformation behavior of electrically conductive nanocomposites was correlated with piezoresistivity, leading to their strain sensing behavior. Structural and morphological characterization of the materials were determined by Fourier transform infrared (FTIR) spectroscopy and microscopic techniques while thermal stability and crystallization behavior were analyzed by thermogravimetric analysis (TGA) and differential scanning calorimetry (DSC), respectively. Comparative analysis of FTIR spectra of PBAT and PBAT/MWCNT nanocomposites suggested a physical matrix-filler binding force to form the composite microstructures. Microscopic techniques revealed an entangled CNT-network uniformly spread in the polymer matrix. Increased thermal stability of the materials was suggested by TGA, attributed to a good filler-matrix interfacial interaction. DSC results revealed the retarded crystallization process of the polymer with the formation of less perfect crystals. Increasing tensile modulus, Martens Hardness (*HM)* and indentation modulus (E_{IT}), and decreasing maximum indentation depth (h_{max}) (by 50%, 50%, 100% and 32% on incorporation of 5 wt-% of fillers, respectively) confirmed the mechanical reinforcement of composites by MWCNT. Volume resistivity observed in the nanocomposites suggested the suitability of nanocomposites for strain sensing applications. An exponential-like increment of relative resistance change ($\Delta R/R_0$) of the nanocomposites as a function of strain confirmed their piezoresistivity. Applicability of nanocomposites as low-strain sensing materials was suggested by their reproducible $\Delta R/R_0$ values from 2% to 8% strain during cyclic strain test. Electron beam (EB) irradiation induced crosslinking of the nanocomposites was employed as a strategy to improve the strain sensing behavior of the nanocomposites. Cyclic strain test of irradiated samples (dose: 150 and 200 kGy) exhibited the improvement (up to 10% strain), attributed to their enhanced elastic deformability. The nanocomposites irradiated with the highest dose (300 kGy) exhibited no correlation between $\Delta R/R_0$ and strain, attributed to the formation of a 3D network of polymer crosslinks restricting the homogeneous deformation of the CNT-network. Moderate degree of EB irradiation induced crosslinking of polymer nanocomposites can be a strategy to improve their strain sensing behavior.

Keywords: *nanocomposites, biodegradability, electrical conductivity, piezoresistivity, strain sensing, electron beam irradiation, crosslinking*

सारांश

जैविक विधिद्वारा कुहाउन सकिने एक कुचालक प्लास्टिक [को-पोलिस्टर, अंग्रेजीमा Poly(butylene adipate-*co*-terephthalate) (PBAT)] र कार्बन नानोट्यूबको असमान मिश्रणलाई १८० डिग्री सेल्सिएस तापक्रममा फरक-फरक अनुपातमा पगालेर सुचालक समिश्रणहरु (Nanocomposites) तयार गरि तिनीहरुको विरुपण व्यवहार (Deformation behavior) र पिजोरेसिस्टिभिटि (Piezoresistivity) को अध्ययनको अधारमा यान्त्रिक तनाव सुचक क्षमता (Strain sensing behavior) को अन्वेषण गरिएको थियो। समिश्रणको रासायनिक संरचना र स्वरुपको अध्ययन क्रमशः फोरियर ट्रान्सफर्म इन्फ्रारेड (FTIR) स्पेक्ट्रोस्कोपी र सुक्ष्मदर्शक यन्त्रको प्रयोगद्वारा गरिएको थियो भने तापस्थिरता (Thermal stability) र मणिभिकरण (Crystallization) को अध्ययन क्रमशः थर्मोग्राभिमेट्रिक विश्लेषण (TGA) र डिफरेन्सिअल स्क्यानिङ क्यालोरिमेट्री (DSC) द्वारा गरिएको थियो। शुद्ध प्लास्टिक र समिश्रणको FTIR पटको तुलनात्मक विश्लेषण गर्दा समिश्रणको सुक्ष्म-संरचना बन्नको लागि प्लास्टिक र फिलरको बीचमा भौतिक प्रकारको आकर्षण बलको प्रमुख भूमिका रहेको कुरा पुष्टि भयो। एक आपसमा जोडिएका कार्बन नानोट्यूबहरूद्वारा समिश्रणको भित्री भागसम्म समान रुपमा फैलिएको जालीजस्तो संरचना निर्माण भएको पाइयो। TGA परिक्षण समिश्रणको बढ्दो तापस्थिरताको कारण फिलर र म्याट्रिक्स बिचको बलियो इन्टरफेसियल अन्तरक्रिया रहेको देखायो। DSC द्वारा मापन गरिएका नतिजाहरूले कार्बन नानोट्यूबले समिश्रणमा अपूर्ण मणिभहरू बन्न प्रेरित गर्दै मणिभिकरणको दर घटाएको पाइयो। समिश्रणमा कार्बन नानोट्यूबको मात्राअनुसार बढ्दो टेन्साइल मापांक तथा यान्त्रिक कडापन सम्बन्धी अन्य गुणहरु जस्तै बढ्दो मार्टेन्स कडापन (HM) र इन्डेन्टेसन मापांक (E_{IT}) तथा घट्दो अधिकतम इन्डेन्टेसन गहिराइ (h_{max}) ले समिश्रणको यान्त्रिक सुदृढिकरणलाइ पुष्टि गर्‍यो। समिश्रणको विद्युतिय आयतन प्रतिरोधात्मक परिमाणले यान्त्रिक तनाव सुचकको रूपमा तिनीहरुलाई प्रयोग गर्न सकिने सम्भाव्यता देखायो। चक्रीय यान्त्रिक तनाव परिक्षण समिश्रणको $\Delta R/R_0$ मान २ % देखि ८ % तनावसम्म फलनको रुपमा वृद्धि हुनुले तिनीहरूलाई कम-तनाव सुचकको रुपमा चित्रण गर्‍यो। उल्लेखित कार्यको अलावा उक्त पदार्थको उच्च-तनाव सुचक क्षमता विकास गर्ने उद्देश्यका साथ इलेक्ट्रोनपुञ्ज विकिरणद्वारा गरिएको समिश्रणभित्र रहेको प्लास्टिकको आणविक सञ्जालिकरण कृया (Crosslinking) लाई एक रणनीतिको रूपमा परिक्षण गरिएको थियो। विकिरणित (क्षमता: १५० र २०० kGy) समिश्रणले चक्रिय तनाव परिक्षणमा सुधारिएको तनाव सुचक क्षमता (१० % सम्म) प्रदर्शन गर्‍यो जवकी ३०० kGy क्षमताको इलेक्ट्रोनपुञ्जद्वारा सञ्जालिकरण गर्दा त्यस्तो कुनै फलनरूपी व्यवहार प्रदर्शन गरेको पाइएन। यसरी मध्यम क्षमताको इलेक्ट्रोनपुञ्जद्वारा गरिने सुचालक प्लास्टिकजन्य समिश्रणको आणविक सञ्जालिकरण तिनीहरुको यान्त्रिक तनाव सुचक क्षमता अभिवृद्धि गर्ने एक उपयुक्त उपाय हुन सक्छ भन्ने निष्कर्ष निकालिएको थियो।

कुञ्जीपदावली: *सुचालक समिश्रण, पिजोरेसिस्टिभिटी, तनाव सुचक क्षमता, आणविक सञ्जालिकरण कृया इलेक्ट्रोनपुञ्ज*

LIST OF ACRONYMS AND ABBREVIATIONS

CPC   : Conductive polymer composites

DSC   : Differential scanning calorimetry

EB   : Electron beam

FTIR   : Fourier transform infrared spectroscopy

MWCNT   : Multiwalled carbon nanotubes

PBAT   : Poly(butylene adipate-co-terephthalate)

PLA   : Poly(lactic acid)

PA   : Polyamide

PPy   : Polypyrrole

rpm   : Round per minute

SEM   : Scanning electron microscopy

TGA   : Thermogravimetric analysis

TPE   : Thermoplastic elastomer

3D   : Three dimensional

TEM   : Transmission electron microscopy

TLM   : Transmission light microscopy

LIST OF SYMBOLS

a.u.	: Arbitrary unit
A/A_0	: Area ratio
σ_0	: Conductivity of percolating network
T_c	: Crystallization point
$°C$	: Degree Celsius
χ_c	: Degree of crystallinity
We	: Elastic work done
ΔH_c	: Enthalpy of crystallization
ΔH_m	: Enthalpy of melting
=	: Equal to
et al.	: Et alia (and others)
etc.	: Et cetera
T_f	: Final degradation temperature
T_g	: Glass transition temperature
E_{IT}	: Indentation modulus
T_{onset}	: Initial degradation temperature
J	: Joule
K	: Kelvin
kGy	: Kilo Gray
HM	: Martens Hardness
T_{max}	: Maximum degradation temperature
μ_{max}	: Maximum indentation depth
MPa	: Mega Pascal
T_m	: Melting Point
μm	: Micrometer
$\Omega.cm$	: Ohm.centimeter
%	: Percentage
W_p	: Plastic work done
$\Delta R/R_0$	: Relative resistance change
ϵ	: Strain

LIST OF TABLES

LIST OF FIGURES

TABLE OF CONTENTS

CHAPTER 3

CHAPTER 1

1. INTRODUCTION

This chapter introduces the survey of similar works reported in the literature in brief. It lists out the similar and somehow modified works related to the topic of this thesis in preface and introduces a research gap in rationale. The aim of this research work is mentioned in general and specific objectives. Specific objectives list out the different steps of the work conducted to meet the overall goal. Scope and limitations of the studies are also introduced.

1.1. Preface

Substitution of traditional non-degradable petroleum based polymers by degradable polymers of natural as well as synthetic origin is given emphasis these days to address existing problems of plastic waste management and e-waste (Feig *et al*., 2018; Fukushima *et al*., 2012; Qazi *et al*., 2020; Sirisinha & Somboon, 2011).

Poly(butylene adipate-*co*-terephthalate) (PBAT), a fully biodegradable, synthetic type of aromatic-aliphatic copolyester exhibiting easy properties of its processing. It undergoes the enzymatic degradation *via* ester group present in it producing environmentally benign bi-products such as biomass and carbondioxide, making contribution to address the environmental problems of solid waste management (Gan *et al*., 2004; Guo *et al*., 2021; Han *et al*., 2022). Most of the properties (physical) of PBAT are similar to that of low density polyethylene (LD-PE). Therefore, it can be taken as a biodegradable alternative of LD-PE. Due to its flexibility, high toughness, high ductility (>700% elongation at break), it was commercialized by BASF for the preparation of degradable packaging materials. PBAT is derived from 1, 4-butandiol, adipic acid, and terephthalic acid. It is composed of a soft aliphatic butylene adipate (BA) unit and a rigid aromatic terephthalate (BT) unit in alternate manner (Al-Itry *et al*., 2015; Behera *et al*., 2020; Calderaro *et al*., 2021; Cranston *et al*., 2003; González Seligra *et al*., 2016; Hong *et al*., 2012; Li *et al*., 2015; Sarul *et al*., 2021). It possesses sufficient mechanical strength, elasticity, hydrolytic and thermal resistance etc. (Duan *et al*., 2019; Rzepna *et al*., 2018; Zhang *et al*., 2019). These properties of PBAT make it a suitable candidate to prepare high performance biodegradable nanomaterials with required modifications (Hong *et al.,* 2012*).

Poly(lactic acid) (PLA), the best taken candidate among the biodegradable polymers with respect to its availability, natural sources and renewability. It can be prepared from

plant sources, however, it is limited to its applications practically due to its poor mechanical performance and thermal stability (Al-Itry *et al.*, 2012; Ko *et al.*, 2009). Biodegradable and cost effective polymeric materials with improved thermo-mechanical properties are being demanded these days (Mohanty & Nayak, 2009). Blending PLA with a soft and elastomeric polymer is a reported strategy to address its limitations. Variety of polymer blends can be prepared with their improved thermo-mechanical properties employing this strategy (Signori *et al.*, 2009).

Meanwhile, the soft and tough blending counterpart should also be biodegradable to keep the biodegradability of resulting polymer blends. PBAT, in terms of its toughness, flexibility, comparable melt viscosity and biodegradability can complement the aforementioned limitations of PLA (Al-Itry *et al.*, 2012). It can be used as a toughening agent for PLA (Ko et al., 2009). PBAT performs the highest elongation at break among other biodegradable polymers (Fukushima *et al.*, 2012). Hence PBAT/ PLA blends are preferred to prepare cost effective biodegradable materials for the substitution of prevailing non-degradable commodity plastics. **Table 1** summarizes the reported works of PBAT and PBAT/PLA blends based biodegradable composites and blends filled with natural fibers, biopolymers and nano-carbons based conductive fillers.

It is shown by **Table 1** that a lot of research works focused on the preparation of biodegradable materials filled with natural fibers and biopolymers are carried out. Similarly, works about PBAT and PBAT/PLA based electrically conductive nanocomposites are reported in the literature focusing only on their electrical conductivity and electrochemical properties. On the other hand, PBAT and PLA are immiscible polymers to each other due to which segregation occurs between them. Therefore, tensile mechanical properties of PBAT can't be maintained in PBAT/PLA blends despite their electrical conductivity and even a lower percolation threshold. Hence, it seems that PBAT alone should be preferred as a polymer matrix to fabricate biodegradable and electrically conductive polymer composites.

Table 1: Summary of PBAT and PBAT/PLA blends based biodegradable composites

S. N.	Composite formulation	Method	Scope	Reference
1.	PBAT + bamboo flour (BF)	Melt-mixing	Structure-property correlation	(Adhikari *et al.*, 2012)
2.	PBAT + bamboo flour (BF)	Melt-mixing	Morphology,mechanical, thermal and water absorption behavior	(Bhandari *et al.*, 2013)
3.	PBAT + chitosan (CS)	Melt-mixing	Structural and thermal properties, and biodegradability	(Pokhrel *et al.*, 2016)
4.	PBAT + thermoplastic starch (TPS), plasticized by glycerol	Extrusion	Morphology, structural and thermal properties, biodegradability	(González Seligra *et al.*, 2016)
5.	PBAT + starch	Solution casting	Morphology, mechanical and thermal properties, biodegradability	(Pokhrel *et al.*, 2021)
6.	PBAT + nanocellulose (NC)	Melt-mixing	Mechanical properties and biodegradability	(Pinheiro *et al.*, 2017)
7.	PBAT + microcrystalline cellulose (MCC), PBAT + nanocellulose (NC)	Melt-mixing	Morphology, surface properties and biodegradability	(Giri *et al.*, 2019)
8.	PBAT + microcrystalline cellulose (MCC)	Melt-mixing	Structural, thermal and mechanical properties	(Giri *et al.*, 2021)
9.	PBAT/PLA + MWCNT	Melt-mixing	Morphology and Electrical conductivity	(Urquijo et al., 2017)
10.	PBAT/PLA + MWCNT (surface modified) + EBAGMA as a compatibilizer *EBAGMA: ethylene-butyl acrylate glycidyl methacrylate*	Melt-mixing	Morphology, thermal and mechanical properties	(Zhou *et al.*, 2018)
11.	PBAT/PLA + graphene nanoplateletes (GNP)	Melt-mixing	Thermal properties and electrical conductivity	(Guo *et al.*, 2020a)
12.	PBAT/PLA + MWCNT	Extrusion	Morphology, thermal and rheological properties	(Ko *et al.*, 2009)
13.	PBAT/PLA + MWCNT	Electrospinning (composite fiber)	Morphology, structural, thermal and electrochemical properties, electrochemical sensor	(Rosenberger *et al.*, 2020)
14.	PBAT/PLA + MWCNT	Electrospinning (composite fiber)	Wettability, mechanical, thermal and electrochemical properties, electrochemical sensor	(Gusmão *et al.*, 2021)
15.	PBAT/PLA + MWCNT	Melt-mixing	Morphology and rheological properties	(Salehiyan *et al.*, 2020)
16.	PBAT/PLA + MWCNT	Melt-mixing	Morphology, structural, thermal and mechanical properties, and electrical conductivity	(Dhakal *et al.*, 2022a)

17.	PBAT/PLA + MWCNT, PBAT + MWCNT	Melt-mixing	Morphology, rheological properties and electrical conductivity	(Dil *et al.*, 2020)
18.	PBAT + MWCNT (functionalized)	Melt-mixing	Structural, mechanical and antibacterial properties, electrical conductivity	(Wu, 2009)
19.	PBAT + MWCNT	Extrusion	Thermal and mechanical properties	(Hong *et al.*, 2012)
20	PBAT + MWCNT	Melt-mixing	Viscoelasticity, dynamic rheology, model simulation	(Ding *et al.*, 2016)
21.	PBAT + MWCNT	Electrospinning (composite fibers)	Morphology, structural, mechanical and thermal properties, and biological (cell) viability	(Ding *et al.*, 2016)

1.2. Rationale

Electrically conductive polymer composites (CPC) find wide applications in different fields such as elctronics, sensors, actuators, sports, construction, robotics etc. Among various polymeric materials used these days, CPC based strain sensors are being applied in different fields i.e. robotics, wearable and portable electronics, health care monitoring, diagnosis of materials and structural damage, sports etc. (Liu *et al.*, 2019). Whatever may be the mode of use of such materials, they ultimately cause the problem of electronic waste (e-waste) along with the environmental pollution (Guo *et al.*, 2020b; Liu *et al.*, 2019) because most of the polymers used in daily life are petro-based non-degradable polymers. Therefore, there is an emergence of development of materials using degradable polymers to address these problems. CPC based strain sensors are taken as the superior ones rather than the metal and semi-conductor (conventional) based strain sensors. However, CPC, composed of degradable polymers used in this regard are rarely found. Poly(butylene adipate-*co*-terephthalate) (PBAT), a biodegradable copolyester was initially commercialized by BASF to develop the degradable packaging materials. Many research works on PBAT based composite materials are reported, targeted to develop the degradable packaging and furnishing materials for household applications. Bhandari prepared natural fibers reinforced melt-nixed biodegradable PBAT/natural fibers composites and investigated their structure-property correlations (Bhandari, 2014). Pokhrel *et al*. fabricated PBAT/chitosan composites by solution casting method and investigated their spectroscopic, thermal and mechanical properties along with the soil burial test for their biodegradability (Pokhrel *et al*., 2016). Giri *et al*. prepared melt-mixed micro and nanocomposites with

micro and nanocrystalline cellulose derived from wheatstalk and investigated their biodegradability along with mechanical and thermal properties (Giri *et al*., 2019, 2021). Similarly, electrically conductive PBAT based composites with conductive fillers such as nanocarbons have also been reported as listed in **Table 1**.

Many research works corresponding to PBAT based conductive composites have focused only on their electrical conductivity and electrochemical properties. However, no researcher has paid attention to piezoresistivity and strain sensing capacity of PBAT based CPC to investigate their potential to use them to fabricate biodegradable strain sensors. This research work is mainly focused on the investigation of piezoresistivity and strain sensing behavior of PBAT/MWCNT nanocomposites.

1.3. Objectives

General and specific objectives of the studies and research works are outlined as follows.

1.3.1. General Objective

Fabrication of flexible, stretchable and electrically conductive polymer nanocomposites by the incorporation of multiwalled carbon nanotubes (MWCNT) into poly(butylene adipate-*co*-terephthalate) (PBAT) and investigate their piezoresistivity and strain sensing behavior is the general objective of this research work.

1.3.2. Specific Objectives

The specific objectives of this research work are as follows.

➢ To prepare PBAT/MWCNT nanocomposites; carry out their morphological, structural and thermal characterization, and investigate their deformation behavior

➢ To investigate of electrical conductivity, piezoresistivity and strain sensing behavior of PBAT/MWCNT nanocomposites

➢ To crosslink the PBAT/MWCNT nanocomposites by electron beam (EB) irradiation as a strategy to improve their strain sensing behavior

➢ To investigate of effect of EB irradiation on deformation behavior, strain sensing behavior and thermal properties of nanocomposites

1.4. Scope of the Studies

Technological advancement has made the lifetime of electronics and devices shorter leading to the problem of electronic waste (e-waste). Meanwhile, the use of non-degradable petro-based polymers has led to a serious problem of plastic waste management contributing to the global environmental problem (Irimia-Vladu *et al*.,

2012; Liu *et al*., 2019). Development of biodegradable as well as biocompatible electronic and biomedical devices, and sensors only can address both of these problems at a time (Irimia-Vladu *et al*., 2012; Li *et al*., 2015). Substitution of traditional non-degradable commodity plastics by the degradable counterparts is the sustainable solution (Deshmukh *et al*., 2017).

PBAT, a biodegradable and biocompatible synthetic copolyester can be a suitable candidate in this regard. On the other hand, PBAT and multiwalled carbon nanotubes (MWCNT) pair up to prepare functional PBAT/MWCNT nanocomposites with electrical conductivity, improved mechanical, thermal and rheological properties. These functional polymer nanocomposites find their applications in biodegradable electronics (Hong *et al*., 2012; Liu *et al*., 2019). Investigation of strain sensing behavior of electrically conductive and piezresistive PBAT/MWCNT nanocomposites carried out in this work has drawn the conclusion of strain-sensing potential of the nanocomposites. In this way, PBAT/MWCNT nanocomposites will be potential candidates to develop biodegradable strain sensors. Similarly, electrically conductive PBAT/MWCNT nanocomposites can find the applications in biodegradable and flexible electronics and biocompatible biomedical devices.

1.5. Limitations of the Studies

PBAT, a commercial product of BASF, as a biodegradable polymer, however, the rate of degradability is quite slow which takes ~4 months (González Seligra *et al*., 2016). Despite of its flexibility, toughness and high elongation at break, it is not like rubber which limit it to its direct applications in biodegradable and flexible high performance materials (Rzepna *et al*., 2018). This limitations can be overcome only by tuning the molar ratio of butylene adipate (BA) and butylene terephthalate (BT) units of PBAT keeping biodegradability (González Seligra *et al*., 2016; Rzepna *et al*., 2018). On the other hand, low tensile strength and tensile modulus of PBAT limit it to load bearing smart applications such as in construction sites (Calderaro *et al*., 2021). Blending PBAT with another biodegradable polymer counterpart can be a strategy to improve its mechanical properties. PLA best suits with PBAT in this regard in terms of tensile strength, tensile modulus, melt viscosity, cost effectiveness and biodegradability, however, they are immiscible polymers to each other (Dhakal, Krause, et al., 2022; Teamsinsungvon et al., 2013). Similarly, they possess a good compatibility at a high

melt processing conditions only which hampers the thermomechanical properties of resulting PBAT/PLA blends (Rzepna *et al*., 2018).

In this work, PBAT/MWCNT nanocomposites exhibited only a low strain-sensing potential which is a disadvantage to fabricate a strain sensor with a good performance despite its degradability. Such a behavior of these nanocomposites can be improved employing strategic techniques such as crosslinking, varying the molar ratio of BA unit during the synthesis of polymer to provide it with higher elastic deformability.

CHAPTER 2

2. LITERATURE REVIEW

A critical review of the related works reported in the literature are discussed in this chapter. It reviews the biocompatible and biodegradable synthetic polymers applicable for the fabrication of biocompatible and biodegradable electronics and sensors. It discusses the background of related research works. It discusses about the general methods of fabrication of electrically conductive polymer composites (CPC), theory behind the development of electrical conductivity and piezoresistivity in CPC and application of piezoresistive CPC as strain sensing materials. It also introduces electron beam (EB) irradiation induced crosslinking of polymer matrix as a strategic technique to improve the strain sensing behavior of CPC and the corresponding mechanism of crosslinking of polymer matrix.

2.1. Electrically Conductive Polymer Composites (CPC)

Electrical insulators can be imparted with conductive properties by the incorporation/adjustment of conductive fillers into/with them. Insulating polymers can be turned into conductive blends or composites following this route. Blending insulating polymers with conducting polymers and diluting the master batches of the corresponding polymers produce electrically conductive polymer blends (Dhakal *et al*., 2022a; Dhakal *et al*., 2022b; Zhang *et al*., 2007). Similarly, one of the approaches to impart electrical conductivity is to combine them with conductive additives. Inorganic conductive fillers can be incorporated into polymers to prepare electrically conductive polymer composites (CPC) (Dhakal *et al*., 2022a; Foulger, 1999; Natarajan *et al*., 2017). A simple additive law may not be followed by the combination of insulating polymers and conductive fillers, however, electrical conductivity is achieved by the resulting composite materials at a certain concentration of conductive additives (Foulger, 1999). Metal particles, carbonaceous conductive fillers such as carbon black (CB), graphite, carbon nanotubes (CNT) etc. and their hybrids are commonly used conductive fillers in this regard. Metal particles deteriorate the properties (mechanical) of the resulting composites despite their better electrical conductivity. On the other hand, nanocarbons improve both electrical and mechanical properties of the resulting composite materials (Natarajan *et al*., 2017). On the other hand, nanocarbons based conductive fillers perform high electrical conductivity which produce the composites with their good mechanical properties and processability along with cost effectiveness

(Chodák *et al*., 2001). Hence, nano-carbons based polymer composites are preferred these days than metal particles incorporated polymer composites (Dhakal *et al*., 2022a; Natarajan *et al*., 2017). Cost effectiveness, easy processability, flexibility, low density, variability of mechanical and electrical properties are the advantages of CPC over metallic conductors (Folorunso *et al*., 2019; Zhang *et al*., 2007).

Carbon nanotubes (CNT) are the most preferred conductive nanofillers than other nanocarbons whose 1D structure of CNT is responsible for the transport of electrons (Ponnamma *et al*., 2014). This is because of their high aspect (length-to-diameter) ratio (100-10,000), low density, high electrical (10^6-10^7 S/m, higher than conductivity of copper) and thermal (3000 W/mK) conductivity, high thermal stability (2800 °C), outstanding mechanical properties (tensile strength: 50 GPa, bending strength: 14.2 GPa, elastic modulus: 4.15 TPa, stronger than steel), high flexibility and toughness, good load bearing capacity (matrix to fillers), chemical inertness etc. (Dhakal *et al*., 2022b; Ponnamma *et al*., 2014; Silva *et al*., 2021). High strength, modulus and flexibility of CNT is associated with sp^2 hybridization of C-C bond of CNT (MacDiarmid, 2001; Salvetat-Delmotte & Rubio, 2002). CNT are also taken as a toughening agents for brittle polymers due to their high flexibility and toughness (Kuan *et al*., 2008; Salvetat-Delmotte & Rubio, 2002).

CNT have many contact points to connect with neighbouring counterparts to form a conductive path because of high aspect ratio and many C=C π-bonds. As a result, a low CNT content will be sufficient to provide electrical conductivity to the nanocomposites (Georgousis *et al*., 2017; Kuan *et al*., 2008; Mičušík *et al*., 2011; Ponnamma *et al*., 2014). Due to such outstanding electrical, mechanical, and thermal properties and the nano-dimension of CNT, they highly reinforce the resulting polymer/CNT composites improving the same properties, when incorporated into a polymer matrix. Incorporation of CNT into polymers makes many positive effects in addition to electrical conductivity. As a consequence, polymer/CNT nanocomposites with improved electrical, mechanical and thermal properties will be obtained (Mičušík *et al*., 2011; Qazi *et al*., 2020; Salvetat *et al*., 1999). Moreover, novel nanocomposites with tailored properties can be prepared combining the outstanding properties of CNT with that of polymer matrix (Gao *et al*., 2005). These are the reasons for scientists for the research of CNT based nanocomposite (Yu *et al*., 2010).

CNT can be incorporated and adjusted into polymers by both wet and dry approaches (Yee *et al*., 2019). Solution casting, spray coating, sonication, spin coating, layer-by-layer assembly, dip coating, vacuum filtration, in-situ polymerization etc. belong to wet approach (Bokobza, 2007; Liu *et al*., 2018; Yee *et al*., 2019). Similarly, melt mixing, direct transfer, mechanical peeling, vapour deposition etc are the methods of dry approach (Mehmood *et al*., 2020; Qazi *et al*., 2020; Yee *et al*., 2019).

Melt-mixing is one of the most preferred method to prepare polymer/CNT composites in commercial scale. It is the mostly preferred method to prepare thermoplastic elastomers (TPE)/CNT nanocomposites. This is due to the environment friendly nature of this method in which no solvent and other chemicals are used (N. Dubey *et al*., 2020; Wang *et al*., 2020). The desired composite materials are prepared only by the wetting of CNTs by polymer melts. Moreover, the various properties of resulting composite materials can be tuned, varying the CNT concentration, their physical and chemical modification, shear change, CNT-matrix interfacial interaction, percolation threshold *etc*. (Bokobza, 2007).

2.2. Electrical Conductivity of CPC

Electrical conductivity of the polymer/nanocarbons composites is developed not only by the CNT-CNT connections, but also by electron hopping and electron tunneling. End-to-end connection of individual CNT particle is not mandatory for the electrical conductivity, which can also be carried out by electron hopping that occurs through the gaps of CNTs at a low CNT concentration. Similarly, electron tunneling between CNT particles maintaining the tunneling distance also contribute to the electrical conductivity (Dhakal *et al*., 2022b; Yu *et al*., 2010).

Development of electrical conductivity of polymer/CNT composites is shown by the schematic illustration presented in **Figure 1**. At a very low concentration of CNT, the conductivity of the composites is very close to that of neat polymer matrix. From **Figure 1**, it seems that conductivity of the nanocomposites gradually increases with the addition of even a low content of fillers.
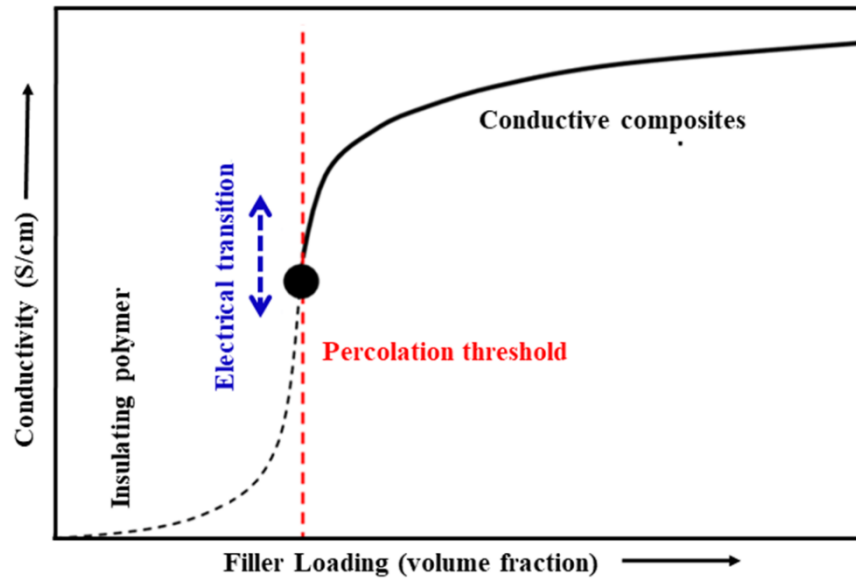
Figure 1: Schematic diagram showing electrical conductivity of CPC (Alamusi *et al*., 2011)

This increment of the conductivity is carried out by electron hopping as well as tunneling effect in which electrical conductivity is provided by close CNT particles without their end-to-end connections (Alamusi *et al*., 2011; Foulger, 1999; Yu *et al*., 2010; Stübler *et al*., 2011). In other words, electrical transport occurs by the hopping of electrons (from one site to another) in the materials (Last & Thouless, 1971). For electron tunneling, filler particles should be close enough (2-8 nm) to each other due to which the electrons can cross the inter-particle gap (Georgousis *et al*., 2018; Krause *et al*., 2019).

The conductivity of nanocomposites remains low before percolation threshold (Baltá Calleja *et al*., 1988). At a certain filler concentration during continuous addition of fillers, an electrical transition (insulator-to-conductor) occurs by the formation of a complete conductive path throughout the composites by which insulating polymer/CNT composites convert into conductors. The transition is called percolation process and the corresponding filler concentration is known as percolation threshold (P_c) or critical concentration. An electrically conductive pathway, necessary for the electrical

conductivity of the composites is formed by the inter-particle physical connections of CNTs at percolation threshold (Baltá Calleja *et al.*, 1988; Krause *et al.*, 2019).

A complete electrical short-circuiting of the charges throughout the materials takes place at percolation threshold making it electrically conductive. Both tunneling effect and the electrical path contribute to the total conductivity of the composites at this stage (Foulger, 1999; Georgousis *et al.*, 2018), however, the electrical conductivity of composites at this phase is mostly due to Ohmic conductance. Therefore, the conductivity of nanocomposites shifts from tunneling effect to Ohmic conductance (Jin *et al.*, 2013; Vilcakova *et al.*, 2002; Xu *et al.*, 2013; Yu *et al.*, 2010). Optimum conductivity of the composites is achieved after percolation threshold depending on the properties of both matrix and fillers, filler concentration as well as the mixing conditions (Folorunso *et al.*, 2019). Conductivity of the composites resulted in this way is carried out by the intrinsic conductivity of CNT incorporated into the polymer matrix (Guo *et al.*, 2020a). The percolation phenomenon and the filler concentration required are based on the aspect ratio, number of contact points and other physical properties of conductive fillers (Stübler *et al.*, 2011). The first completely connected conductive path, formed by the end-to-end connections of CNT governs the electrical conductivity of the nanocomposites. The conductive path thus formed causes the whole composite system to percolate (Weber & Kamal, 1997). A steep and abrupt increment of electrical conductivity of CPC (by multiple decades) as shown in **Figure 1** occurs by the formation of a continuous filler network throughout the composites. In other words, a morphological change of CPC also takes place at percolation threshold in addition to the electrical conductivity (Mičušík *et al.*, 2011; Ponnamma *et al.*, 2014).

Development of a conductive path at percolation threshold has a positive effect on electrical properties of the composites, but adverse effects on their mechanical properties. Cracks, voids and more failure sites can be formed in the nanocomposites at higher filler concentration (Chodák *et al.*, 2001). Therefore, a possible low value of percolation threshold is always desired (when CPC are prepared) for better mechanical properties of the composites as well as cost effectiveness (Dhakal *et al.*, 2022a; Zhang *et al.*, 2007). However, percolation threshold depends also on many other factors except filler concentration such as properties and dimensions of fillers, properties of polymer matrix (adhesion capacity on filler particles, viscosity, crystallinity etc), methods and conditions of preparation etc. (Dhakal *et al.*, 2022a; Dhakal *et al.*, 2022b; Ponnamma *et al.*, 2014). Low percolation threshold of thermoplastic polymers/MWCNT

12

nanocomposites is reported in the literature. Low percolation threshold and high electrical conductivity of the composites signify the homogeneous dispersion of fillers throughout the materials (Georgousis *et al.*, 2018).

Electrical conductivity of nanocomposites is explained in accordance with percolation theory. Moreover, an empirical percolation power law, explained by percolation theory is followed by the nanocomposites above percolation threshold as given by equation (1). It relates the electrical conductivity of nanocomposites with the concentration of conductive fillers quantitatively (Alamusi *et al.*, 2011; Jin *et al.*, 2013; Knite *et al.*, 2007; Liu *et a*l., 2018; Vilcakova *et al.*, 2002; Xu *et al.*, 2013; Yu *et al.*, 2010)

$$\sigma = \sigma_0 (P - P_c)^\wedge t \tag{1}$$

where, σ = Conductivity of CPC

σ_0 = Conductivity of fillers

P = Filler fraction

P_c = Percolation threshold

t = Scaling factor signifying filler dimensionality and the change of conductivity with respect to filler concentration = 1.3 to 4 for MWCNT

Here, $P > Pc$ should come true (above percolation threshold) for the validity of this power law. It is used to determine the value of P_c fitting the experimental data (Weber & Kamal, 1997).

After percolation threshold, multiple number of conductive paths can be formed producing a 3D conductive filler network and the conductivity gradually levels off (Alamusi *et al.*, 2011; Liu *et al.*, 2018; Xu *et al.*, 2013) as shown in **Figure 1**. A high and stable conductivity of the composite materials is acquired at this stage.

Electrical conductivity of polymer composites can also be expressed in terms of volume resistivity. Volume resistivity is the reciprocal of volume conductivity and can be expressed as (Natarajan *et al.*, 2017).

$$\rho = \frac{1}{\sigma} \tag{2}$$

where, ρ = volume resistivity (Ω.cm)

σ = volume conductivity ($\Omega^{-1}.cm^{-1}$)
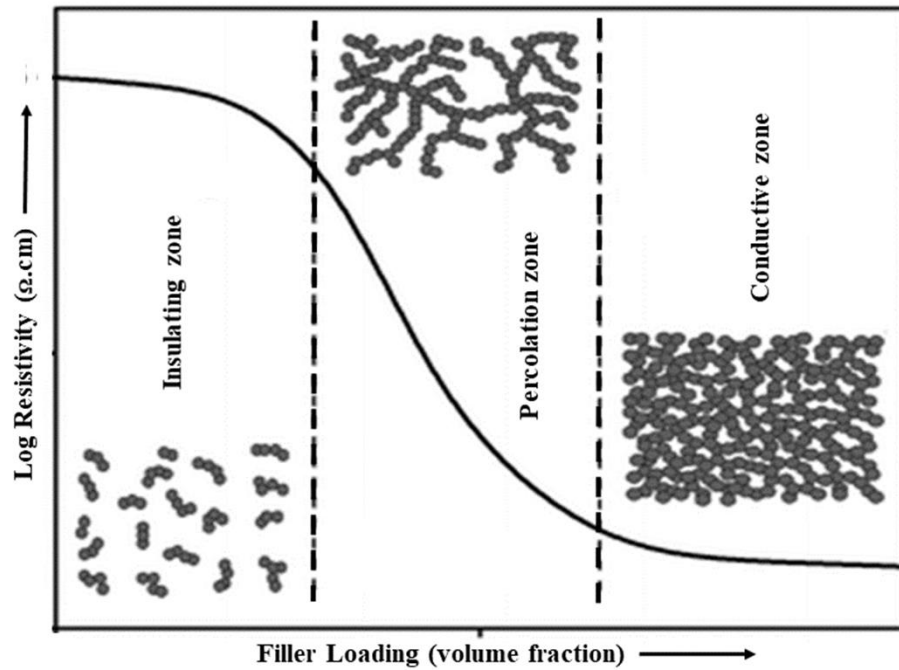
Figure 2. Schematic diagram showing volume resistivity of CPC as a function of filler wt. fraction (Rahaman *et al*., 2019)

Volume resistivity, as a reciprocal of volume conductivity, decreases with increasing filler concentration. At percolation threshold, a steep decrease in volume resistivity with a small rise in filler content takes place. In other words, all the trends of volume conductivity will occur in an opposite way as a function of filler content as illustrated by **Figure 2**.

2.3. Piezoresistivity of CPC

Electrical properties of CPC respond to the mechanical deformation by virtue of which their resistance or capacitance changes reversibly (Amjadi *et al*., 2014; Natarajan *et al*., 2017). These materials convert stimuli of mechanical deformations (pressure, stress, strain etc.) into electrical signals (Alamusi *et al*., 2011; Shintake *et al*., 2018). Their electrical resistance or capacitance changes with external stimuli due to the induced mechanical deformation that is retained on the removal of these stimuli (Gong & Zhu, 2014; Liu *et al*., 2018; Zheng *et al*., 2014). Such a reversible change of electrical resistance of the materials carried out by mechanical deformation is called piezoresistivity and the materials are said to be piezoresistive in nature. Hence, electromechanical response is performed by the piezoresistive materials towards the external mechanical deformation (Costa *et al*., 2017; D. Guo *et al*., 2019; Natarajan *et al*., 2017).

Deformation induced piezoresistivity of CPC is carried out by (i) the destruction of conductive path (ii) change in the tunneling effect in the nanocomposites (iii) change in the piezoresistivity of CNT (iv) change in geometry and orientation of fillers, and (v) formation and the propagation of micro-cracks in the nanocomposites carried out by the mechanical deformation (Amjadi *et al.*, 2015; Canavese *et al.*, 2012, 2014; Georgousis, Pandis, Kalamiotis, *et al.*, 2015; Vidhate *et al.*, 2009; Zheng *et al.*, 2014). Piezoresistivity depends also on dimensionality and aspect ratio of conductive fillers, filler concentration and viscosity, crystallinity and mechanical properties of the polymer matrix (Natarajan *et al.*, 2017; Selvan *et al.*, 2016). It can be tuned by the variation of filler concentration, their orientation, and selection of suitable polymer matrix as per the mode of applications of nanocomposites. The composites with filler concentration near to percolation threshold are more sensitive to the deformation due to the less dense network and vice versa (Chen *et al.*, 2007; Natarajan *et al.*, 2017). Generally, positive and negative type of piezoresistivity are observed depending on the nature of deformation. Electrical resistance increases in positive piezoresistivity which is performed by tensile deformation. Similarly, it decreases in negative piezoresitivity which is exhibited by compressive type of deformation (Natarajan *et al.*, 2017).

Quantified change of electrical resistance of CPC as a function of strain induced deformation (mechanical) is useful to the strain sensitivity of these materials. In other words, these materials can be integrated as strain sensors which become applicable in wearable electronics and sensors, monitoring human health and body motion, structural damage sensation etc. (Alamusi *et al.*, 2011; Lee *et al.*, 2017). CPC based strain sensors work on the basis of principle of piezoresistivity and they are of low impedance with low power consumption (Chen *et al.*, 2007; Georgopoulou & Clemens, 2020). The reason of piezoresistive effect of CPC is described on the basis of statistical percolation model as follows (Chen *et al.*, 2007).

At percolation threshold, electrical conductivity of nanocomposites is given by (from equation (1) stated above)

$$\sigma \sim (P - Pc)^t \qquad\qquad (3)$$

where, σ = Conductivity of CPC

P = Filler fraction

P_c = Percolation threshold

t = Scaling factor

Similarly, the correlation length (ξ) between the adjacent filler particles at percolation threshold is given by

$$\xi \sim (P - Pc)^{-v} \qquad\qquad (4)$$

where, v = critical index

The same value, $P - Pc$ is exponented to different power values in equation (3) and (4) signifying the values of conductivity and the average distance between filler particles, respectively. This is the reason behind the performance of piezoresistivity by CPC but not that by metals and semiconductors (Alamusi *et al*., 2011; Chen *et al*., 2007). Capacitive and resistive type of strain sensors are designed on the basis of deformation induced change of electrical resistance and capacitance respectively (Shintake *et al*., 2018; Xie *et al*., 2019). Capacitive strain sensors perform low sensitivity range in comparison to that by resistive type of sensors (Amjadi *et al*., 2015; Shintake *et al*., 2018). Capacitive sensors are useful mainly for thermal, biological and chemical sensing purpose (Xie *et al*., 2019). Resistive type of strain sensors perform high sensitivity with easy signal collection despite their high hysteresis (Niu *et al*., 2018; Shintake *et al*., 2018). Deformation induced reversible change of electrical resistance of CPC and their ability to transduce the deformations into electrical signals are the basis to integrate them as strain sensors (Pissis *et al*., 2015; Shintake *et al*., 2018; Vidhate *et al*., 2009; Yu & Kwon, 2009).

Highly ductile and deformable polymers and elastomers based nanocomposites comprising of conductive nanocarbons with high aspect ratio are taken as suitable piezoresistive materials for strain sensing and soft robotic applications (Canavese *et al*., 2014; Guo *et al*., 2019; Hwang *et al*., 2013). CPC are deformable materials with

flexibility and easy processability which can be prepared in a cost effective way. Deformability and flexibility of CPC can be tuned optimizing the filler concentration, conditions of their preparation and selection of suitable polymer matrix *(Canavese et al.*, 2014; Qu & Wong, 2007). The percolated conductive filler network formed by the incorporated conductive fillers into the polymer matrix is sensitive to the external deformation stimuli such as strain, stress, pressure etc. High conductivity of the nanocomposites at a low filler loadings is desired to minimize the mechanical hysteresis of polymer matrices. In other words, low percolation threshold of CPC protects their mechanical properties providing them with electrical conductivity and piezoresistive sensitivity (Dubey *et al.*, 2020). Flexibility and the elasticity are the fundamental requirements for CPC to find their applications for strain sensing (Ryu *et al.*, 2015). Stretchability, conductivity and the sensitivity of the materials should be addressed at a time for this goal (Georgopoulou & Clemens, 2020). Flexibility of these materials is conferred by the corresponding polymer matrix whereas conductivity and the mechanical properties can be tuned varying the concentration, aspect ratio and orientation of conductive fillers. These composite materials can endure high strain applied. The corresponding resistance change carried out by the strain induced deformation of CPC will be reversible up to a certain extent due to their elastic properties (Amjadi *et al.*, 2015; Kumbay Yildiz *et al.*, 2016).

CNT, the mostly used conductive nano-fillers are piezoresistive themselves and perform outstanding electrical, mechanical and thermal properties in comparison to other nanocarbons. Therefore, CNT are chosen as suitable conductive nano-fillers in the preparation of piezoresistive materials applicable for strain sensing. MWCNT are mostly preferred in this regard due to their high purity and low cost if compared to single walled carbon nanotubes (SWCNT) (Knite *et al.*, 2007; Wu *et al.*, 2017). CNT maintain the electrical conductivity of nanocomposites even under stretched condition due to their own stretchability. They alone as well as in compounded state with elastic and soft matrix can be integrated into strain sensors (Amjadi *et al.*, 2015; Ryu *et al.*, 2015). Moreover, CNT compounded with an elastomeric matrix are found to perform stable and reproducible electromechanical response with less vulnerability (Kumbay Yildiz *et al.,* 2016*).* Even graphene based strain sensors perform low stretchability because of the brittle behavior of graphene sheets regardless their electrical conductivity (Amjadi *et al*., 2014; Niu *et al*., 2018). Similarly, graphene based strain sensors perform low sensitivity due to its zero band gap of graphene (Zhao *et al*., 2015).

Piezoresistive flexible polymer/MWCNT nanocomposites can easily be prepared compounding MWCNT with ductile and deformable polymer matrices (Alamusi *et al*., 2011; Gau *et al*., 2009). Both filled and sandwiched type of composites, applicable for strain sensors can be prepared using suitable polymer matrices and MWCNT. However, strain sensors based on filled type of composites perform good mechanical properties with ease of mass production and cost effectiveness (Chen *et al*., 2021). Higher strain sensitivity (in micro level) can be achieved from polymer/MWCNT nanocomposites than that from conventional strain gauzes (macro level) (Alamusi *et al*., 2011; Ponnamma *et al*., 2014). Furthermore, the range of sensitivity of CPC based strain sensors can be tuned varying the filler concentration, their orientation and choosing the suitable polymer matrix (Hwang *et al*., 2013).

Flexible and stretchable strain sensors with their high sensitivity range are desired these days to substitute the traditional strain sensors with low strain range (Amjadi *et al*., 2014). CPC based on elastomers and the flexible thermoplastic polymers with high elongation at break and easy processability can be the suitable candidates (Georgousis *et al*., 2017; Vidhate *et al*., 2009). Flexibility and stretchability are not provided by the traditional metal and semiconductors (rigid) based strain sensors which have a low sensitivity range (Amjadi *et al*., 2014; Tang *et al*., 2015). Ceramics based piezoresistive sensors are also reported, however, they are found brittle and costly with poor matrix adhesion (Vidhate *et al*., 2009). Thus, electrically conductive CNT/ flexible polymer nanocomposites based strain sensors can be the alternatives to the conventional strain sensors (Amjadi *et al*., 2014; Ferreira *et al*., 2013). Easy deformation and higher piezoresistive effect of CPC is required for the best strain sensing applications (Narongthong *et al*., 2018). High aspect ratio of the conductive fillers and low loading provides the high piezoresistive effect whereas soft and flexible polymer matrix provides the easy deformation (Chen *et al*., 2007; Narongthong *et al.,* 2018*).*

Thermoplastic elastomers (TPE) generally possess a low yield strain as well as a narrow elastic region in comparison to the elastomers. However, they perform higher sensitivity range (up to 50 %) strain of piezoresistive sensing than that of conventional strain gauze (>5%) (Ke *et al*., 2017; Wu *et al*., 2017) Due to the piezoresistive nature of CNT, polymer nanocomposites reinforced by CNT also become piezoresistive in nature. Hence, CNT filled CPC can directly be integrated into piezoresistive strain sensors (Ciselli *et al*., 2010; Gau *et al*., 2009; Ryu *et al*., 2015). Individual CNT perform linear piezoresistivity with mechanical strain whereas polymer/CNT

composites exhibit non-linear exponential-like piezoresistivity as presented in **Figure 3a** and **3b** respectively (Gau *et al*., 2009).
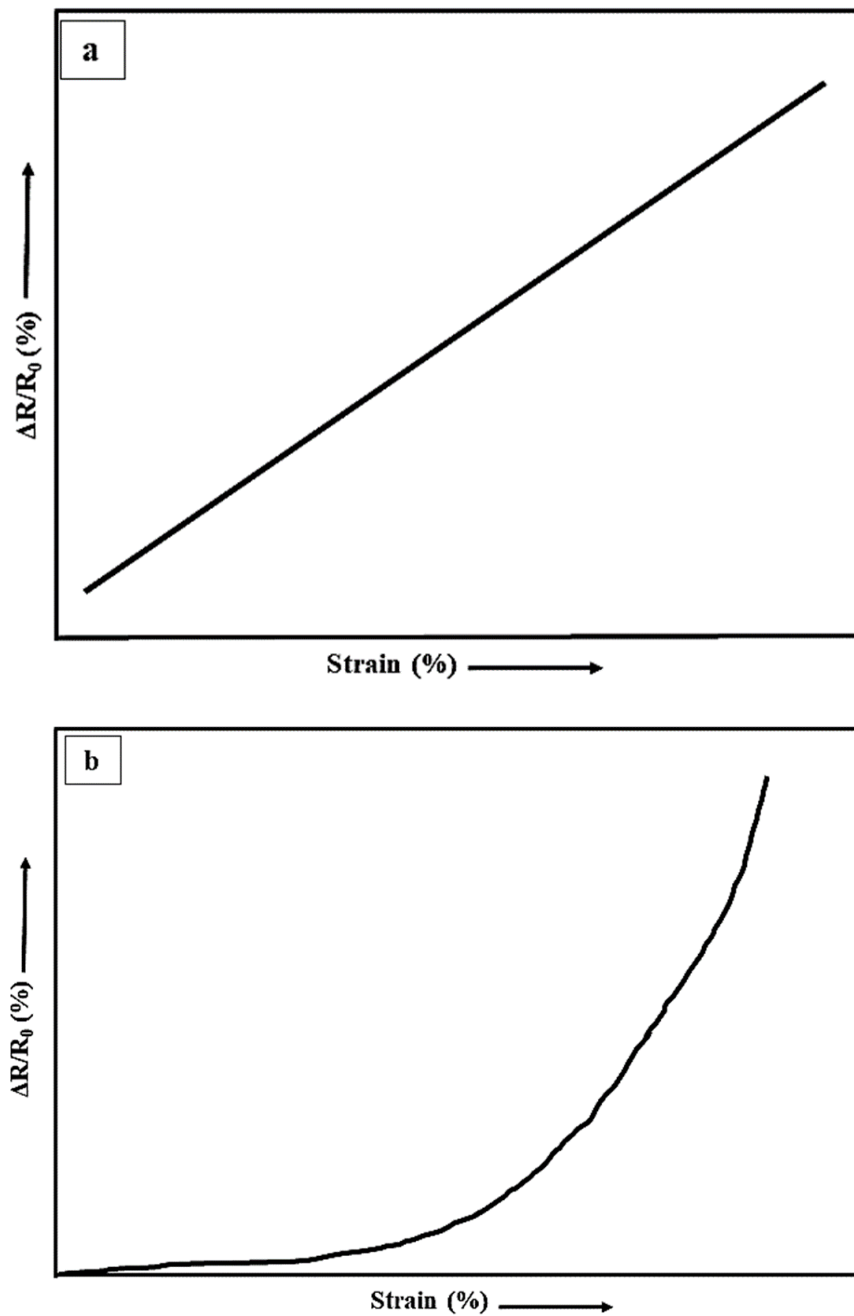
Figure 3: Schematic diagrams illustrating (a) linear piezoresistivity of CNT and (b) exponential-like piezoresistivity of CPC (Gau *et al*., 2009)

The exponential-like piezoresistivity curve of the polymer/CNT composites is due to the increased tunneling effect between neighboring CNT-particles during deformation of the composites which causes the decrease in resistance of the nanocomposites to some extent restricting its linear increment. Under deformed conditions, electron tunneling becomes dominant in nanocomposites (Gau *et al*., 2009). Viscoelasticity of

the polymer matrices causes the rearrangement of filler particles during deformation by which tunneling effect increases controlling the linear increase of the relative resistance change ($\Delta R/R_0$) (Cravanzola *et al*., 2013).

Recovery of the initial resistance of nanocomposites becomes possible by the presence of conductive filler network throughout the composites, and flexibility and stretchability of polymer matrices. Hence, intrinsic piezoresistivity of CNT, tunneling effects, deformability of individual CNT and that of conductive CNT network, stretchability and flexibility of the polymer matrix are combined together in piezoresistive effect of CPC (Cravanzola *et al*., 2013; Zheng *et al*., 2014). In other words, conductivity of polymer/nanocarbons composites is piezoresistive in nature. Electrical conductivity is similar to that of conventional metals and semiconductors based strain gauzes, however, it additionally performs sensitivity towards external mechanical stimuli due to piezoresistivity (Gong & Zhu, 2014).

Total electrical resistance of CPC can reversibly be varied applying external stimuli by virtue of piezoresistivity (Chen *et al*., 2021). An overall change in resistance of CPC depends on inter-chain contact of CNT in the conductive network which is a basis to apply them in strain sensors (Vidhate *et al*., 2009). Change in electrical resistance of CPC as a function of tensile deformation is measured quantitatively for the evaluation of strain sensitivity. Stress-strain behavior of CPC and the relative resistance change with strain applied are measured simultaneously (Georgousis *et al*., 2018). Hence, $\Delta R/R_0$ of CPC, as a suitable candidates, find their applications to design resistive type of strain sensors (Yu & Kwon, 2009).

2.4. Strain Sensing Behavior of CPC

Flexible and stretchable piezoresistive CPC are the suitable sensing materials for different external deformation stimuli such as, stress, strain, pressure, etc. They can be integrated into piezoresistive strain sensors whose sensitivity is established by the quantified conversion of mechanical strain into electrical signals. They can be cost effective and flexible new generation strain sensors (Alamusi *et al*., 2011; Almahri *et al*., 2022; Selvan *et al*., 2016; Zhang *et al*., 2007). Poor stretchability and flexibility of conventional metallic strain sensors can be compensated by the CPC based strain sensors, maintaining their electromechanical stability even at high strain range (Almahri *et al*., 2022; Amjadi *et al*., 2015). Deformation sensing performance of CPC is due to the increased tunneling resistance and the decreased contacts between filler

particles by which overall resistance of the composites increases (Ke *et al.*, 2016). Therefore, relative variation in electrical resistance of CPC, commonly called relative resistance change ($\Delta R/R_0$) is evaluated as a function of mechanical strain to investigate the sensitivity of piezoresistive strain sensors as presented in **Figure 4**.
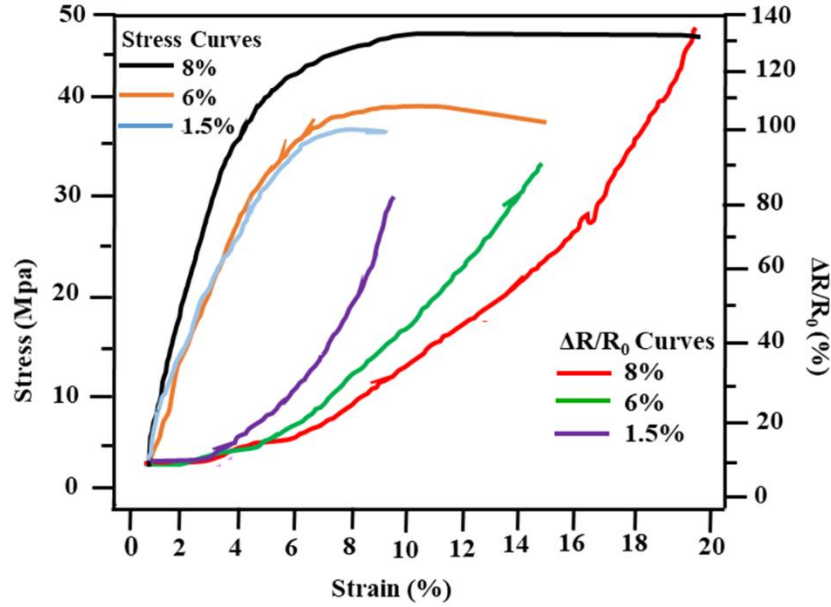
Figure 4: Relative resistance change of polymer/CNT nanocomposites as a function of mechanical strain with stress-strain curves (Georgousis *et al.*, 2015)

$\Delta R/R_0$ measures the extent of piezoresistivity by which degree of sensitivity is provided (Georgopoulou & Clemens, 2020; Georgousis *et al.*, 2018; Wu *et al.*, 2017). The entire resistance of CPC is determined not only by the filler concentration, but also by network density, correlation length between filler particles, properties of polymer matrix etc. Therefore, $\Delta R/R_0$ of nanocomposites changes due to the deformation induced destruction of nanocomposites, tunneling effect and change in micro and nanostructure of composites carried out by deformation (Georgousis *et al.*, 2018; Zhao *et al.*, 2017) . It changes almost linearly at lower strain level which later increases exponentially as shown in **Figure 4**.

Gauze factor (GF) which is the ratio of $\Delta R/R_0$ to the strain (ε) applied of a strain sensors is evaluated to quantify the sensitivity of the sensors (Chen *et al.*, 2021; Georgousis *et al.,* 2018*)*. GF is calculated from the slope of exponential-like piezoresistive curve obtained by plotting $\Delta R/R_0$ versus strain (ε) applied as presented in **Figure 5**.
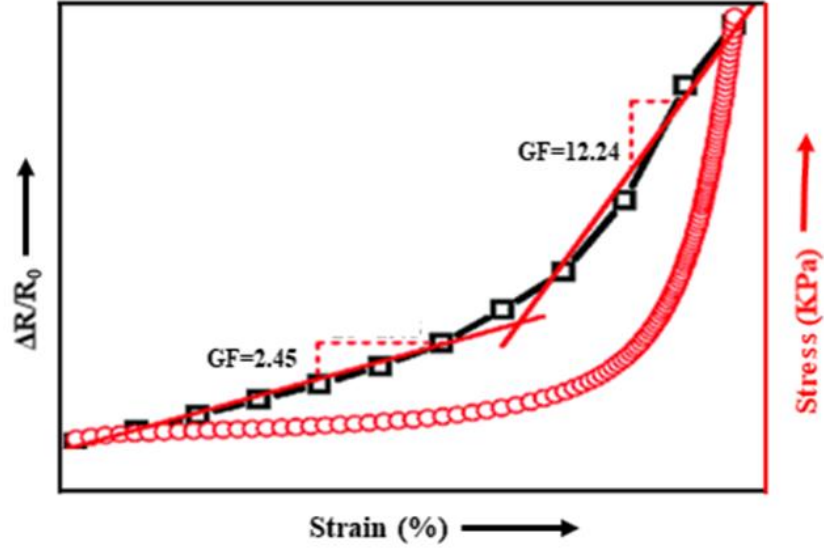
Figure 5: Calculation of gauze factor (GF) from piezoresistive curve of graphene/TPU foam (Liu *et al.*, 2017)

Despite the quantitative indication of sensitivity of piezoresistive strain sensors, GF can't provide the information about their applicable strain sensitivity range. The product of GF and mechanical strain applied is taken for the evaluation of overall performance of strain sensors (Georgopoulou & Clemens, 2020; Sang *et al.*, 2019; Zhao *et al.*, 2017). i.e.

$$\frac{\Delta R}{R0} = GF \times \varepsilon \qquad (5)$$

where, $\frac{\Delta R}{R0}$ = Relative resistance change, GF = Gauze factor, ε = Strain applied

Strain sensing applications of CPC is based on their piezoresistivity i.e. on the quantified resistance change with respect to mechanical deformation carried out by the loss of CNT connections (Sang *et al.*, 2019). More smooth change in *ΔR/R₀* is observed in densely percolated (well above percolation threshold) nanocomposites. Sparse type of conductive CNT-network is formed in CPC by the loose connection of CNT near percolation threshold. Therefore, a minimum deformation makes CNT apart from each other in the direction of stretching. On the other hand, an abrupt change occurs in the nanocomposites filled with lower filler content (close to percolation threshold). High piezoresistivity is performed by the CPC containing filler concentration close to percolation threshold due to loose CNT connections. It means that a lower strain value can cause a higher strain sensitivity in the nanocomposites with low filler concentration. Such nanocomposites are applicable for low strain-sensing purposes. Similarly, the

densely filled nanocomposites with higher filler concentration can withstand higher strain without failure of conductive filler networks the materials themselves. They can be applicable for high strain-sensing purposes (Dhakal *et al*., 2022b; Georgousis *et al*., 2015a; Narongthong *et al*., 2018).

Stable and reproducible resistance change may not be achieved from the nanocomposites with filler concentration close to percolation threshold. This is due to the sparse filler network which can be permanently destructed even at low strain. Similarly, recovery of original resistance of nanocomposites after deformation in a sparse network is low (Georgousis *et al*., 2017; Wu *et al*., 2017). Noisy electrical signals are obtained from the CPC, close to the percolation threshold. Meanwhile, instrumental drawbacks can be dominant while quantifying such a sensitivity. Even a very high resistance change can be obtained while using CPC with filler concentrations near to the percolation threshold. It can be out of range of measurements using the available instruments (Sang *et al*., 2019).
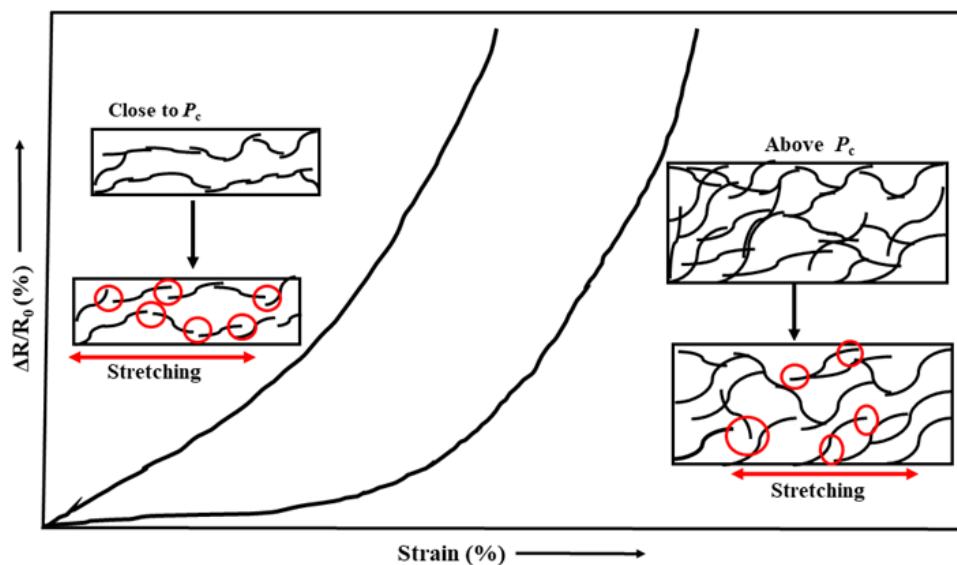
Figure 6: Schematic illustration of piezoresistive sensitivity of CNT filled CPC close to and above percolation threshold (P_c)

An abrupt (close to percolation threshold) and a smooth (above percolation threshold) resistance change is illustrated in **Figure 6**. Inter-particle distance of CNT overcomes the tunneling distance soon (illustrated by red circles). There will be a very low probability for the formation of alternative conductive pathways with the deformation. These phenomena are the reasons for an abrupt increase of electrical resistance.

Moreover, dense filler networks and the corresponding deformation induced smooth resistance change are also illustrated in **Figure 6**. Higher probability of formation of new conductive pathways (illustrated in Figure) and the maintenance of tunneling distance due to higher concentration of CNT are the reasons for a smooth increase in resistance. The detached CNT due to deformation immediately connect to other CNT forming new conductive paths. Similarly, CNT which can't maintain the tunneling distance to each other may maintain that distance with neighbouring CNT particles. Therefore, linear part of piezoresistive curve as well as a smooth increment of resistance change can be clearly observed.

Stress-strain behavior of polymer matrix used for the preparation of CPC is correlated with the $\Delta R/R_0$ of the composites over a range of mechanical strain. Therefore, stress-strain behavior of polymer matrix deserves a significance in this regard. Percolation threshold and volume resistivity of CPC provide the information about the formation of conductive pathway throughout the composites and their electrical conductivity. However, deformation of CPC and the deformation induced CNT disconnection, their reorientation and resistance change depends also on mechanical toughness of the polymer matrix. In other words, piezoresistivity and the piezoresistive strain sensing behavior of CPC depends on the toughness of CPC. Therefore, piezoresistivity of CPC differs from matrix to matrix under same experimental conditions and filler concentration. E.g. Elastomers based CPC are more susceptible to mechanical deformation than TPE based CPC. Similarly, Thermosets based CPC are less susceptible to mechanical deformation than TPE based CPC (Ke, 2016).
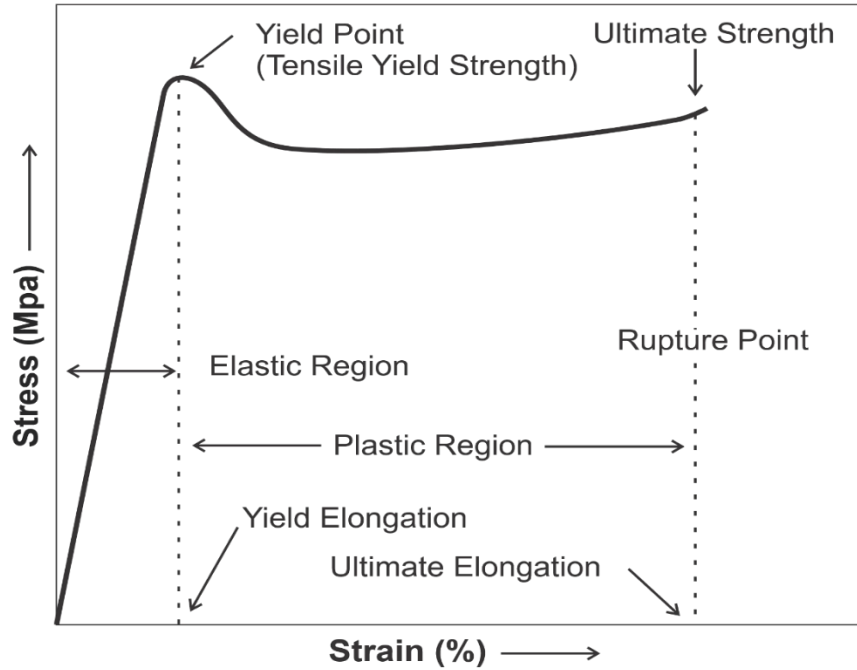
Figure 7: Typical stress-strain behavior of thermoplastic elastomers (Ke, 2016)

Typical stress-strain plot of a thermoplastic elastomer is presented in **Figure 7**. It involves an elastic region followed by a plastic region with strain yield point. After yield point, the corresponding stress value decreases as shown in **Figure 7**.(Kai-Ke, 2016). Reversible deformation of conductive network and piezoresistivity of TPE based CPC can be obtained only below yield point. $\Delta R/R_0$ increases in a linear way in elastic region whereas it increases faster in exponential manner till the failure of the material (Georgousis *et al*., 2018; Pissis *et al*., 2015).

Strain sensitivity and deformability only are not the sufficient characteristics for CPC for their strain sensing applications. Strain dependent resistance change of materials and its stability and repeatability over a range of strain is necessary in this regard. It is investigated by continuous strain cycles in cyclic strain experiment (dynamic cyclic test) (Ji *et al*., 2014; Liu *et al*., 2021; Zhang *et al*., 2013). Mostly, equal tensile speeds are employed in piezoresistive experiement and cyclic strain experiment for the comparative analyses. Occurence of a stable and repeatable electromechanical response of CPC upto a number of cycles is expected. A consistent and stable $\Delta R/R_0$ value as a function of mechanical strain applied over a range of strain confirms the excellence of materials for strain sensing applications (Christ *et al*., 2017; Georgopoulou & Clemens, 2020). Fitting of $\Delta R/R_0$ with the mechanical strain and its repeatability in a number of cycles is investigated.

In cyclic strain experiment, electrical resistance of TPE based CPC is not fully recovered during strain unloading process i.e. $R/R_0 \neq 1$ after unloading. It is reported that $R/R_0 = 1$ for an ideal strain sensor. In other words, conductive CNT-network can't be reformed completely during unloading. Full recovery of the resistance of these CPC is limited by hysteresis effect which is carried out by the process of energy dissipation in which reconstruction of conductive network is partially hindered. Repeatedly applied strain to the CPC carries out a semi-permanent type of change in the conductive filler network and the composite microstructures (Cetin & Karahan Toprakci, 2021; Christ *et al*., 2017; Kumar *et al*., 2019; Liu *et al*., 2015; Liu *et al*., 2021; Zhang *et al*., 2013). Therefore, resistance recovery in a cyclic strain experiment is related not only to the removal of mechanical strain, but it is a time dependent phenomenon (Zhang *et al*., 2013). In the first few cycles, the amplitude of resistance change goes in decreasing manner. Such an amplitude decay of electrical resistance is stabilized after a few cycles (Sang et al., 2019). Several constructions and destructions of conductive paths balance each other after several loading and unloading processes. Hence, resistance change drifts less and stabilizes with higher number of cycles. Rearrangement of polymer chains occurs at higher number of cycles to minimize the strain induced deformation called strain softening that leads to the stability of resistance change (Christ *et al*., 2017; Georgopoulou & Clemens, 2020; Kumar *et al*., 2019; Liu *et al*., 2021; Xiang *et al*., 2019; Zhang *et al*., 2013).

In case of thermoplastic elastomers based CPC, single peak resistance response is observed only at lower strain range (mostly below 5 % strain) whereas second peaks called shoulder peaks are also observed at higher strain values as shown in **Figure 8** (Christ *et al*., 2017; Kumar *et al*., 2019; Zhang *et al.*, 2013). The first peak is due to the increase in electrical resistance called positive piezoresistive effect and carried out by the breakdown of the conductive network and increasein tunneling distance (Liu *et al*., 2015). Development of second peaks in this experiment is not a separate phenomenon which is generally performed by thermoplastic elastomers and rubber composites.
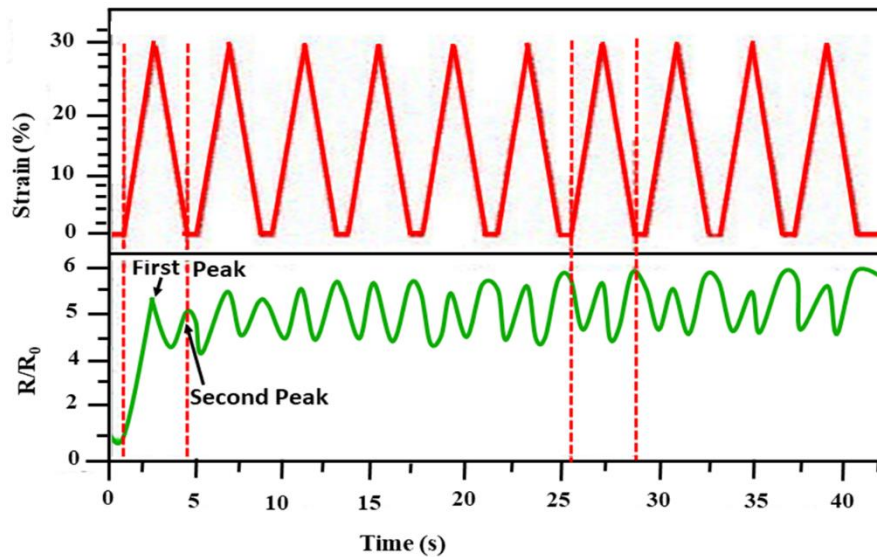
Figure 8: Cyclic strain test of polyurethane-urea/MWCNT composites (Zhang *et a*l., 2013)

Mechanical hysteresis causes the destruction of the conductive network whereas the retraction of polymer chains attempt for its reconstruction. Two opposite competitive phenomena i.e. destruction of old conductive pathways and the reconstruction of new conductive pathways during loading and unloading cycles of this experiment occurs, respectively. A full retraction of the polymer chains to reform the conductive pathways is not possible by which the network is partially destroyed and the resistance increases even in unloading process that produces the shoulder peaks (Xiang *et al*., 2019). As shown in **Figure 8**, strain is loaded continuously up to a certain value and unloaded to zero value. Zhang et al. has provided an interval of 6 seconds at the end of unloading of each cycle for the relaxation of stretched specimen (Zhang *et al*., 2013). This time interval can be altered in various experiments. Meanwhile, relaxaion time can be provided at the end of every unloading and loading in each strain cycle.

Unloading process is also performed in a similar way to that of loading process (Zhang *et al*., 2013). At higher strain values in each cycle, *ΔR/R₀* does not compulsorily decreases during unloading. It is observed that the resistance decreases to certain minima at the begining of strain unloading and increases before the next cycle which is the reason to appear shoulder peaks (Christ *et al*., 2017; Liu *et al*., 2021; Zhang *et al*., 2013). A single-peak resistance response of the materials is desired for their strain sensing applications. However, shoulder peaks are negative piezoresistive response which can also be taken as strain sensitivity in opposite direction (Christ *et al*., 2017; Kumar *et al*., 2019; Salaeh *et al*., 2020).

The possible mechanism of stretching and relaxation of CPC during cyclic strain experiment is illustrated in **Figure 9.**

Original state: The original (strain unloaded) state corresponds to have a conductive network formed by CNT-CNT connections with some tunneling distance maintained (red encircled). Multiple conductive paths formed by end to end connections of CNT as well as electron tunneling contribute to the conductivity of CPC in this state.
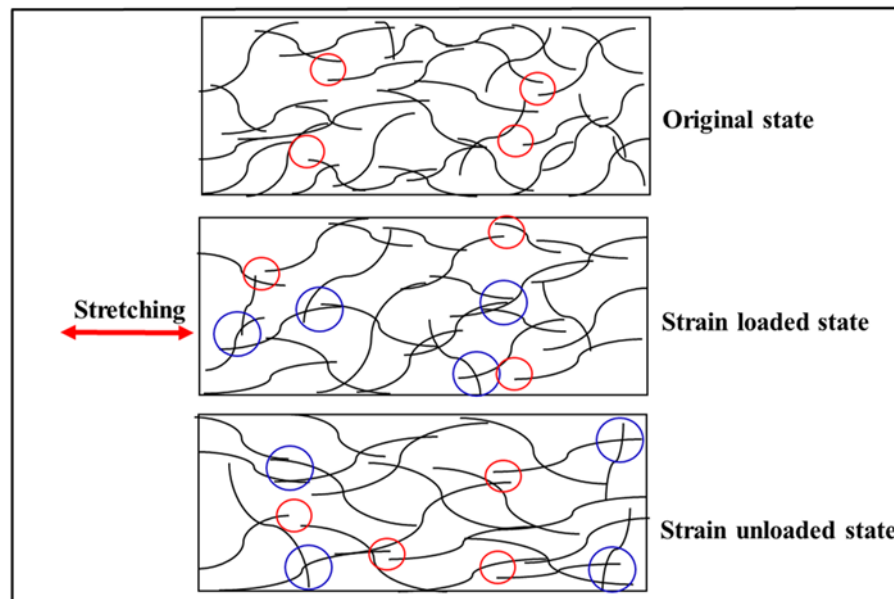
Figure 9: Schematic illustration of change of microstructures of CPC during cyclic strain experiment (Liu *et al*., 2015, 2018)

Strain loaded state: During tensile stretching (strain loaded state), CNT connections are lost (red encircled). Meanwhile, new CNT connections are formed (blue encircled) producing new conductive pathways. At lower strain values, the disconnected CNT particles can maintain the tunneling distance between them as well as with the neighbouring CNT particles which contribute to the electrons-tunneling induced conductivity of CPC. Therefore, a linear and smooth resistance change occurs at such lower mechanical strain. At higher strain values, both the loss of CNT connections and inter-particle distance (greater than tunneling distance) contribute to an abrupt increment of electrical resistance.

Strain unloaded state: The applied mechanical strain is removed in this state by which a slightly different conductive CNT-network can be developed. New conductive pathways and the new CNT-to-CNT gaps (red encircled) are developed. As mentioned previously, TPE based CPC suffer from hysteresis effect by which original value of

resistance (R_0) is not retained. Hence, amplitude of resistance change decreases (also called resistance decay) in first few cycles in this experiment.

Each strain cycle goes through strain loading and unloading as mentioned above. Repeatedly applied strain loading and unloading stabilizes the resistance amplitude due to Mullin's effect and strain softening (Salaeh *et al*., 2020).

2.5. Crosslinking CPC by Electron Beam (EB) Irradiation

Structural modification and the change in properties of neat polymers, polymeric materials and rubber can be carried out by the irradiation of ionizing type of radiation. Electron beam (EB) and the gamma radiation are the mostly used ionizing radiations (Clough, 2001; Iuliano *et al*., 2020; Kobayashi *et al*., 2013). They are irradiated to the materials mainly for crosslinking and sterilization (Clough, 2001; Madera-Santana *et al*., 2016). EB irradiation is used as an advanced technique these days for the processing of polymeric and rubber materials such as medical and packaging materials, aircraft cables, emulsions, acrylates, tires etc. (Clough, 2001). Even the packaged materials can be processed by this method by which undesired degradation of materials can be controlled (Haji-Saeid *et al*., 2007). This method is taken as a green and comparatively faster method for the processing of polymeric materials in industrial level because it involves no additives and leaves no chemical residues which is not possible in other methods such as sulphur crosslinking, peroxide crosslinking etc. It can also be carried out at room temperature and provides green strength even to uncured rubber (Choi *et al*., 2013; Chongcharoenchaikul *et al*., 2022; Clough, 2001; Dubey *et al*., 2020; Haji-Saeid *et al*., 2007; Hwang *et al*., 2010; Iuliano *et al*., 2020).

Radiation induced crosslinking provides homogeneous crosslinking throughout the irradiated materials (Chaudhari *et al*., 2012). Moreover, this method consumes low energy, requires no radioactive source to operate and it can be controlled during the operation in terms of duration and dose of irradiation. Comparatively, higher irradiation dose than that by gamma radiation, in a changeable mode can be applied using electron beam. Processing of a material can be carried out under selective conditions. Therefore, the exact conditions and the irradiation dose required for a particular processing can be experimentally determined. It is well accepted processing method with high curing capacity, however, EB performs less penetrating capacity in comparison to gamma radiation (Clough, 2001; Iuliano *et al*., 2020; Kobayashi *et al*., 2013; Lappan *et al*.,

2001; Zhao *et al*., 2020). Meanwhile, it possesses higher throughput efficiencies than gamma radiations (Haji-Saeid *et al*., 2007).

EB irradiation leads to the formation of covalent bonds between the chains of polymer without any additives due to which chain mobility of the polymers is controlled. When EB is irradiated to the polymers, reactive intermediates are formed which on excited state causes the rearrangement of the polymer chains and formation of covalent bonds (Clough, 2001; Haji-Saeid *et al*., 2007). This method of crosslinking is applicable even to the polymers without active functional groups for the chemical reaction. The polymeric materials crosslinked by EB irradiation have superior properties and can find advanced applications. It is reported that styrene butadiene rubber (SBR) crosslinked by EB irradiation performed better wear properties and ozone resistance in comparison to SBR crosslinked by Sulphur (Clough, 2001).

EB irradiation on polymeric materials carries out two major phenomena. They are chain scission and crosslinking of polymers. Chain scission leads to the degradation of polymers at higher dose by which molecular weight (MW) of the polymers decreases causing the decrease in melting point, thermal stability, mechanical strength etc. (Clough, 2001; Haji-Saeid *et al*., 2007; Zhao *et al*., 2020). On the other hand, crosslinking of polymers by EB irradiation leads to increase in MW and changes in physicochemical properties. Generally, decreased elongation at break, crystallinity, solubility etc. and increased tensile strength, elastic modulus, melt-viscosity etc. of the polymers are carried out by the irradiation induced crosslinking (Choi *et al*., 2013; Clough, 2001; Haji-Saeid *et al*., 2007; Rzepna *et al*., 2018; Zhao *et al*., 2020). Crosslinking of the irradiated materials occurs dominantly under reduced pressure and inert gas atmosphere (Iuliano *et al*., 2020). Advantages of EB irradiation induced crosslinking are outlined as follows *(*Dubey *et al*., 2015).

➢ Electron tunneling and hopping rate will be higher with higher network density

➢ The polymer chains will be less flexible and inter-chain slippage will also decrease which can withstand more strain

➢ Dynamics of filler aggregation is also changed in which disaggregation and re-aggregation dynamics occurs. It leads to increase the gauge factor (piezoresistive sensitivity) of electrically conductive polymer nanocomposites and significantly changes their electromechanical response

Biodegradable copolyesters are mostly crosslinked by the method of EB irradiation. A successful and irradiation dose dependent crosslinking of PBAT and its nanocomposites by EB irradiation is reported in the literatures (Iuliano *et al*., 2020; Rzepna *et al*., 2018; Zhao *et al*., 2020). Although PBAT is commercialized as a biodegradable packaging materials, it is being researched for advanced applications after modification (Rzepna et al., 2018). PBAT is resistant to EB irradiation to some extent because of the presence of an aromatic ring in its butylene terephthalate (BT) segment, however, irradiation induced crosslinking occurs *via* ester bond present in butylene adipate (BA), an aliphatic segment (Burillo *et al*., 2007; González Seligra *et al*., 2016; Rzepna *et al*., 2018). Inter and intra-chain free radical mechanism of EB induced PBAT crosslinking and the corresponding species are as in **Figure 10**.

PBAT molecule

↓ EB

$PH + electron\ beam \rightarrow PH^{*}$ *(excited state)*

$PH^{*} \rightarrow PH^{+} + e^{-}$ *(ion and secondary electron)*

$PH^{*} \rightarrow P^{\bullet} + H^{\bullet}$ *(free radical)*

$PH + PH \rightarrow P^{\bullet} + PH_2^{+}$ *(free radical and ion)*

$P^{\bullet} + PH_2^{+} + e^{-} \rightarrow P^{\bullet} + P^{\bullet} + H_2$ *(free radical)*
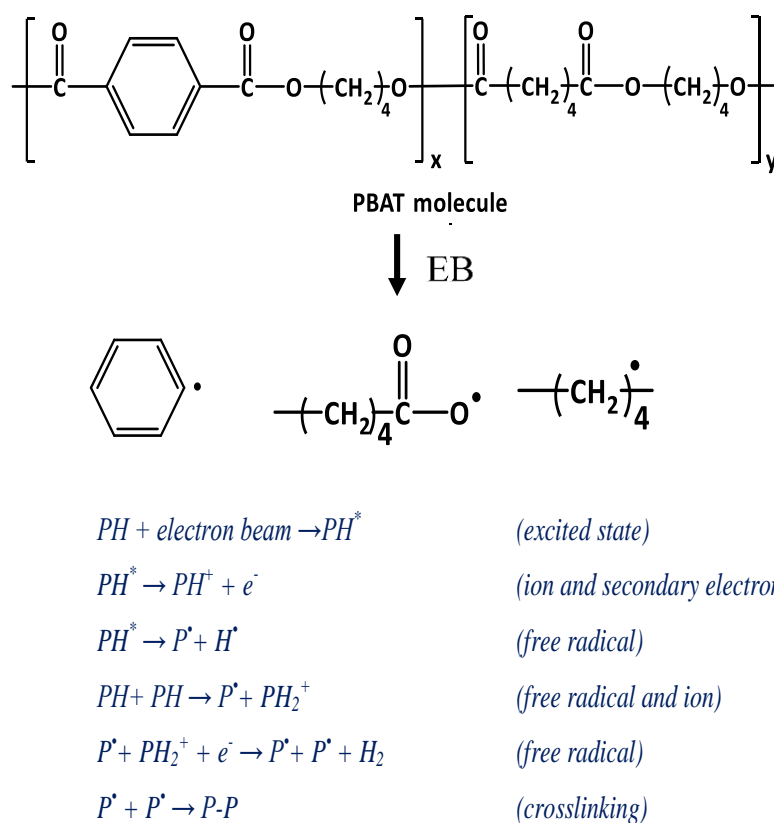
$P^{\bullet} + P^{\bullet} \rightarrow P\text{-}P$ *(crosslinking)*

Inter and intrachain crosslinking at various reactive sites

Figure 10: Mechanism of electron beam irradiation induced crosslinking of PBAT (Khatiwada *et al*., 2019; Rzepna *et al*., 2018)

Minor degradation of PBAT during EB irradiation is also reported (Choi *et al*., 2013; Hwang *et al*., 2010; Rzepna *et al*., 2018) however, crosslinking and chain scission balance each other at higher irradiation dose. Aromatic domain of PBAT partly

participates in radiation effects (Iuliano *et al*., 2020). **Table 2** summarizes the PBAT and PBAT/PLA based blends and composites irradiated with EB.

Table 2: List of EB irradiated PBAT, PBAT/PLA blends and the related composites

S.N.	Materials	Thickness	Dose (kGy)	Remarks	Reference
1.	PBAT/PLA Blends-film	120 µm	5, 13, 26	More ductile at higher dose, no change in barrier properties	(Iuliano *et al*., 2020)
2.	PBAT/PLA Blends-film	>20 mm	10, 40, 90	Crosslinking at 10 and 40 kGy, material degradation at 90 kGy, PBAT is less susceptipble due to aromatic domain (protective effect)	(Malinowski *et al*., 2020)
3.	PBAT and PBAT/POSS	-	20-200	Crosslinking (PBAT:17% and PBAT/POSS: 61% at 200 kGy)	(Choi *et al*., 2013)
4.	PBAT and PBAT/PLA Blends-films	0.5 mm	25-100	decrease in elongation at break	(Zhao *et al*., 2020)
5.	PBAT-film	130 µm	20-200	Crosslinking (52% at 200 kGy), decreased elongation at break and increased tensile strength (at higher doses)	(Hwang *et al*., 2010)
6.	PBAT-film	-	0-200	Change in elongation at break at higher dose	(Rzepna *et al*., 2018)

POSS: *polyhedral oligomeric silsesquioxane*

In polymer/CNT nanocomposites, degree of crosslinking can increase also with the CNT concentration. This is because of the absorption of energy of radiation by the CNT particles. Meanwhile, reinforcement of polymer/CNT nanocomposites by the filler particles checks the reorientation of polymer chains, Filler particles may form physical and chemical crosslinks on the chains of polymer leading to the immobilization of polymer chains (Chaudhari *et al*., 2012).

2.6. Biodegradable CPC

Polymers and polymeric materials have become a part of our daily life which is because of their low weight, cost effectiveness, better processability, mechanical performance, and variability of the physical properties. Meanwhile, they can be benefitted from different aspects such as materials design, synthetic routes, methodologies etc. This is due to their better proceessability by which they can be modified into different polymeric micro and nanomaterials. Therefore, more than 250 metric tons plastic products are produced annually in the world to meet the daily requirements of human life *(*Dil *et al*., 2020; Gan *et al*., 2004; Li *et al*., 2015; Liu *et al*., 2022; Tran *et al*., 2019). Such a large volume of plastics and plastic based products is causing waste disposal crisis and environmental problems (Gan *et al*., 2004; Sirisinha & Somboon, 2011). Meanwhile, it causes aquatic and marine pollution badly affecting the ecology. It is estimated that the fish population in the ocean will be exceeded by the plastic products by 2050 (Barron & Sparks, 2020). On the other hand, technological advancement is making the useful age of electronics shorter these days. The electronic gadgets become obsolete shortly and get replaced by their superior model successors of new generation (Guo *et al*., 2020a; Qazi *et al*., 2020; Silva *et al*., 2021). It is causing the problems of electronic waste (e-waste) ultimately leading to environmental, land and aquatic pollution (Guo *et al*., 2021; Liu *et al*., 2019). Non-degradable polymers, harmful chemicals and heavy metals are being released to the environment from e-wastes (Liu *et al*., 2019).   Hence, mitigation as well as eradication of plastic and e-waste pollution is an urgent task in the world. It is possible by the development and promotion of bioplastics and biodegradable and biocompatible polymers to substitute the existing petro-based non-degradable commodity plastics (Deshmukh *et al*., 2017; Guo *et al*., 2020a; Qazi *et al*., 2020).

Biodegradable polymers undergo microbial and enzymatic degradation under environmental conditions from which bi-products, harmless to the environment are produced during their degradation (Han *et al*., 2022; Liu *et al*., 2022). They undergo the change in chemical structure and properties under environmental conditions (Qazi *et al*., 2020). Otherwise, polymers require up to 1000 years and even more for degradation. Similarly, promotion of advanced degradable polymeric materials, finding their applications in stretchable and flexible electronics is the strategic solution to overcome the problem of e-wastes. Multifunctional polymeric materials with

degradability, flexibility along with electrical conductivity are required in this regard. Biodegradability of polymeric materials is the most to address the global environmental and e-waste problems. However, biodegradability, low density, flexibility and electrical conductivity of same materials at a time is a challenge (Guo *et al*., 2021; Kumar *et al*., 2012; Soares *et al*., 2020; Tran *et al*., 2019).

If electrical conductivity is provided to a biodegradable, flexible and stretchable polymer, they can replace the conventional rigid, metal based conductors and semi-conductors. Most of the biodegradable polymers are found to be biocompatible as well. Therefore, flexible polymers with required electrical conductivity find their applications not only in electronics but also in biomedical field (Liu *et al*., 2019). Commercially available biodegradable polymers are applicable in electronics and sensors which can compete with the traditional non-degradable petro-based polymers. However, these polymers are limited to apply in electronics, actuators and sensors due to the lack of electrical conductivity (Dil *et al*., 2020; Qazi *et al*., 2020; Tran *et al*., 2019).

These materials can easily be prepared introducing the electrically conductive inorganic fillers into biodegradable polymers along with their flexibility and stretchability. Biodegradability and better mechanical performance of the resulting nanocomposites are provided by the matrix whereas electrical conductivity is provided by the inorganic fillers incorporated into them. Elastic inorganic fillers like CNT partially contribute to the enhancement of mechanical properties of nanocomposites. Electrically conductive bio-nanocomposites using eco-friendly polyesters find their applications in flexible electronics, sensors, actuators, transistors, EMI-shielding, optoelectronics etc. Biodegradable polymers and biopolymers based electronics is a long awaited agenda for advanced level research (Dil *et al*., 2020; Qazi *et al*., 2020; Tran *et al*., 2019).

Table 3: List of some biodegradable/biocompatible polymers

S.N.	Type	Name	Remarks	Reference
1.	Natural	Cellulose, alginate, collagen, silk, shellac, gelatin, chitosan, chitin *etc*.	Insulators, biodegradable and biocompatible	(Han *et al*., 2022; Liu *et al*., 2021)
2.	Synthetic polymers	Polyvinyl alcohol (PVA), polydimethylsiloxane (PDMS), poly (lactic acid) (PLA), poly (caprolactone) (PCL), poly(3-hydroxybutyric acid) (PHB), poly (lactic-co-glycolic acid) (PLGA), Polyhydroxy alkanoates PHA), polybutylene succinate PBS), polyuraethane (PU), poly(acrylic acid) (PAA), thermoplastic starch (TPS), poly(butylene adipate-co-terephthalate) (PBAT) *etc.*	Insulators, biodegradable and/or biocompatible	(Barron & Sparks, 2020) (Gan *et al*., 2004; Han *et al*., 2022; Sirisinha & Somboon, 2011)
3.	Synthetic and thermosetting polymers	Poly (glycerol sebacate) (PGS), poly (octamethylene maleate citrate) (POMaC) *etc*.	Insulators, Covalent crosslinking structure, difficulties in processing	(Guo *et al*., 2021)

Smart and intelligent materials can be prepared using biodegradable polymers (B. Kumar *et al*., 2012). Natural and synthetic biodegradable polymers and their major characteristics are summarized in **Table 3.**

There are varieties of natural sources of degradable polymers as listed in **Table 3**, however, natural sources based polymers perform poor mechanical and processing properties (Li *et al*., 2015). Aliphatic polyesters are biodegradable polymers which are more susceptible to hydrolysis and thermal degradation and perform poor mechanical performance. E.g. poly(lactic acid) (PLA), poly(butylene terephthalate) (PBT), poly(3-hydroxy butyrate) (PHB), poly(butylene succinate) etc (Chivrac *et al*., 2006; Iuliano *et al*., 2020; Rzepna *et al.*, 2018). Similarly, there are aliphatic-aromatic copolyesters which are synthetic copolymers comprising both aliphatic and aromatic segments. They are prepared by introducing the corresponding aromatic unit into aliphatic unit. Resulting aromatic-aliphatic copolyesters, thus, possess the combined properties of both aliphatic and aromatic polyesters. The aromatic groups always have better thermal and mechanical properties. Hence, the combination of aromatic and aliphatic units in a same backbone of a polyester improves the physical properties of copolyesters keeping

their biodegradability (Chivrac *et al.*, 2006; Cranston *et al.*, 2003; Fukushima *et al.*, 2012; Gan *et al.*, 2004; Rzepna *et al.*, 2018). Cost effective random copolymers can be prepared by this approach whose physical properties can be tuned varying the molar fraction of aromatic and/or aliphatic units (Gan *et al.*, 2004). Biodegradability of the copolyesters depends on the content of aliphatic part whereas physical and thermal properties depend on aromatic part (Chivrac *et al.*, 2006). Poly(butylene adipate-*co*-terephthalate (PBAT), poly(hydroxyl butyrate-*co*-valerate) (PHBV) etc. are aromatic-*co*-aliphatic copolyesters in which aromatic and aliphatic units are arranged in an alternate manner (Fukushima *et al.*, 2012; Mochane *et al.*, 2020; Pokhrel *et al.*, 2021; Rzepna *et al.*, 2018; Zhang *et al.*, 2019).

PBAT is a 100% degradable and biocompatible aromatic-aliphatic copolyester which undergoes both enzymatic and hydrolytic degradation (Ferreira *et al.*, 2019). It performs better physical properties than most of other degradable polymers due to which it finds applications in diverse fields like packaging materials, biomedical devices, electronics and sensors etc. (Pinheiro *et al.*, 2017). Degradation process of PBAT is comparatively, a long process (~4 months) which is due to the presence of aromatic ring. However, it can be tuned by the variation of molar ratio of aliphatic and aromatic parts of PBAT molecule.

Natural fillers and polymers based PBAT composites and blends possess a higher degradation rate (Ferreira *et al.*, 2019; González Seligra *et al.*, 2016; Rzepna *et al.*, 2018). **Figure 11** presents the soil burial test of biodegradability of PBAT, PBAT/PLA blends and PLA for 4 months.
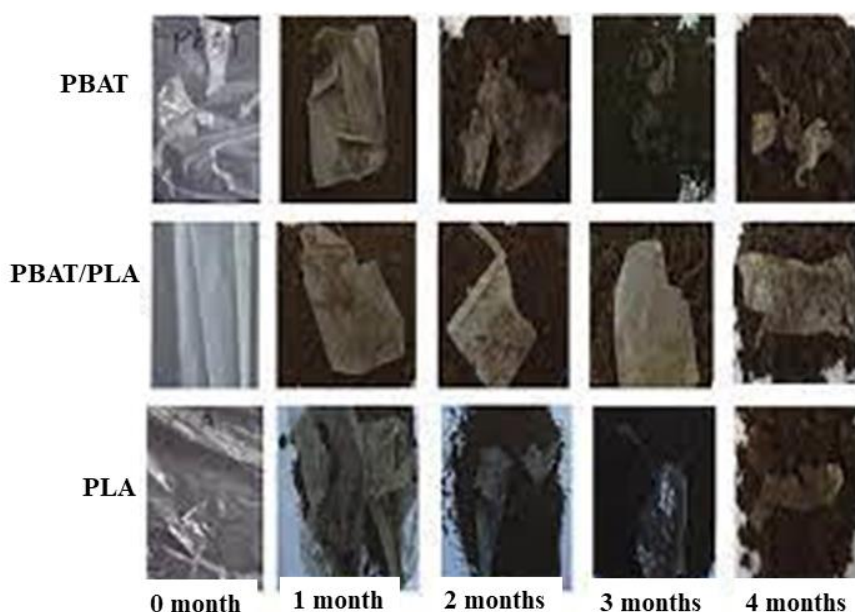
Figure 11: Soil burial test of biodegradability of PBAT, PBAT/PLA blends and PLA (Weng *et al*., 2013)

CNT are the highly preferred nano-fillers to prepare flexible and stretchable CPC than metal particles as well as other carbon fillers. It is because of their high availability, low density, flexibility and outstanding mechanical, electrical, and thermal properties. MWCNT also contribute to improve the flexibility of the nanocomposites to which they are incorporated because of their own flexibility and elasticity (Qazi *et al*., 2020). In this way, PBAT and PBAT/PLA blends will best pair up with MWCNT to prepare biodegradable, flexible and stretchable CPC.

It seems that both problems of plastic waste management as well as electronic waste (e-waste) are prevalent these days. Commercially available biodegradable polymers like PLA, PBAT and their blends have not been researched in the direction of their applications in degradable electronics and sensors. They are mostly used to prepare the packaging materials. On the other hand, flexible electronics and sensors are mostly fabricated using non-degradable synthetic and petroleum based polymers. There is a research gap to use biodegradable polymers to fabricate flexible and degradable electronics. In this way, study of feasibility of using degradable polymers to prepare eco-friendly electronics and sensors and the promotion of these materials should be the future direction of research.

CHAPTER 3

3. MATERIALS AND METHODS

The starting materials i.e. polymer matrix and conductive nanofillers used for the fabrication of nanocomposites and their structure and physical properties will be discussed in this chapter. Moreover, the scheme, procedure and the conditions of sample preparation will be summarized. Similarly, characterization techniques, instrumental detail, calibration and the conditions for the measurements will be discussed in this chapter.

3.1. Materials

3.1.1. Poly(butylene adipate-co-terephthalate) (PBAT)

Poly(butylene adipate-co-terephthalate), a commercial product of BASF, Germany with the trade name 'Ecoflex FBX7011' was used in this work as a polymer matrix. It is an aromatic-aliphatic copolyester whose most of the physical properties resemble to that of low density polyethylene (PE-LD). It is composed of BA and BT units comprising 44 and 56 mole-% of a PBAT molecule, respectively. PBAT is a copolymer of BA and BT units due to which, it is also represented as P(BA-*co*-BT). Presence of aliphatic unit in PBAT makes it biodegradable, while aromatic units in the same copolymer imparts novel and high performance properties. The structure of PBAT is presented in **Figure 12** where x and y are the degrees of polymerization of polyester of dimethyl terephthalate and polyester of adipic acid, respectively.
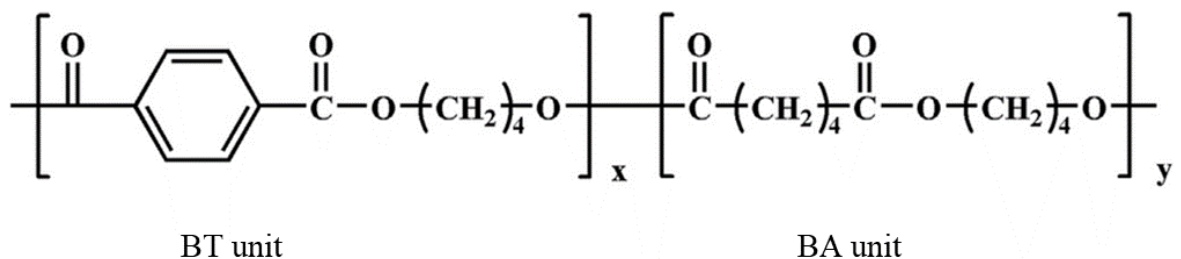
Figure 12: Chemical structure of PBAT (González Seligra *et al*., 2016; Jian *et al*., 2020).

Biodegradability of PBAT makes it deserving candidate for replacing the traditional commodity plastics and the corresponding materials to address the existing global environmental and waste management problems. Biodegradability, high elongation at break, flexibility, water and heat resistance of PBAT are the motivational factors to use

it as a polymer matrix in this research work. Physical properties of PBAT according to data sheet are presented in **Table 4**.

Table 4: Physical properties of PBAT according to the data sheet

Properties	Values
Molecular weight (M_w)	150,000 g/mole
Melting point (T_m)	120 °C
Glass transition temperature (T_g)	-30 °C
Density	1.27 g/cc
Melt flow	4.9 g/10 minutes

3.1.2. Multiwalled carbon nanotubes (MWCNT)

MWCNT, Nanocyl NC7000^{TM} from Nanocyl S.A., Belgium were used as conductive nanofillers. MWCNT is preferred as a conductive nanofillers because of their high aspect ratio, good mechanical properties, high thermal stability and electrical conductivity, and low density. Physical properties (from datasheet) of MWCNT used in this work are presented in **Table 5.**

Table 5: Physical properties of MWCNT according to the data sheet

Properties	Values
Diameter (average)	9.5 nm
Length (average)	1.5 µm
Purity	90 %

3.2. Methods of Sample Preparation

Solution casting and melt-mixing are commonly used methods in the fabrication   of polymer/CNT composites. In this work, melt-mixing followed by compression moulding methods were employed to fabricate the PBAT/MWCNT nanocomposites and prepare the composite plates, respectively. Melt-mixing is a cost effective and, solvents and chemicals free method, commonly employed to prepare polymers/CNT composites in industrial scale (Ke *et al.*, 2012). This method is suitable to prepare polymers/CNT composites with higher concentration of CNT (beyond percolation threshold) in comparison to solution casting method. Comparatively low CNT-aggregation and a good matrix-filler interfacial adhesion can be achieved by this method which provide enhanced tensile mechanical properties to the composite materials. Cavitation and voids formation in the composites at higher filler

concentration occur during solvent removal procedure of solvent casting methods. These limitations can be overcome adopting the non-toxic and environment friendly melt-mixing method to prepare electrically conductive polymer/CNT nanocomposites (Bhawal *et al.*, 2019; Ke *et al.*, 2012).

The processes of melt-mixing and compression moulding to prepare PBAT/MWCNT nanocomposites are illustrated in **Figure 13a** and **13b,** respectively.

a.
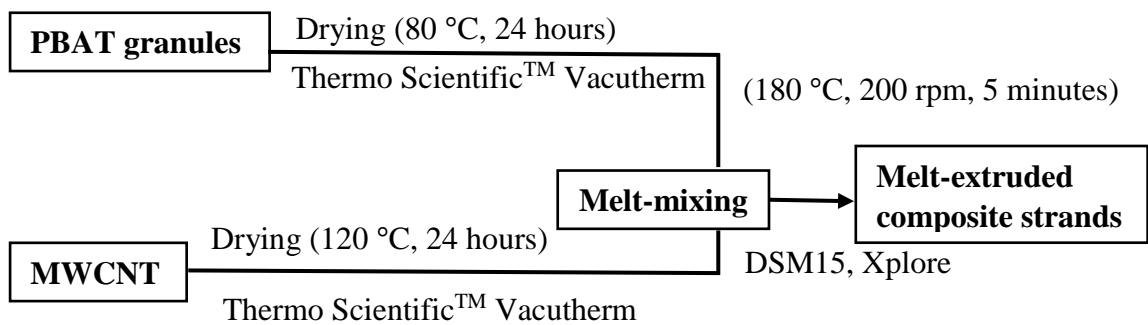
b.
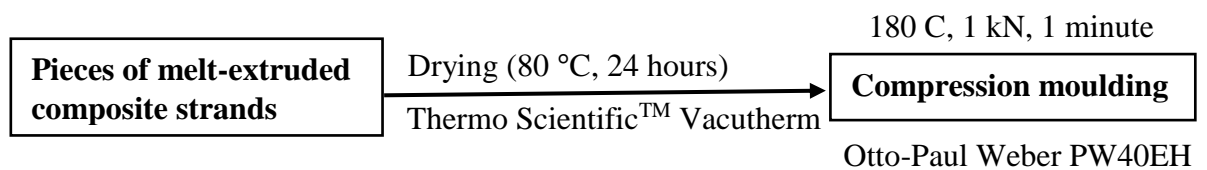
Figure 13: Illustration of (a) melt-mixing and (b) compression moulding for the preparation of PBAT/MWCNT nanocomposites

The granules of PBAT were dried (at 80 °C) using vacuum oven (Thermo Scientific™ Vacutherm, Thermo Fisher Scientific Inc.). Melt-mixing of polymer with MWCNT was carried out using DSM15 (Xplore Instruments BV, Sittard, The Netherlands) a twin-screw micro compounder while, compression moulding was carried out by PW40EH hot press (Otto-Paul-Weber GmbH, Remshalden, Germany).

3.3. Measurement Techniques

3.3.1. Microscopic Techniques

Transmission light microscopy (TLM), scanning electron microscopy (SEM), and transmission electron microscopy (TEM) were used to investigate the fillers agglomeration, morphology (surface), and the dispersion of fillers throughout the polymer matrix and composite microstructure, respectively. These characterization were conducted at Leibniz-Institut für Polymerforschung (IPF) Dresden e.V., Germany.

Transmission light microscopy (TLM): BH2 microscope in combination with DP71 camera (Olympus Deutschland GmbH, Germany) in transmission light mode was used for TLM. A thin section (5 μm thick, -30 °C, liquid N_2) of PBAT/MWCNT nanocomposites cut from the melt extruded strand using RM2265 microtome (Leica Mikrosysteme Vertrieb GmbH, Bensheim, Germany) was taken for this investigation.

Scanning Electron microscopy (SEM): A scanning electron microscope (Ultra plus microscope, Carl Zeiss GmbH, Germany) was used to investigate the surface morphology of fractured (cryo) surfaces of PBAT/MWCNT nanocomposites. The sample specimens, prepared by breaking the composites (in liquid nitrogen) and sputter coating their fractured surfaces with platinum thin film (~80 nm) were used. Furthermore, another set of composite samples were characterized using next scanning electron microscope (Carl Zeiss Ultra plus microscope in combination with a SE2 detector) with the voltage of 3 kV. The strands of melt-extruded composites were cryo-fractured (in liquid nitrogen) and the surfaces were sputter-coated with platinum (thickness: 30 nm).

Transmission Electron microscopy (TEM): Filler dispersion and the nanocomposites microstructures were investigated by transmission electron microscopy using TEM, LIBRA-120, Carl-Zeiss GmbH, Oberkochen, Germany, a transmission electron microscope with acceleration voltage of 120 kV. Ultra-thin sections (thickness: ~50 nm) of nanocomposites, cut using an ultra-microtome (at –100 °C) were used for this investigation. Another set of composites were investigated using TEM LIBRA-200MC (Carl-Zeiss, Oberkochen, Germany), a TEM microscope. Thin sections (thickness: 60 nm) of the composites were cut using an ultramicrotome EM UB6/FC6 (Leica, Austria) at -160 °C and the sectioning speed of 2 mm/s. Carbon filmed Cu-grids were used the sectioning in DMSO medium.

3.3.2. Spectroscopic Technique

Fourier transform infrared (FTIR) spectroscopy was employed to investigate the structure of PBAT/MWCNT nanocomposites. FTIR spectra of nanocomposites and polymer matrix were measured in the wavenumber range of 4000-500 cm^{-1} with the resolution of 10 cm^{-1} in attenuated total reflectance (ATR) mode of a FTIR-2000 spectrometer with diamond crystal (Perkin Elmer). FTIR spectra were measured at Polymer Service GmbH Merseburg (PSM), Germany.

3.3.3. Tensile Test

Tensile mechanical test was performed to investigate the deformation behavior of PBAT/MWCNT nanocomposites. Zwick/Roell 1456 tensile machine (ZwickRoell GmbH & Co. KG, Ulm, Germany) located at Leibniz-Institut für Polymerforschung (IPF) Dresden e.V., Germany was used to investigate stress–strain behavior of PBAT/MWCNT nanocomposites and neat PBAT. Five different compression moulded plate specimens (dog bone-shaped, length: 50 mm thickness: 0.5 mm, length and width of parallel parts: 12 and 2 mm) of each type of nanocomposites were measured and the mean values are reported. Tensile speed of 1 mm/minute (at low-strain range) and 50 mm/minute (at high-strain range) at 23 °C were employed for these measurements.

3.3.4. Microhardness Measurements

Microindentation test was performed to assess the deformation behaviour of nanocomposites under the influence of low load (up to 300 mN). Microhardness of the nanocomposites was measured at Polymer Service GmbH, Merseburg, Germany using Fischerscope H100C microhardness tester with a Vickers diamond indenter (pyramidal) (Helmut Fischer GmbH, Sindelfingen, Germany). Compression moulded plate specimens (1×1 cm^2 and 0.5 mm thick) were used for indentation to make the measurements of loads (F) *versus* indentation depth (h). Five different measurements were taken by the indentation at different positions of the specimens applying a force of 300 mN at the rate of 15 mN/second in each loading and unloading cycles at 23 °C. Average parameters of surface hardness i.e. Martens hardness (HM), indentation modulus (E_{IT}), maximum indentation depth (h_{max}) and work of deformation were calculated from the measured data. Different parameters of the work of deformation i.e. elastic and plastic work of deformation (W_e and W_p), total work of deformation ($W_t = W_e + W_p$) and the work ratio (W_e/ W_p) were calculated.

3.3.5. Electrical Measurements

Electrical volume resistivity and piezoresistivity of the nanocomposites were measured also at Leibniz-Institut für Polymerforschung (IPF) Dresden e.V., Dresden, Germany.

Volume Resistivity: An electrometer, Keithley E6517A (Keithley Instruments, Solon, USA) in combination with Keithley 8009 (Keithley Instruments, Solon, USA) was used to measure the volume resistivity $>10^7$ Ω·cm. Similarly, the same electrometer, in combination with a 4-point test fixture (with 1 cm apart gold electrodes and 1.6 cm apart source electrodes) was used to measure the volume resistivity $<10^7$ Ω·cm. Compression moulded plates of composite (in case of highly resistive samples) and dumbbell specimens (ISO 527-2 standard, type S3), cut from compression moulded plates (in case of conductive samples) were taken for this measurement.

Piezoresistivity: An instrumental set of an electrometer, Keithley DMM2001 (Keithley Instruments, Solon, USA) measuring the maximum resistance of 20 GΩ in combination with a tensile machine (Zwick/Roell 1456, ZwickRoell GmbH & Co. KG, Ulm, Germany) applying the maximum strain of 300% and the force of 1 kN was used to measure the piezoresistivity of electrically conductive composite samples (ISO 527-2, S3 type, dumbbell specimens) at 23 °C and 50% humidity. The specimens were stretched at a tensile speed of 0.5 mm/minute and the change in electrical resistance was measured simultaneously until the sample rupture. Relative resistance change ($\Delta R/R_0$) of the composite samples was calculated using **equation (6).**

$$\frac{\Delta R}{R_0} = \frac{R - R_0}{R_0} \tag{6}$$

where, ΔR = resistance change*,*

$\qquad R$ = resistance of specimen at a certain strain

$\qquad R_0$ = resistance of specimen at zero strain.

Cyclic Strain Test: Same set of tensile machine and electrometer used in the measurement of piezoresistivity was used to conduct cyclic strain test. Dumbell specimens (ISO 527-2 standard, type S3), fixed at the two clamps of tensile machine were stretched (speed: 0.5 mm/minute) with strain applied (1 to 10 %, 3 loading cycles in each strain) in increasing manner. Similarly, another set of test specimens were carried out their cyclic strain test with a fixed strain (7%) and 15 loading cycles. The specimens were allowed to relax for 90 seconds after each loading and unloading cycle in this test.

3.3.6. Electron Beam (EB) Irradiation

The compression-moulded composite plates were irradiated with electron beam (EB) for crosslinking using ELV-2 electron accelerator (energy: 1.0 MeV, current: 4 mA, Budker Institute of Nuclear Physics, Novosibirsk, Russia) at a dose rate of 12.5 kGy per irradiation at room temperature. Mass of gel content, formed in the polymer (by the irradiation) was taken into account to determine the degree of crosslinking. Degree of crosslinking was calculated using **equation (7)**.

$$Degree\ of\ crosslinking\ (\%) = \left(\frac{w_1}{w_2}\right) \times 100\ \% \qquad (7)$$

where, w_1 = weight of gel formed, w_2 = total weight of the irradiated sample.

3.3.7. Thermal Techniques

Thermogarvimetric analysis (TGA) and differential scanning calorimetry (DSC) of the nanocomposites were performed to analyze their thermal stability and crystallization behavior, respectively. TGA was carried out at Leibniz-Institut für Polymerforschung (IPF) Dresden e.V., Dresden, Germany while DSC was conducted at Leibniz-Institut für Polymerforschung (IPF) Dresden e.V., Dresden, Germany and Polymer Service GmbH Merseburg (PSM), Germany. TGA measurements of polymer matrix and that of nanocomposites were conducted using TGA Q 5000 (TA instruments) with standard aluminium pans. The experiment was run at the heating rate of 10 °C min^{-1} (range of temperature: room temperature (RT) to 800 °C, N_2-atmosphere), and mass flow rate of 100 and 50 mL min^{-1} before and after equilibration, respectively (at 35 °C, isothermal for 10 minutes). Similarly, DSC measurements of neat PBAT and PBAT/MWCNT nanocomposites were carried out using a DSC 2500 calorimeter (TA instruments) with standard aluminium pans. Heating-cooling-heating scans were performed under N_2-atmosphere ~6.0 mg of the sample was heated from –120 °C to 180 °C, then cooled to -120 °C and again heated to 180 °C at the rate of 10 °C/minute. Glass transition temperature (T_g), crystallization temperature (T_c), melting temperature (T_m), enthalpy of crystallization (ΔH_c) and enthalpy of melting (ΔH_m) were calculated from the measured data. Degree of crystallization was calculated using **equation (8)**.

$$\chi_c = \frac{\Delta H_m}{f \times \Delta H_m^{\infty}} \times 100\ \% \qquad (8)$$

where, χ_c = degree of crystallization (%), ΔH_m = enthalpy of melting, f = weight ratio of PBAT in the composites ΔH_m^{∞} = enthalpy of melting for the crystal with infinite thickness = 114 J/g (adapted from literature) (Giri *et al*., 2021; Mohanty & Nayak, 2009).

CHAPTER 4

4. RESULTS AND DISCUSSION

Results of deformation behavior of the nanocomposites, correlated with their piezoresistivity leading to the strain sensing behavior are discussed in this chapter. Similarly, structure and morphology of fabricated materials are analyzed employing spectroscopic and microscopic techniques. Additionally, results of thermal stability and crystallization behavior of the nanocomposites, evaluated by thermogravimetric analysis (TGA) and differential scanning calorimetry (DSC), respectively are presented. Electron beam irradiation induced crosslinking of polymer matrix and its effect on deformation behavior, strain sensing behavior, thermal stability, and crystallization behavior of the nanocomposites will also be discussed.

4.1. Morphologies and Structure of Nanocomposites

Dispersion of MWCNT throughout the polymer matrix and their agglomeration determine the morphology and the microstructures of nanocomposites. They ultimately affect the electrical, mechanical and thermal properties of nanocomposites. Similarly, mode of matrix-filler interaction and their structure also determines the properties of the nanocomposites. Therefore, morphologies and the structure of nanocomposites will be discussed in this chapter. Macrodispersion of MWCNT in the nanocomposites will be analysed by transmission light microscopy (TLM). CNT agglomeration and the dispersion of the agglomerates will also be assessed by TLM. Agglomerate size will be evaluated taking agglomerate area ratio (A/A_0) into account. Surface morphology of nanocomposites are investigated by scanning electron microscopy (SEM) whereas microdispersion of MWCNT, their agglomeration and orientation are assessed by transmission electron microscopy (TEM). Furthermore, structure of PBAT/MWCNT nanocomposites are investigated by Fourier transform infrared (FTIR) spectroscopy.

4.1.1. Transmission Light Microscopic Investigation

Transmission light micrographs of PBAT/MWCNT nanocomposites, taken to assess the macrodispersion of the filler particles are presented in **Figure 14.** TLM micrographs suggest a random distribution of CNT-aggregates throughout the polymer matrix. These agglomerates increase with increasing CNT concentration in the composites because of strong Van der Waals force of attraction between MWCNT particles. As the nanocomposites, prepared by melt-mixing are used which are relaxed during

compression moulding, the agglomerates formed during melt-mixing are relaxed during compression moulding. Agglomerate area ratio (A/A_0) of nanocomposites with different CNT concentration were calculated from TLM micrographs and analyzed comparatively whose values are depicted in the corresponding micrographs. This value of the nanocomposites increases from 0.27 to 1.26 % with 0.5 to 2 wt.-% of MWCNT, respectively. TLM investigation of the nanocomposites containing 3 wt.-% MWCNT and higher concentration could not be carried out in this experiment because high CNT content hampers the transmission of light through them (Rodrigues *et al.*, 2016).
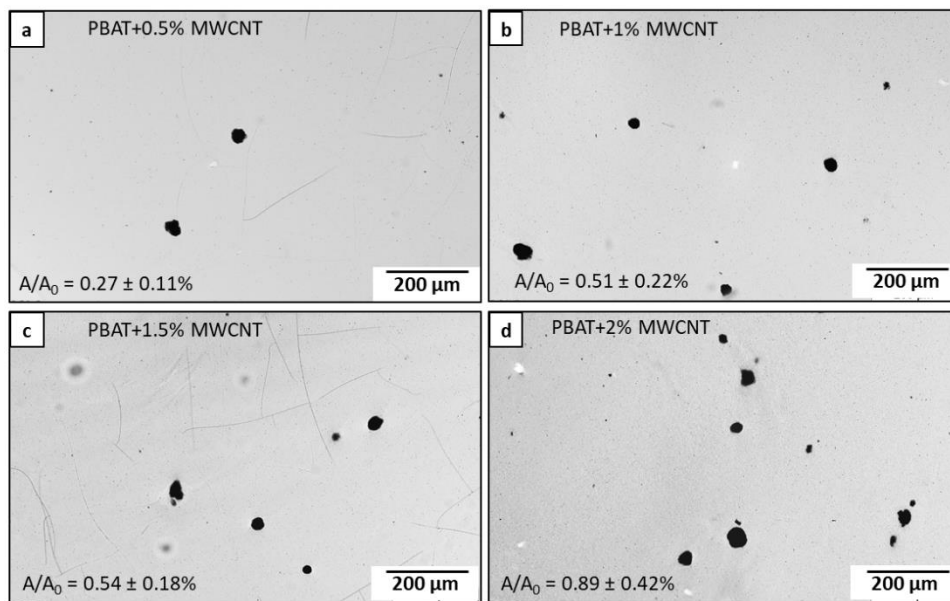
Figure 14: Transmission light micrographs of PBAT/MWCNT nanocomposites

A quite low agglomeration rate can be deduced from *A/A_0* values calculated in this work are quite low in comparison to that reported in the literature. Staudinger *et al.* has reported *A/A_0* value of 0.68% in styrene-butadiene triblock copolymer/1% MWCNT nanocomposites which were prepared by melt-mixing under same conditions (c). Moreover, it is implied by TLM images that number of agglomerates is quite low (compared to that reported in literature) regardless their size (Staudinger *et al.*, 2019, 2020). It is further implied that CNT-agglomerates are also uniformly distributed which compensate (to some extent) the descent of mechanical properties of the nanocomposites due to filler agglomeration.

4.1.2. Morphological Studies

Scanning electron micrographs of PBAT/MWCNT nanocomposites, used to analyze their surface morphology are presented in **Figure 15** and **16**. Morphology of stained thin sections and that of cryo-fractured surface were investigated by SEM as presented in **Figure 15** and **16**, respectively.
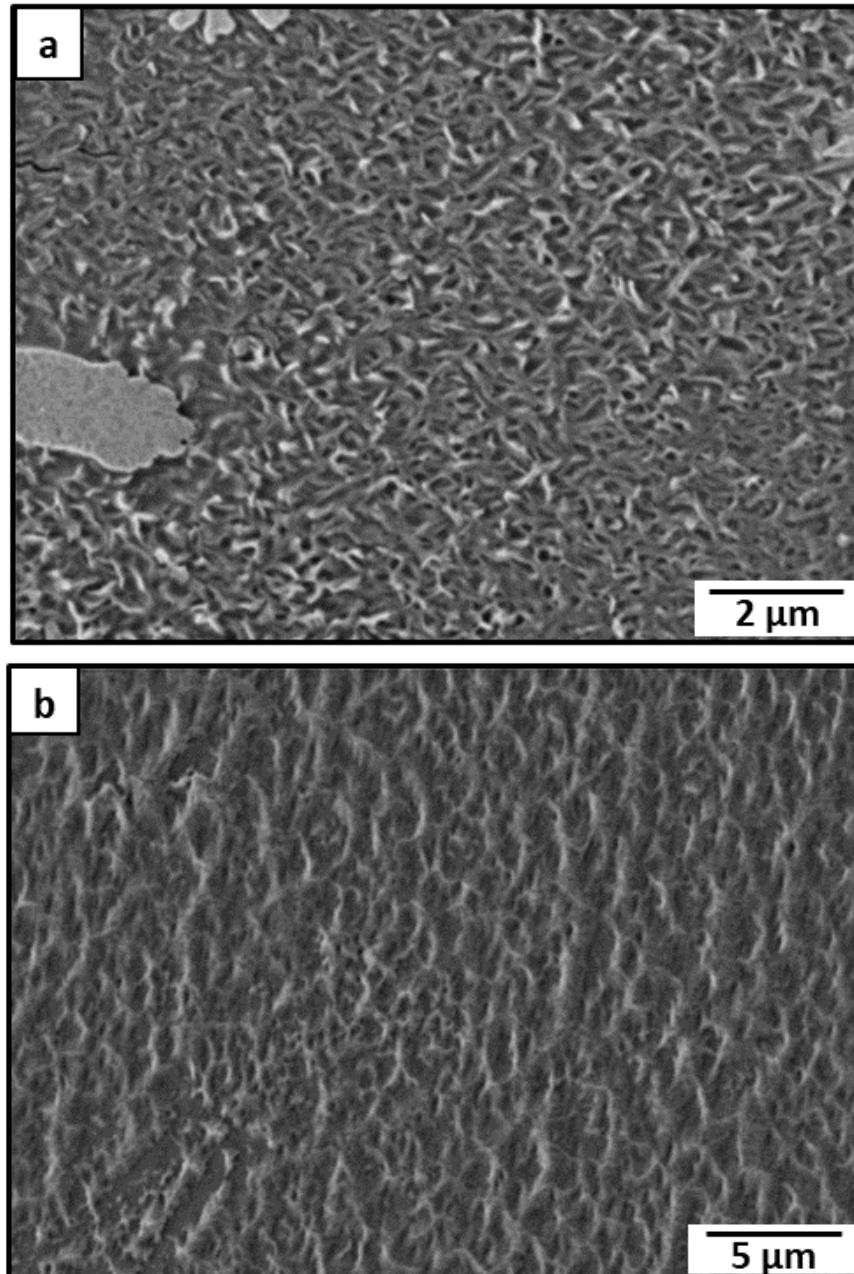
Figure 15: SEM micrographs of stained thin section of PBAT/1% MWCNT nanocomposites under different magnification
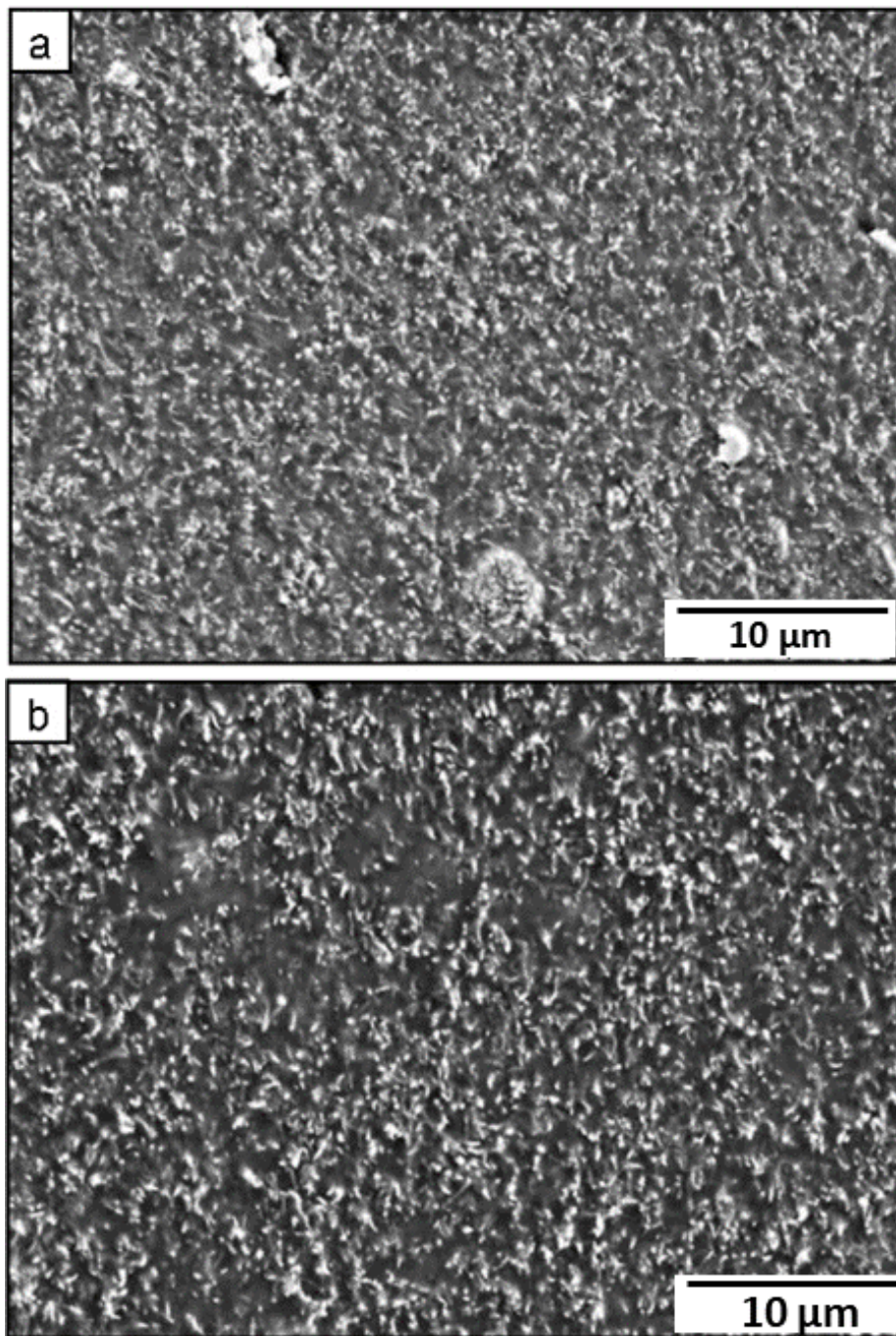
Figure 16: SEM micrographs of cryo-fractured PBAT/MWCNT nanocomposites with different filler content: (a) 3 wt.-% MWCNT and (b) 10 wt.-% MWCNT

A clear net-like entangled and interconnected CNT-network throughout the surface of PBAT/MWCNT nanocomposites is suggested by these micrographs (clear at higher magnification). It is developed by the homogeneous dispersion of MWCNT through the matrix. SEM micrographs of cryo-fractured surface of the nanocomposites with higher MWCNT content (3 and 10 wt.-%) are presented in **Figure 16**. They imply the similar surface morphology of nanocomposites as discussed before, however, higher

surface roughness and progressively developed ductile-to-brittle morphology can be inferred from these micrographs. No CNT-agglomerates are visible on the surface of the nanocomposites. Filler aggregation, network density and the microstructure of nanocomposites as a function of filler content are hardly detectable from these images for which transmission electron microscopy (TEM) was employed.

TEM micrographs of a thin section of PBAT/MWCNT nanocomposites are presented in **Figure 17**. The micrographs suggest a uniform distribution of CNT particles in PBAT with partial CNT-agglomeration which are encircled in the images. The CNT-flocs can be observed rather than the individually distributed CNT particles. The CNT-agglomeration is attributed to the strong van der Waals force of attraction between CNT particles. Comparative analyses of TEM images in **Figure 17 (a** and **c)** and **(b** and **d)** reveal the higher agglomeration with increasing CNT content which is also implied by TLM images and the corresponding A/A_0 values.
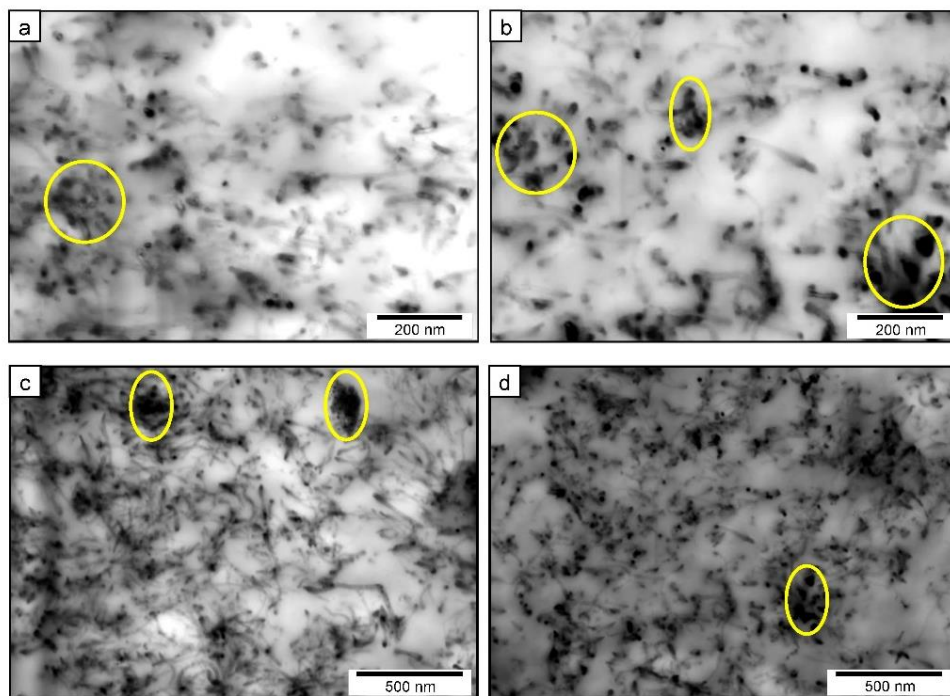
Figure 17: TEM micrographs of cryo-fractured PBAT/MWCNT nanocomposites with different filler content under different magnification: (a, c) 3 wt.-% MWCNT and (b, d) 10 wt.-% MWCNT

TEM images of PBAT/3% MWCNT nanocomposites under high magnification is presented in **Figure 18.** It clearly shows the evenly embedded individual carbon nanotubes in the polymer matrix, connected to each other forming an interconnected CNT-CNT network with minor aggregates (encircled). Agglomerates with clustered hair-like structure are formed by the aggregation of a number of individual tubes which

are encircled in the image. Carbon nanotubes, embedded in PBAT seem like fibers because of their higher length (1.5 µm) and small diameter (9.5 nm). Similar results of morphology and microstructure of PBAT/MWCNT nanocomposites have been reported in the literature (Dil *et al.*, 2020; Ding *et al.*, 2016; Hong *et al.*, 2012; Rodrigues *et al.*, 2016).
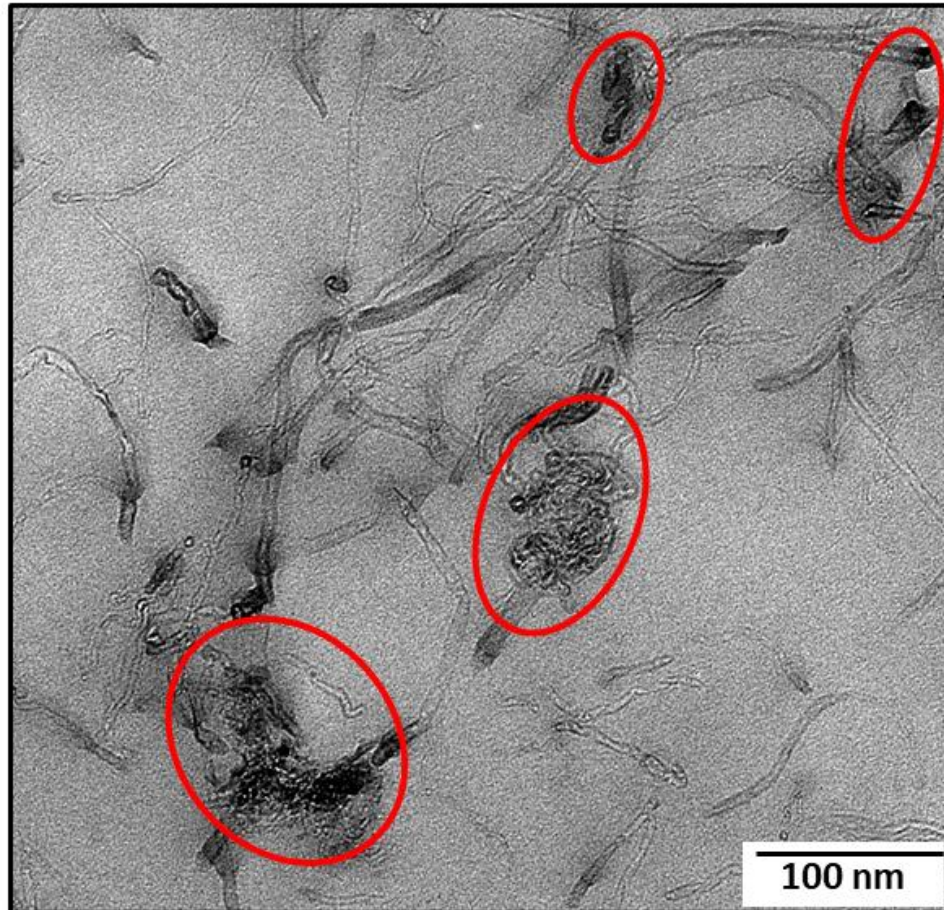
Figure 18: TEM micrograph of PBAT/3 wt.-% MWCNT nanocomposites at higher magnification

Homogeneous fillers-network of entangled and interconnected MWCNT with partial CNT-agglomerates can be inferred from the morphology suggested by TEM micrographs. It is ascribed to the flexibility of PBAT chains and the aromatic ring present in PBAT, leading to a good interfacial matrix-filler interaction (Ko *et al.*, 2009). CNT-agglomerates too are uniformly distributed by which deterioration of mechanical properties of nanocomposites is compensated to some extent. The agglomerates also contribute to the electrical conductivity of nanocomposites although they cause somewhat higher percolation threshold. However, only a limited part of a TEM micrographs may not inform completely about the MWCNT distribution and the formation of CNT-network throughout the sample. Results of volume resistivity of the

nanocomposites are taken as an indirect method to correlate the dispersion level of MWCNT which are discussed in section 4.3.1.

4.1.3. Structural Characterization

Chemical structure of PBAT/MWCNT nanocomposites were investigated by FTIR spectroscopy in comparison to that of neat PBAT. Chemical bonding between matrix and fillers, development of any new bands and peaks as well as peak-shifts in the FTIR spectra of nanocomposites in comparison to that of neat PBAT were investigated. Melt processed PBAT and PBAT/MWCNT composites with the filler concentration 0.5, 1, 3, 6 and 10 wt.-% were taken for this measurement whose FTIR spectra are presented in **Figure 19**.
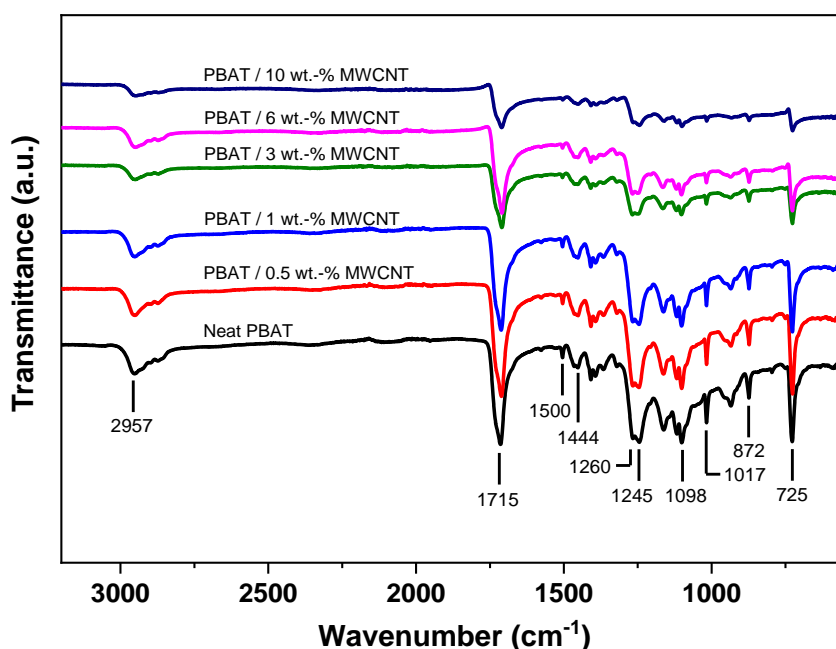
Figure 19: FTIR spectra of neat PBAT and PBAT/MWCNT nanocomposites

The significance of major peaks appeared in FTIR spectra of PBAT-neat and PBAT/MWCNT nanocomposites are mentioned in **Table 6**.

Table 6: Major peaks of functional groups of neat PBAT and PBAT/MWCNT nanocomposites with their significance

Wavenumber(cm^{-1})	Significance	Reference
724	-C-H$_2$ stretching	(Al-Itry *et al.*, 2015; Giri *et al.*, 2021; Pokhrel *et al.*, 2016; Siyamak *et al.*, 2012)
1444	-C-H$_3$ bending	(Al-Itry *et al.*, 2015; Giri *et al.*, 2021; Pokhrel *et al.*, 2016), Sirisinha *et al.*, 2012)
1715	C-O stretching (ester linkage)	(Sirisinha *et al.*, 2012; Pokhrel *et al.*, 2016; Al-Itry *et al.*, 2015; Giri *et al.*, 2021; Rodrigues *et al.*, 2016)
1260	C=O (ester linkage)	(Al-Itry *et al.*, 2015; Giri *et al.*, 2021)
2957	asymmetric -C-H stretching	(Sirisinha *et al.*, 2012; Al-Itry *et al.*, 2015; Rodrigues *et al.*, 2016)
1500	phenylene group (aromatic ring)	(Giri *et al.*, 2021; Rodrigues *et al.*, 2016; Siyamak *et al.*, 2012)

A close and comparative analysis of the FTIR spectra of neat PBAT with that of PBAT/MWCNT nanocomposites reveals that no new bands were developed by the incorporation of MWCNT into PBAT. Similarly, no distinguished peak shift can be observed in any of the spectra which confirms that no chemical bonding between PBAT and CNT has occurred instead of which, a net physical matrix-filler interaction develops microstructures of PBAT/MWCNT nanocomposites. These results are found consistent with the results reported in literature (Rodrigues *et al.*, 2016).

4.1.4. Summary of Morphologies and Structure of Nanocomposites

➤ Homogeneous filler dispersion with partial agglomeration of MWCNT, and the entangled net-like MWCNT-network in the nanocomposites are deduced. It is further supported by the electron microscopic studies of the nanocomposites.

➤ A low CNT agglomeration is attested by the comparative analysis of *A/A₀* values with the reported values which is further supported by their electron microscopic studies.

➤ Development of no new bands as well as no significant peak shifts has occurred in FTIR spectra of PBAT/MWCNT nanocomposites in comparison to that of pure PBAT. It reveals a physical type of PBAT-CNT interfacial interaction and a physical binding force is responsible for the formation of the nanocomposite microstructures. Such a net physical interaction between MWCNT and PBAT will be beneficial to the piezoresistivity of the nanocomposites that will support the evaluation of their strain sensing behavior.

4.2. Deformation Behavior of Nanocomposites

Mechanical properties of polymeric nanomaterials play a pivotal role to find their suitability for practical applications. Load bearing capacity, ductility, fracture etc. determine the suitability of the materials in this regard. Tuned elasticity and flexibility of the nanocomposites are the major properties to be considered for strain sensing applications of polymer composites. Therefore, deformation behavior and micromechanical properties of PBAT-neat and PBAT/MWCNT nanocomposites are discussed in this chapter. Deformation behavior of nanocomposites was analysed by tensile mechanical test and their micromechanical properties were investigated by microindentation test. Tensile mechanical properties were evaluated taking tensile strength, tensile modulus and elongation at break, into account. Similarly, Martens hardness (HM), indentation depth (h_{max}), indentation modulus (E_{IT}), and works of deformation (elastic and plastic) recorded from microindentation test and their ratio were taken into account to analyse the microhardness of the materials.

4.2.1. Tensile Mechanical Properties

Tensile stress–strain behavior of PBAT-neat and PBAT/MWCNT nanocomposites (0.5, 1, 2, 3, 4, and 5 wt.-% of MWCNT) are presented in **Figure 20**. Similarly, the tensile data (tensile modulus, tensile strength and elongation at break) obtained from the tensile test of these samples are presented in **Table 7**. Stress-strain curves of nanocomposites presented here can be differentiated on the basis of the values of elongation at break, tensile strength, and their slopes in correlation with CNT concentration in the nanocomposites.

Neat PBAT and all of the composite samples seem ductile and tough in nature. Elongation at break of pure PBAT is more than 900% (showing a large plastic deformation) while that of the composites range in 159 – 500% based on the filler concentration. All of the PBAT/MWCNT nanocomposites presented here seem ductile in nature (Giri *et al*., 2021). Even the PBAT/10% MWCNT nanocomposites perform ductile nature which were prepared as another batch of samples in this work and the results are reported in Dhakal *et al*, 2022 (Dhakal *et al.*, 2022b). Such a ductility and the flexibility of PBAT/MWCNT nanocomposites are advantageous to their applications in a strain sensor.
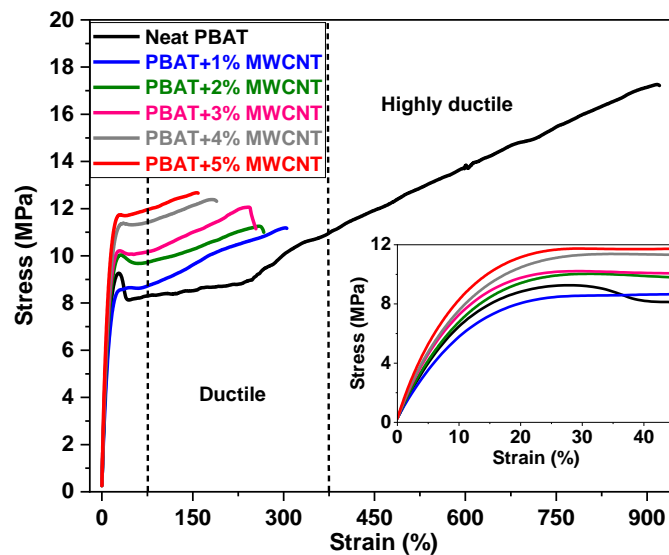
Figure 20: Tensile stress-strain curves of neat PBAT and PBAT/MWCNT nanocomposites with different filler content

The increasing slope of stress–strain curves (in low-strain level, in inset) with increasing MWCNT content implies the increasing elastic modulus of nanocomposites. Similarly, improved tensile stress and tensile modulus of the nanocomposites with increasing filler content is also implied by the stress-strain curves. Presence of MWCNT in polymers controls the chain mobility of polymers during deformation resulting in the higher tensile modulus (González Seligra *et al*., 2016). Increased tensile stress and tensile modulus imply the reinforcement of the nanocomposites and a matrix-to-fillers stress transfer by the presence of MWCNT (Yu & Li, 2014). Homogeneous CNT-distributiom, outstanding mechanical properties of MWCNT, low agglomeration rate and good PBAT-MWCNT interfacial interaction (physical) are responsible for the improved mechanical properties (Hong *et al*., 2012; Chiu *et al.*, 2013; Zhang *et al*., 2019; Pinheiro *et al*., 2017). Morphological and structural results of the nanocomposites can be correlated with their mechanical properties. Similarly, yield point of the nanocomposites, shifting to higher stress values at higher filler concentration corresponds to higher mechanical strength and the stiffness (Zhang *et al*., 2019). It suggests an increased strength of recovery of the nanocomposites from deformation (Ge *et al*., 2021). Meanwhile, yield point followed by necking is performed by the tensile stress strain curves of nanocomposites which also implies the ductile nature of the nanocomposites (Jalali Dil *et al*., 2016). It seems that PBAT/MWCNT nanocomposites have maintained their ductility even with high MWCNT content which

is found consistent with the results reported in literature (Urquijo *et al*., 2017). This is advantageous to the nanocomposites for their applications in strain sensing.

Table 7: Tensile mechanical properties of PBAT/MWCNT nanocomposites

Sample	σ (MPa)	Et (MPa)	ε_B (%)
Neat PBAT	83 ± 5.6	17 ± 0.8	920 ± 45
PBAT/0.5% MWCNT	79 ± 0.5	11 ± 0.2	508 ± 59
PBAT/1% MWCNT	75 ± 0.9	12 ± 2.1	376 ± 29
PBAT/2% MWCNT	92 ± 7.6	11 ± 0.8	267 ± 21
PBAT/3% MWCNT	107 ± 5.9	11 ± 1.5	254 ± 11
PBAT/4% MWCNT	112 ± 4.5	12 ± 0.6	189 ± 19
PBAT/5% MWCNT	125 ± 2.5	13 ± 0.8	159 ± 15.6

σ: Tensile modulus, Et: Tensile strength, ε_B: Elongation at break

From **Table 7**, decreasing performance of both tensile strength (*Et*) and strain at break (*ε_B*) with higher filler content of the nanocomposites can be observed in the high-strain range. A significant declination of elongation at break of nanocomposites when compared neat PBAT is implied by the stress-strain curves. Physical type of matrix-filler interaction to form the nanocomposites (as suggested by FTIR spectra) can be one of the reasons behind it (Ge *et al*., 2021). Similarly, declination of strain at break of nanocomposites with higher MWCNT content can be correlated to the increasing stiffness of the nanocomposites. Development of a ductile-to-stiff morphology (as suggested by SEM micrographs) can be ascribed to it. Partial CNT-agglomeration (as suggested by TEM and TLM micrographs) carried out by van der Waals force of attraction and the effect of non-wetting of fillers by matrix melts in higher filler concentration significantly affect the tensile mechanical properties of nanocomposites (Dhakal *et al*., 2022b). Similarly, formation of cracks and voids, their propagation and the premature rupture of the test specimens can occur in the nanocomposites at higher filler concentration hampering their mechanical performance (Giri *et al*., 2021; La Mantia *et al*., 2020; Chodák, *et al*., 2001). MWCNT, as a nanofiller used in this work is found to reinforce the PBAT/MWCNT nanocomposites largely if compared to that of other nanofillers in the similar works reported in literature (Giri *et al*., 2021; Pinheiro *et al*., 2017).

4.2.2. Micromechanical Behaviour

The same set of the nanocomposites (used for tensile test) were taken for the investigation of micromechanical behavior. Microindentation test of nanocomposites was carried out to investigate their micromechanical properties. Martens hardness (HM), indentation depth (h_{max}) and indentation modulus (E_{IT}) of nanocomposites, calculated from microindentation test were comparatively analysed as a function of increasing filler content. The values of HM are correlated with viscoelastic and viscoplastic properties of the nanocomposites in terms of maximum indentation depth (h_{max}), and elastic (W_e) and plastic work (W_p). W_e and W_p were calculated from F-h plots Variation of these micromechanical parameters of pure PBAT and PBAT/MWCNT nanocomposites are presented in **Figure 21**.
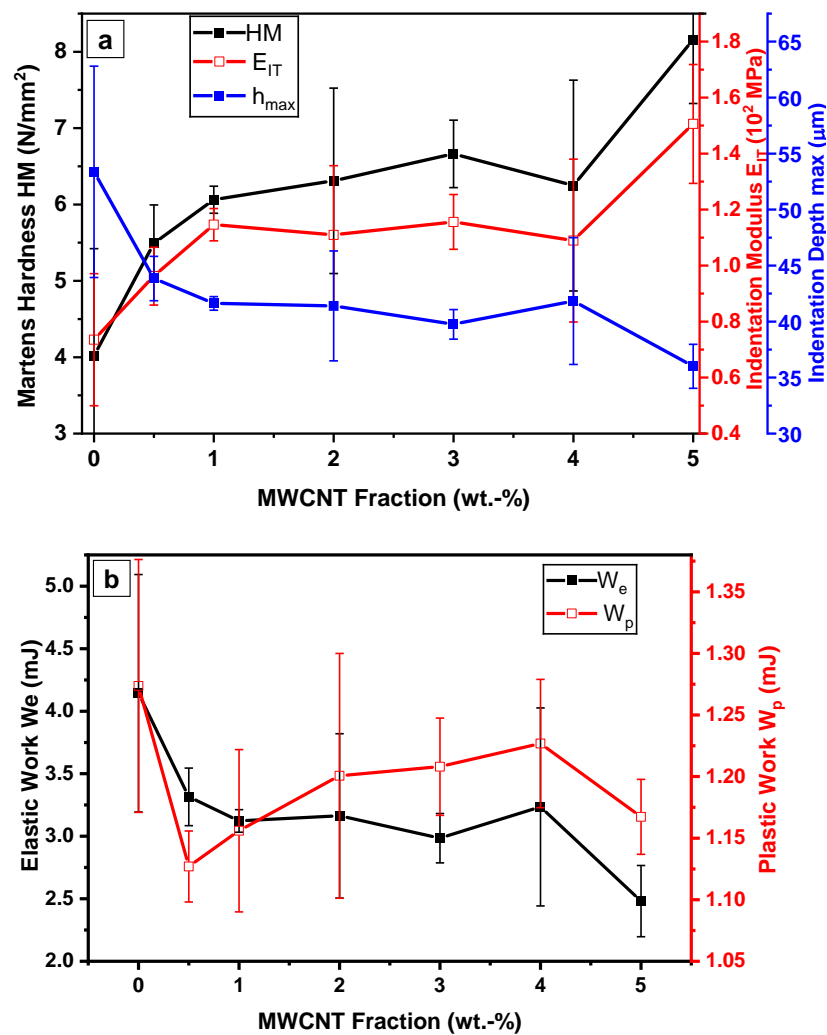
Figure 21: (a) Martens hardness (HM), indentation modulus (E_{IT}) and indentation depth (h_{max}) and (b) work done by elastic deformation (W_e) and plastic deformation (W_p) of PBAT/MWCNT nanocomposites as a function of filler content.

Statistical values (including standard deviations) of *HM*, E_{IT} and h_{max}, are presented in **Table 8.** Similarly, values (including standard deviations) of elastic and plastic work of deformation, and their ratio are presented in **Table 9.**

Table 8: Micromechanical properties of neat PBAT and the PBAT/MWCNT nanocomposites

Sample	E_{IT} (MPa)	HM (N/mm^2)	h_{max} (µm)
PBAT-neat	73.53 ± 10.38	4.017 ± 1.40	53.37 ± 9.43
PBAT/0.5% MWCNT	96.23 ± 10.38	5.50 ± 0.50	43.85 ± 1.10
PBAT/1% MWCNT	114.61 ± 5.75	6.06 ± 0.18	41.62 ± 0.60
PBAT/2% MWCNT	110.95 ± 24.73	6.31 ± 1.21	41.39 ± 4.90
PBAT/3% MWCNT	115.59 ± 9.79	6.66 ± 0.44	39.75 ± 1.32
PBAT/4% MWCNT	108.94 ±29.09	6.25 ± 1.38	41.82 ± 5.66
PBAT/5% MWCNT	150.60 ± 21.22	8.16 ± 0.84	36.01 ± 1.95

HM: Martens hardness, E_{IT}: Indentation modulus, h_{max}: maximum indentation depth

Table 9: Elastic and plastic work (W_e and W_p) of deformation of neat PBAT and PBAT/MWCNT nanocomposites, and their ratio (W_e/W_p)

Sample	W_e (mJ)	W_p (mJ)	W_e/W_p
PBAT-neat	4.14 ± 0.95	1.27 ± 0.10	3.25
PBAT/0.5% MWCNT	3.31 ± 0.23	1.13 ± 0.03	2.94
PBAT/1% MWCNT	3.12 ± 0.09	1.16 ± 0.06	2.70
PBAT/2% MWCNT	3.16 ± 0.66	1.20 ± 0.09	2.63
PBAT/3% MWCNT	2.98 ± 0.19	1.20 ± 0.04	2.47
PBAT/4% MWCNT	3.23 ± 0.79	1.23 ± 0.05	2.64
PBAT/5% MWCNT	2.48 ± 0.28	1.17 ± 0.03	2.13

Mechanical reinforcement of the nanocomposites by MWCNT particles is revealed by the increasing trend of Martens hardness (*HM*) and indentation modulus (E_{IT}) and the decreasing trend of indentation depth (h_{max}) with higher filler concentration in the nanocomposites. These results also suggest the matrix-to-fillers stress transfer. These results are found consistent with increasing tensile strength (recorded by tensile test) in low strain-range. Moreover, decreasing trend of h_{max} refers to the increasing resistance of the materials towards elastic and plastic deformation. This behaviour of nanocomposites is also suggested by the results of tensile mechanical test.

Pure PBAT possess the lowest Martens hardness (~4 N/mm^2) and indentation modulus (~73 MPa), respectively. It exhibits a highest values of indentation depth (~53 µm). Similarly, PBAT/5 % MWCNT performs a minimum indentation depth (~36 µm) with

the maximum value of indentation modulus (~150 MPa). Martens hardness and indentation modulus values of nanocomposites continuously increase while that of $h_{\max}$ decreases with higher filler concentration suggesting the mechanical reinforcement of PBAT by MWCNT. Reinforcement of PBAT by MWCNT in PBAT/MWCNT nanocomposites in this work is found higher if compared that by microcellulose and nanocellulose reported in literature (Giri *et al*., 2021; Giri, 2020).

Trend of change of these parameters (*HM*, E_{IT} and h_{max}) of the nanocomposites is uniform except that of PBAT/4 % MWCNT nanocomposites. The alteration of the trend particularly in one type of materials only can be attributed to the possibility of formation of voids, cracks, uneven filler dispersion as well as the partial CNT non-wetting by polymer-melts (shortcomings during melt mixing). They can lead to the lower reinforcement of the nanocomposites by the filler particles. Filler concentration in nanocomposites determines the maximum indentation depth and indentation modulus values, while *HM* values depend on energy dissipation and composite microstructures. However, all three parameters at a time are in a different trend in comparison to that of other nanocomposites which are nearly equal to that of PBAT/2% MWCNT nanocomposites. Similarly, all of them follow a similar trend of alteration and possess higher and comparable values of standard deviations to each other. Thus, the possibilities of above mentioned shortcomings during material preparation are supported. Higher rate of agglomeration and uneven MWCNT distribution can also be predicted from the higher values of standard deviation of *HM*, E_{IT} and h_{max} of PBAT/2% MWCNT (also supported by TLM images and the corresponding values of A/A$_0$) and PBAT/4% MWCNT nanocomposites than other nanocomposites. In overall, the PBAT/MWCNT nanocomposites are reinforced by the presence of MWCNT regardless a particular case.

Table 9 shows that W_e and W_p are directly correlated to each other. Both W_e and W_p decrease continuously with increasing filler concentration. However, the different trend of PBAT/4% MWCNT nanocomposites is reflected in their values of W_e and W_p also. Progressive decrease in the ratio of work of deformation (W_e/W_p) with increase in MWCNT content implies the decreasing elastic deformation of nanocomposites and also the formation of micro-voids in them at higher MWCNT nanocomposites (Giri *et al*., 2021). These results are found consistent with increasing tensile modulus (in low-strain range) with higher MWCNT content as discussed in previous section.

4.2.3. Summary of Deformation Behavior

➢ A significant reinforcement of PBAT by MWCNT as nanofillers is implied by higher tensile strength and tensile modulus (in low strain range) recorded in the tensile test. It is further supported by higher Martens hardness, higher indentation modulus, and lower indentation depth of PBAT/MWCNT nanocomposites with increasing MWCNT content recorded by microindentation test.

➢ Decreasing trend of indentation depth (h_{max}) with higher filler content implies the increasing resistance of nanocomposites towards elastic/plastic deformation which is further supported by the increasing yield stress of nanocomposites as shown by tensile stress-strain curves.

➢ Decreased tensile strength and strain at break of nanocomposites (at higher strain range) with increasing MWCNT content suggest a decreased elastic deformability and the formation of micro-voids in the materials. It is further supported by the decreasing ratio of elastic work to plastic work of deformation.

4.3. Electrical Properties of Nanocomposites

Electrical conductivity of polymer/MWCNT nanocomposites deserve an importance for their high-tech applications. Range of electrical conductivity and its stability determine the particular field of applications of CPC. Therefore, electrical conductivity of PBAT/MWCNT nanocomposites are investigated quantitatively as a function of filler concentration. Value of volume resistivity of nanocomposites is taken into account to determine the electrical conductivity of nanocomposites. Furthermore, change in resistance of nanocomposites as a function of mechanical deformation (strain) are measured to investigate their piezoresistivity. Finally, reproducibility of change in electrical resistance with quantitatively applied strain is investigated to evaluate the strain sensing behavior of electrically conductive PBAT/MWCNT nanocomposites. In this way, electrical conductivity, piezoresistivity and the strain sensing behavior of PBAT/MWCNT nanocomposites will be discussed in this section.

4.3.1. Volume Resistivity

Volume resistivity of PBAT/MWCNT nanocomposites was measured to determine the percolation threshold and to quantify their electrical conductivity. It is also taken as an alternative method providing information about the formation of CNT-network and the status of filler dispersion in nanocomposites. Formation of conductive filler network throughout the polymer matrix causes insulator-to-conductor electrical transition in nanocomposites imparting them with electrical conductivity. It is described in accordance with percolation theory. The volume resistivity of nanocomposites, plotted as a function of MWCNT concentration and the recorded values are presented in **Figure 22a** and **Table 10**, respectively.
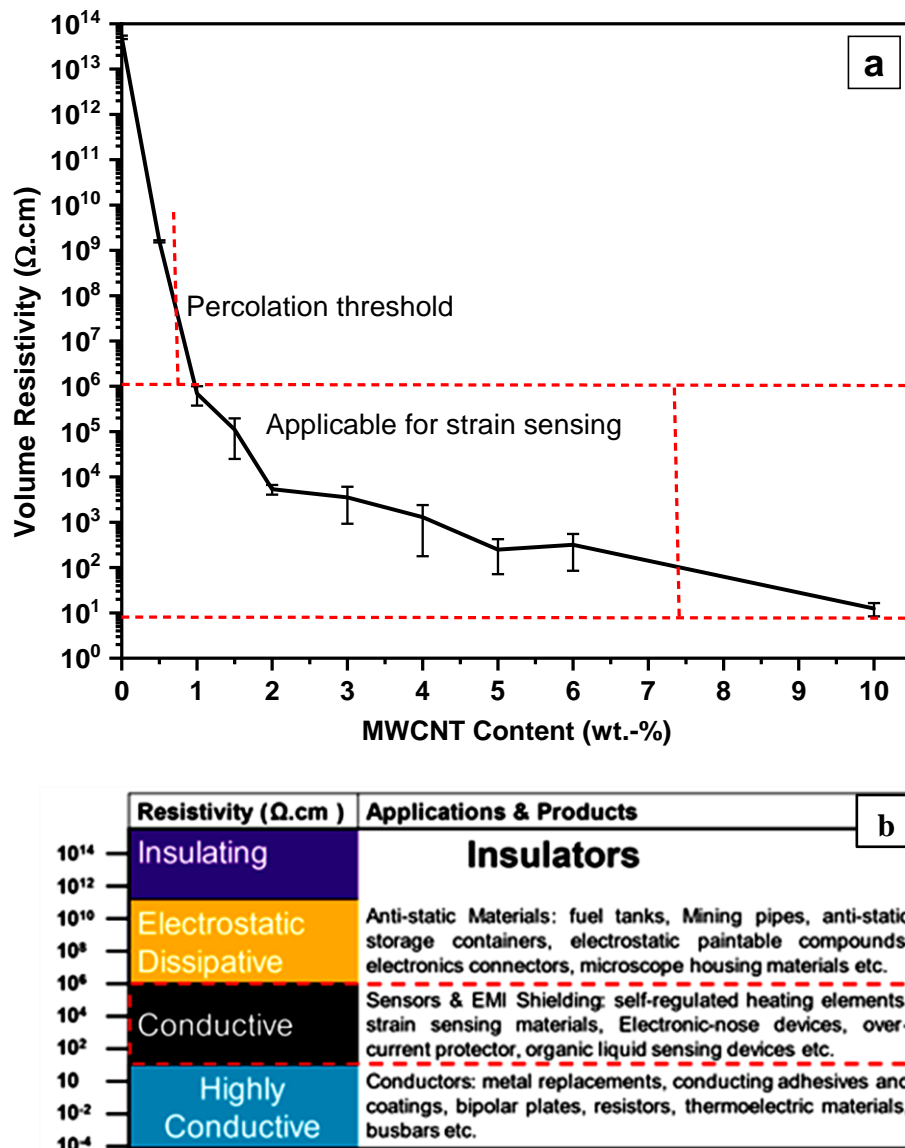
Figure 22: (a) Plot of volume resistivity versus filler content of PBAT/MWCNT nanocomposites and (b) classification of materials according to volume resistivity (Pang *et al*., 2014)

Table 10: Volume resistivity of neat PBAT and PBAT/MWCNT nanocomposites

Sample	Volume resistivity ($\Omega \cdot cm$)
PBAT-neat	$5.03 \times 10^{13} \pm 4.36 \times 10^{12}$
PBAT/0.5% MWCNT	$1.58 \times 10^{9} \pm 8.54 \times 10^{7}$
PBAT/1% MWCNT	$6.90 \times 10^{5} \pm 8.57 \times 10^{4}$
PBAT/1.5% MWCNT	$1.10 \times 10^{5} \pm 8.57 \times 10^{4}$
PBAT/2% MWCNT	$5.36 \times 10^{3} \pm 1.30 \times 10^{3}$
PBAT/3% MWCNT	$3.50 \times 10^{3} \pm 2.58 \times 10^{3}$
PBAT/4% MWCNT	$1.29 \times 10^{3} \pm 1.11 \times 10^{3}$
PBAT/5% MWCNT	$2.46 \times 10^{2} \pm 1.75 \times 10^{2}$
PBAT/6% MWCNT	$3.17 \times 10^{2} \pm 2.32 \times 10^{2}$
PBAT/10% MWCNT	$1.24 \times 10^{1} \pm 4.07$

According to **Table 10**, volume resistivity of nanocomposites is reduced by 4 decades by the incorporation of 0.5 wt.-% of fillers which is further decreased by 5 decades at 1 wt.-% of CNT concentration. This value of volume resistivity and the classification of materials on the basis of volume resistivity (presented in **Figure 22b** suggest the occurrence of insulator-to-conductor transition of nanocomposites between these two filler concentrations signifying percolation threshold (Kaur *et al*., 2015; Pang *et al*., 2014). Percolation threshold below 1 wt.-% MWCNT concentration is taken as comparatively, a low percolation threshold as reported in the literature for similar works. Urquijo *et al.* and Ding *et al.* have reported the percolation threshold above 2 wt.-% of CNT for similar works (Ding *et al*., 2016; Urquijo *et al*., 2017). On the basis of volume resistivity values of the nanocomposites, it seems that PBAT/0.5 % MWCNT nanocomposites are electrical insulators whereas PBAT/1 % MWCNT and all of the composites above this CNT concentration are electrically conductive. Based on the values of volume resistivity listed in **Table 10**, and the classification of the materials presented in **Figure 22b**, PBAT/MWCNT nanocomposites are electrically conductive at and above 1 wt.-% of MWCNT, and applicable for sensors and electromagnetic interference (EMI) shielding (Kaur *et al*., 2015; Pang *et al*., 2014)

Occurrence of electrical transition between 0.5 to 1 wt.-% of MWCNT implies the formation of a conductive continuous MWCNT-network throughout the composites at this filler concentration (Kaur *et al*., 2015). The volume resistivity values of nanocomposites seem continuously decreasing with the increasing filler concentration.

However, the rate of declining these values slows down beyond 2 wt.-% of CNT. Such a trend of volume resistivity values suggests the increasing network density in the composites beyond 2 wt.-% filler content (Christ *et al*., 2017). Achievement of such a low percolation threshold (below 1 wt.-% CNT concentration) and corresponding values of volume resistivity with increasing filler concentration imply the uniformity in the dispersion of MWCNT throughout the nanocomposites (Dil *et al*., 2020). This is in agreement with the results of morphological investigation (suggested by TEM and SEM micrographs) of the nanocomposites. In this way, only partial agglomeration of CNT (suggested by TEM and TLM micrographs) and an even distribution of agglomerates throughout the composite samples are confirmed. It would have resulted into a higher percolation threshold with higher agglomeration despite the contribution of the CNT agglomerates to the electrical conductivity which is not noticed in this work. Uniform dispersion of MWCNT particles in the nanocomposites with minimum agglomeration enhances their electrical as well as mechanical properties which is the advantage to apply the composite materials as strain sensors (Sang *et al*., 2019; Xiang *et al*., 2019). Conductive PBAT/MWCNT nanocomposites were integrated into an electrical circuit as a confirmatory test of their conductivity as shown in **Figure 23**. Electrical conductivity of the nanocomposites was confirmed by the glowing bulb (**Figure 23**) which became significant with PBAT/3% MWCNT nanocomposites.
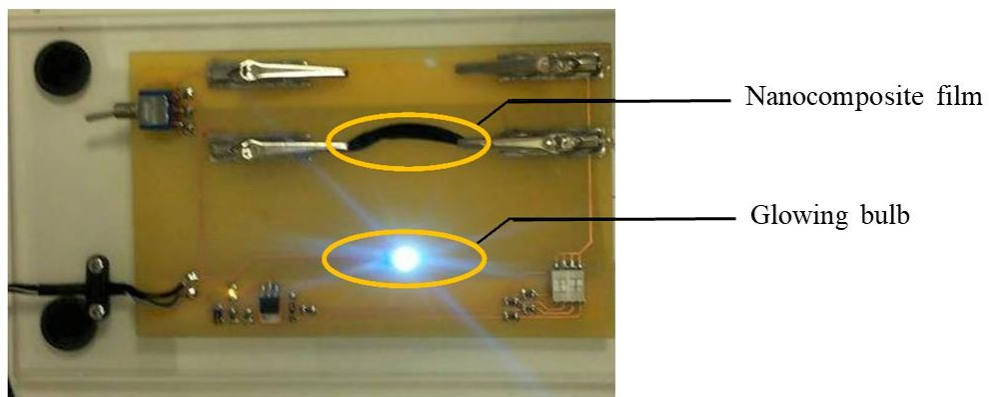
Figure 23: Electrically conductive PBAT/MWCNT nanocomposites integrated into an electrical circuit

The electrical circuit was operated by the voltage (*V*) of 24 V and the resistance of the composite film used in the circuit was measured before experiment which was 2.2×10^4 Ohm. The value of current (*I*) flowing through the electrical circuit was determined by Ohm's equation stated in **equation (9).**

$$V = IR \tag{9}$$

where, V = electrical voltage, I = current, R = electrical resistance of the conductor. Value of the current flowing through the circuit calculated using **equation (9)** was 0.001 ampere.

4.3.2. Piezoresistivity

Piezoresistivity of CPC is their electromechanical response which is determined by the morphology and the microstructure of nanocomposites (Salaeh *et al.*, 2020; Xiang *et al.*, 2019). The trend of change of electrical resistance of PBAT/MWCNT nanocomposites was measured during unidirectional tensile test at a low tensile speed (0.5 mm/ minute) to investigate their piezoresistive behavior. Relative resistance change ($\Delta R/R_0$) of nanocomposites during tensile stretching is taken into account to evaluate their piezoresistive sensitivity. Change in $\Delta R/R_0$ of nanocomposites as a with increasingly applied mechanical strain and their initial resistance (R_0) along with their stress-strain behaviour during the test is presented in **Figure 24**.
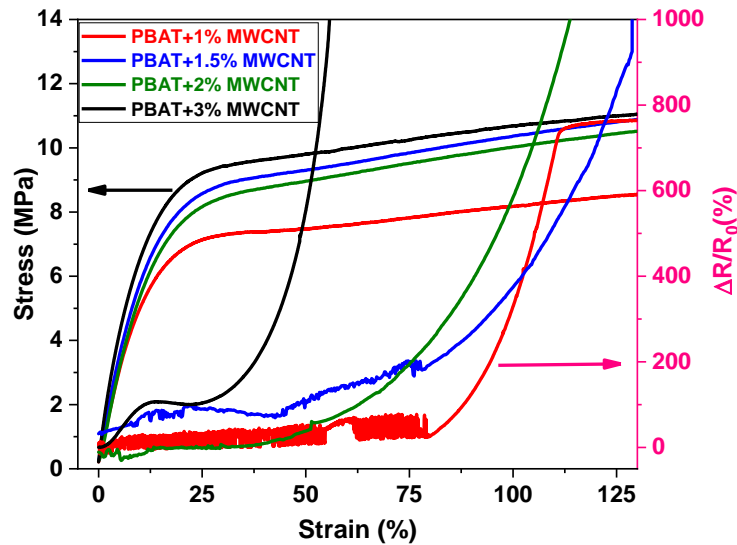
Figure 24: Relative resistance change ($\Delta R/R_0$) of PBAT/MWCNT nanocomposites as a function of mechanical strain

Some of the nanocomposites (1, 1.5, 2 and 3 wt.-%) with CNT cocentration close to as well as above percolation threshold CNT) were taken for this experiment whose electrical resistance change and stress-strain data were recorded simultaneously. Selection of the samples for this experiment is based on the value of electrical volume resistivity, percolation threshold, less dense filler network present in the samples and their mechanical performance. The composite samples with low to moderate stiffness,

high elongation at break and low agglomeration are preferred. Non-linear and exponential-like increase of $\Delta R/R_0$ of nanocomposites with increasing mechanical strain during the experiment confirmed the piezoresistivity of materials (Ke *et al*., 2017; Papageorgiou *et al*., 2020; Tang *et al*., 2020; Xiang *et al*., 2019). This behavior of PBAT/MWCNT nanocomposites signifies the potential of their applications in piezoresistive strain sensors (Ma *et al*., 2022).

Increase in electrical resistance of PBAT/MWCNT nanocomposites with increasing tensile strain in comparison to that at zero strain is carried out by the disconnection of filler particles during mechanical deformation, deformation of CNT particles due to applied strain, tunnelling resistance and the destruction of conductive CNT network by the tensile deformation (Amjadi *et al*., 2015; Park *et al*., 2016). Resistance increases sharply at high-strain region, which is attributed to the irreversible destruction of conductive CNT-networks (Salaeh *et al*., 2020). Similarly, a temporary and reversible breakdown of the CNT-network occurs at low-strain level, mostly below the yield point in elastic region of the electrically conductive composites of thermoplastic elastomers. As suggested by the tensile stress-strain behaviour of PBAT/MWCNT nanocomposites, this region will lie up to around 15% strain.

Among the nanocomposites investigated in this experiment, piezoresistive behavior of PBAT/3% MWCNT nanocomposites are discussed in detail here and the corresponding results and their closer views are presented in **Figure 25**. Entire range of stress strain behaviour and change in $\Delta R/R_0$ as a function of mechanical strain are presented in **Figure 25a**. A Closer regime of **Figure 25a**, presented in **Figure 25b** shows the resistance change up to 10% mechanical strain. Measurement of the change in electrical resistance with increasingly applied mechanical strain in cyclic manner up to this range is carried out to investigate the reproducibility and stability of piezoresistive sensitivity of these nanocomposites. A closest view of **Figure 25a** (below 2% strain) is presented in **Figure 25c**, which follows a different way of resistance change despite an overall exponential-like manner. It is observed that electrical resistance is decreased at a low strain (below 1%) in comparison to the resistance of nanocomposites at zero strain (R_0). This strain value is called the critical strain and the decrease in resistance below this strain value is attributed to the effect of composite conditioning. Unstable and temporary CNT contacts are removed in this effect due to weak filler-matrix interfacial interaction. As a result, alternative CNT-CNT connections will be formed at lower deformation of the composites which reduces the resistance of the nanocomposites. As

a result, additional conductive pathways are formed in nanocomposites due to which electrical resistance decreases (Ji *et al*., 2014; Tang *et al*., 2020). Resistance seems to increase exponentially as a function of increasing strain beyond the critical strain only.
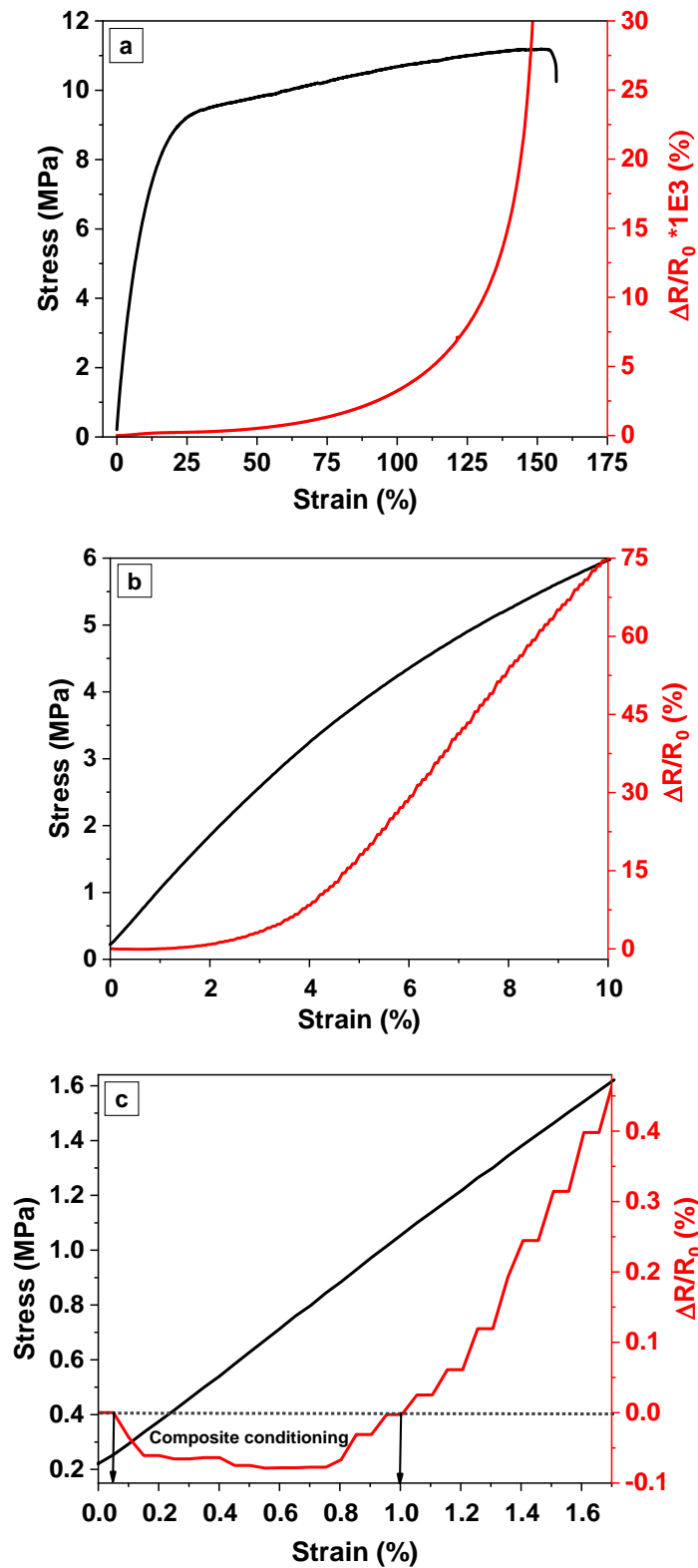
Figure 25: (a) Relative resistance change ($\Delta R/R_0$) of PBAT/ 3% MWCNT nanocomposites as a function of mechanical strain (b) closer regime and (c) closest regime

A rapid change in resistance of the nanocomposites with increasing filler concentration near to the percolation threshold takes place with a low mechanical strain which can be applicable for low-strain sensitivity. Less densified filler networks in such composites will have the probability of formation of alternative conductive paths contributing to the linear piezoresistivity (Costa *et al.*, 2017; Liao *et al.*, 2017). It occurs just beyond the critical strain of the nanocomposites and attributed to the disconnection CNT-CNT connections simultaneously followed by the construction of an alternative CNT-network, however, such nanocomposites are not suitable for higher strain sensitivity. Meanwhile, probability of simultaneous reconstruction of alternative CNT network declines at higher CNT content for which extra strain is required to perform the reversible destruction of the network. Such nanocomposites with higher filler content can be applicable for high-strain sensitivity (Dhakal *et al.*, 2022a).

Conductive CNT-network formed by the CNT connections can be clearly observed by TEM micrograph presented in **Figure 26**. Possible destruction and reconstruction of this network up on mechanical deformation of PBAT/MWCNT nanocomposites and its removal, respectively can also be predicted from this micrograph.
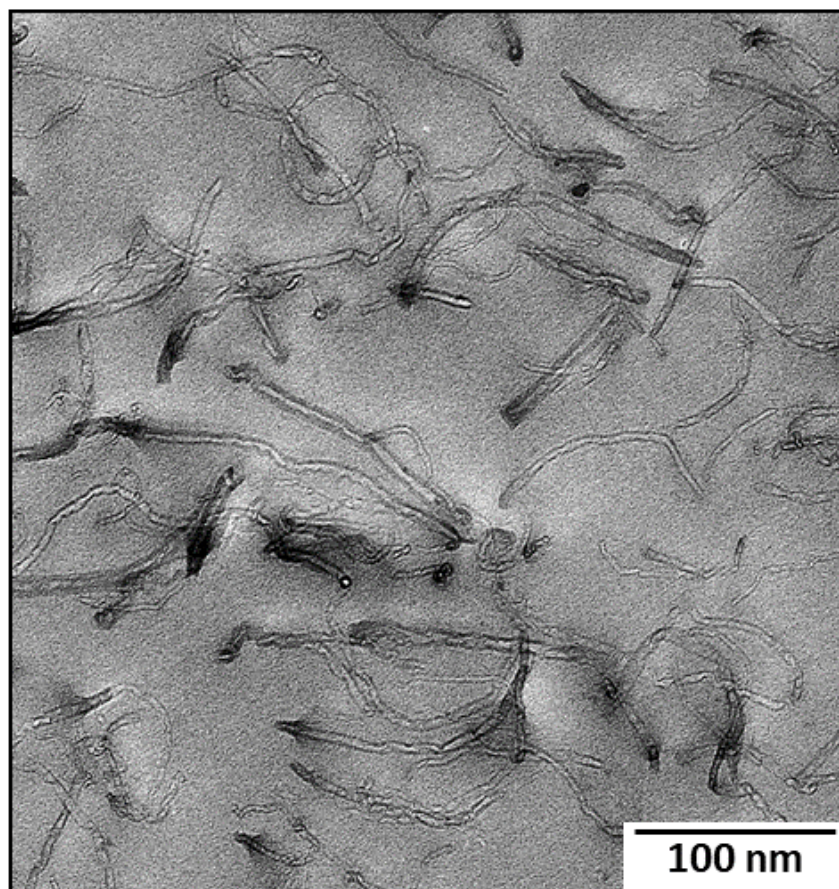
Figure 26: TEM micrograph of PBAT/3% MWCNT nanocomposites

The piezoresistive type of sensitivity of CPC can be tuned altering the filler concentration in them above percolation threshold. Declined recovery of conductive CNT-network of the piezoresistive nanocomposites at higher filler concentration is further supported by the agglomeration. At higher agglomeration, electrical conductivity of nanocomposites is mostly due to tunnelling effect rather than that by the conductive filler network (Ciselli *et al.*, 2010). Based on the electrical conductivity of the nanocomposites, their ductile nature suggested by tensile test and the results of microindentation tests of nanocomposites, PBAT/3% MWCNT nanocomposites were used for further experiments to analyse the stability and reproducibility of piezoresistive sensitivity which are discussed in the next section.

4.3.3. Strain Sensing Behavior

Cyclic strain experiment was performed to assess the strain sensing behavior of PBAT/MWCNT nanocomposites. Electrical resistance of nanocomposites was measured as a function of mechanical strain under cyclic loading/unloading of strain to evaluate their electromechanical response. $\Delta R/R_0$–strain correlation of the nanocomposites during cyclic strain experiment was investigated measuring the electrical resistance simultaneously with increasingly applied mechanical strain. Mechanical strain was exerted on PBAT/3 % MWCNT nanocomposites in increasing manner from 1 to 10 % as presented in **Figure 27** (**a-c**). Three loading and unloading cycles of strain were applied in each value of strain from 1 to 10% with the relaxation period of 90 seconds after each loading and unloading.

From **Figure 27a**, it seems that $\Delta R/R_0$ decreases with mechanical strain up to 1% strain which is highlighted in **Figure 27c**. This result is found consistent with that of uniaxial tensile stretching of PBAT/3% MWCNT nanocomposites discussed in chapter 4.3.2. This value of strain, called critical strain above which the electrical resistance increases. On the other hand, $\Delta R/R_0$ values increases with increasing strain and vice versa in each loading and unloading of mechanical strain, fitting well with strain from 2% to 8% strain as highlighted in **Figure 27b** and indicated by green arrow. A positive correlation between $\Delta R/R_0$ and tensile strain is observed which is required for an electrically conductive nanocomposites based strain sensor (Niu *et al.*, 2018). However, $\Delta R/R_0$ does not fit with applied strain above 8% which changes in an irregular way regardless the loading and unloading of mechanical strain as shown by horizontal green arrow in **Figure 27a**.
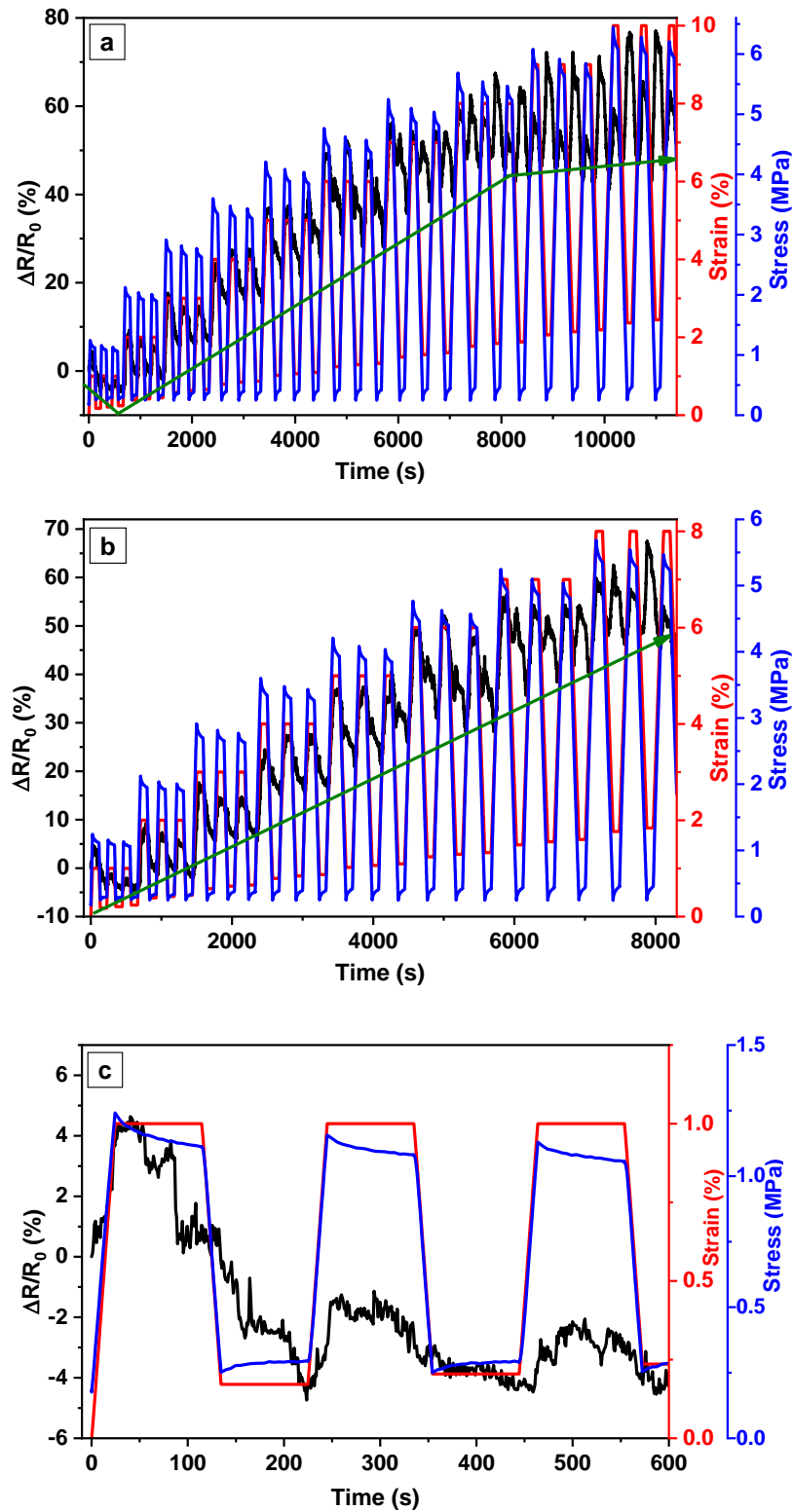
Figure 27: (a) Cyclic strain test of PBAT/3% MWCNT nanocomposites (b) highlighted portion of relative resistance change (ΔR/R₀) fitting with strain and (c) highlighted portion of decreasing ΔR/R₀ up to 1% strain

Increase in $\Delta R/R_0$ values with increasing strain and vice versa signifies the electromechanical response of nanocomposites. Increase in electrical resistance of

nanocomposites upon strain loading corresponds to the increase in distance between CNT-particles and decrease in contact between them up on mechanical deformation. On the other hand, recovery of the resistance upon removal of mechanical strain is due to the viscoelastic flow of PBAT (matrix).

A closer view of **Figure 27b** suggests that second peaks (shoulder peaks) appear at 4% strain which become significant and even higher than the first peaks at higher strain (as seen at 8% strain). In this phenomenon, the first peak corresponds to the resistance change by the maximum strain applied and the second peak is the shoulder peak. This phenomenon is common in thermoplastic elastomers (TPE) based strain sensors. They appear due to competition between destruction and reconstruction of conductive network during loading and unloading of strain, respectively. There will be a compitition between destruction and formation of CNT network during strain loading and unloading (Zhang *et al*., 2013; Salaeh *et al*., 2020). They appear after unloading the strain in cyclic strain test. At higher strain, during unloading, residual relative resistance recovery takes place, however, it can not fully occur. Only a part of resistance is recovered and the resistance change becomes non-monotonic with the strain applied. Hence, it seems a time dependent phenomenon instead of decreasing continuously with decreasing strain during unloading. Shoulder peaks are also called negative piezoresistivity which produce the sensitivity signals in opposite direction which are also applicable for strain sensing purpose. Strain sensors with the dominance of first peaks (positive piezoresistivity) are preferred for strain sensing applications (Salaeh *et al*., 2020).

4.3.4. Summary of Electrical Properties

➤ Comparatively low percolation threshold (lying between 0.5 and 1 wt.-% of MWCNT) of PBAT/MWCNT nanocomposites is suggested. Homogeneous dispersion of MWCNT in the nanocomposites, low filler agglomeration and the uniform distribution of CNT-agglomerates are responsible for such a low percolation threshold. Volume resistivity values of nanocomposites (above percolation threshold) in the range of 10 to 10^6 $\Omega \cdot$cm imply for their potential in strain-sensing.

➤ An exponential-like non-linear increase of $\Delta R/R_0$ of the nanocomposites as a function of mechanical strain confirms their piezoresistivity which is one of the requirements of conductive polymer composites (CPC) for strain sensing

applications. Similarly, decrease in electrical resistance as an effect of composite conditioning up to 1% strain (critical strain) is dominant.

➢ Cyclic strain experiment of PBAT/MWCNT nanocomposites performs reproducibility and fitting of $\Delta R/R_0$ values up to 8% mechanical strain. It implies the potential of nanocomposites for low strain-sensing applications. Shoulder peaks of $\Delta R/R_0$ appear at and above 4% strain which become significant at higher strain. They can also be taken into account for strain sensing purpose, however, the signals will be displayed in opposite direction.

4.4. Crosslinking the Nanocomposites by Electron Beam (EB) Irradiation

Crosslinking PBAT/MWCNT nanocomposites was employed as a strategy to improve their strain sensing behaviour. Crosslinking of the nanocomposites was carried out by the irradiation of electron beam (EB). It was targeted that EB induced crosslinking the nanocomposites would improve their elasticity and controls the viscoelastic flow of PBAT chains enhancing the strain sensing behaviour.

EB irradiation of PBAT/MWCNT nanocomposites, investigation of degree of crosslinking, deformation behavior of irradiated nanocomposites, and evaluation of their strain sensing behavior and its reproducibility are discussed in this chapter.

4.4.1. Investigation of Degree of Crosslinking

In order to determine the exact dose of EB irradiation to PBAT/MWCNT nanocomposites on the basis of degree of crosslinking, EB irradiation of neat PBAT was performed in a irradiation dose range i.e. 25, 50, 75, 100, 150, 200, 250 and 300 kGy. Resulting degree of crosslinking were calculated taking the mass of gel formed by the EB irradiation whose results are presented in **Figure 28**. The mass of gel formed in each irradiated sample was determined by dissolving it in chloroform in which insoluble residue (gel) was weighed after drying.
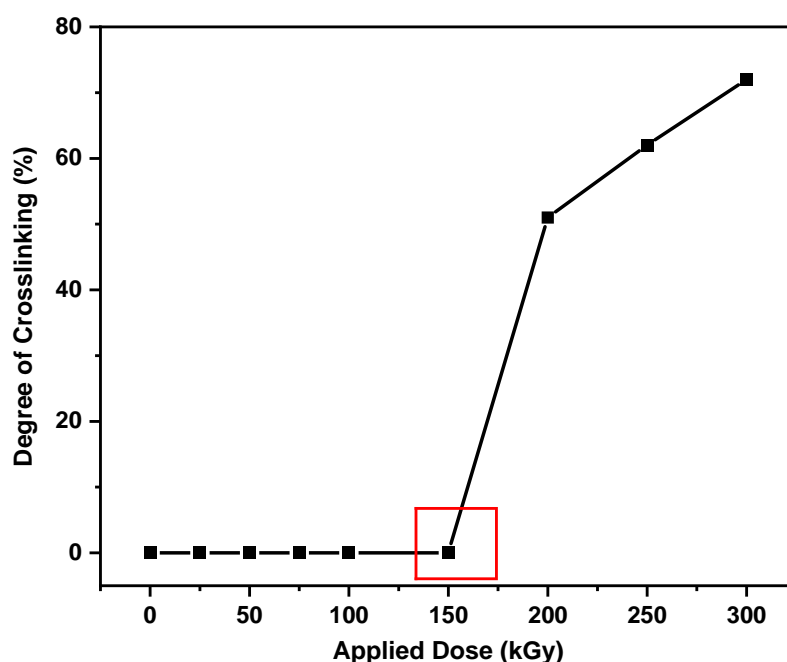
Figure 28: Degree of crosslinking of neat PBAT as a function of applied dose

Degree of crosslinking of PBAT/MWCNT nanocomposites can't be determined exactly because of the insolubility of MWCNT in organic solvents. Therefore, degree of

crosslinking of irradiated PBAT was taken as a reference to irradiate PBAT/MWCNT nanocomposites.

As presented in **Figure 28**, no gel was formed up to the dose of 150 kGy. A viscous PBAT-solution was obtained when PBAT irradiated with 150 kGy (highlighted in **Figure 28**) was dissolved in chloroform. This PBAT solution could not be filtered *via* filter paper although gel was not obtained as a residue. This is attributed to the branching of PBAT by the EB irradiation before crosslinking. Hence, degree of crosslinking is zero up to 150 kGy of irradiation dose.

Table 11: Dose dependent degree of crosslinking of neat PBAT

Dose (kGy)	Degree of crosslinking (%)
0	0
25	0
50	0
75	0
100	0
150	0
200	51
250	62
300	72

Gel formation was observed at the irradiation doses above 150 kGy when PBAT was dissolved in chloroform which confirmed the crosslinking of PBAT. Degree of crosslinking is calculated using **equation (7).**

$$Degree\ of\ crosslinking\ (\%) = \left(\frac{w_1}{w_2}\right) \times 100\% \qquad (7)$$

where, w_1 = weight of gel formed, w_2 = total weight of the irradiated sample

Corresponding degree of crosslinking, calculated are presented in **Table 11**. It seems that degree of crosslinking is dependent on the dose of irradiation which increases with increasing dose and vice versa.

4.4.2. Deformation Behavior

Deformation behavior of EB irradiated PBAT/MWCNT nanocomposites was also investigated by the analyses of their tensile mechanical and micromechanical properties.

4.4.2.1. Tensile Mechanical Properties

Based on the polymer branching and dose dependent degree of crosslinking of EB irradiated PBAT, PBAT/3% MWCNT nanocomposites were irradiated with the dose of 150, 200 and 300 kGy. Tensile stress-strain behavior of EB irradiated PBAT (with 150 kGy and above) and PBAT/3% MWCNT nanocomposites were investigated under the same experimental conditions as discussed in section 4.2.1. The stress-strain curves of irradiated PBAT and PBAT/3% MWCNT are presented in **Figure 29** and the related results are presented in **Table 12**. Tensile strength and tensile modulus of nanocomposites are unchanged. However, significant variation in elongation at break of both irradiated and unirradiated PBAT as well as composites are observed. Dose dependent decrease of elongation at break of composites are implied which are presented in **Table 13**.
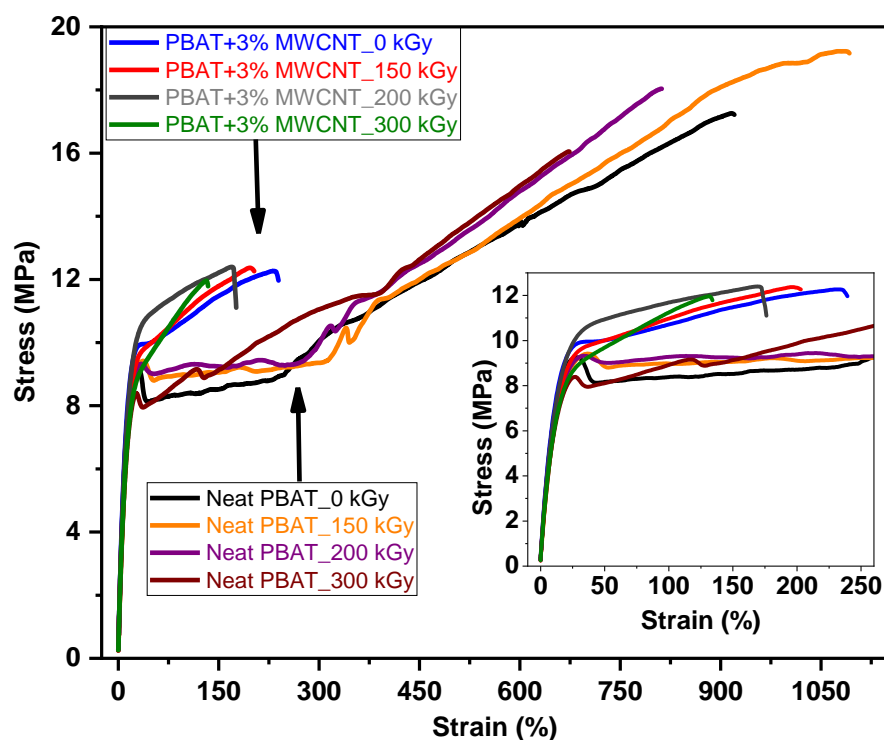
Figure 29: (a) Tensile stress-strain behavior of EB irradiated PBAT with lower dose and (b) EB irradiated PBAT and PBAT/3% MWCNT nanocomposites with higher dose

Table 12: Tensile mechanical properties of EB irradiated PBAT and EB irradiated PBAT/MWCNT nanocomposites

Sample	σ (MPa)	Et (MPa)	ε_B (%)
Matrix			
PBAT-0 kGy	83 ± 5.6	17 ± 0.8	920 ± 45.0
PBAT-150 kGy	71 ± 2.2	19 ± 0.6	1094 ± 10.2
PBAT-200 kGy	82 ± 3.1	18 ± 0.7	812 ± 62.0
PBAT-300 kGy	76 ± 2.6	16 ± 1.7	675 ± 174.2
Composites			
PBAT/3% MWCNT -0 kGy	86 ± 7.0	12 ± 0.5	238 ± 67.6
PBAT/3% MWCNT -150 kGy	84 ± 6.6	12 ± 0.5	211 ± 35.8
PBAT/3% MWCNT -200 kGy	84 ± 7.0	12 ± 1.1	190 ± 47.7
PBAT/3% MWCNT -300 kGy	82 ± 3.0	12 ± 1.1	132 ± 35.4

σ: Tensile modulus, Et: Tensile strength, ε_B: Elongation at break

Table 13: Dose dependent change of elongation at break of EB irradiated PBAT and EB irradiated PBAT/MWCNT nanocomposites

Irradiated PBAT		
Sample	ε_B (%)	Remarks
PBAT-0 kGy	920 ± 45.0	-
PBAT-150 kGy	1094 ± 10.2	Increased by 19 %
PBAT-200 kGy	812 ± 62.0	Decreased by 12 %
PBAT-300 kGy	675 ± 174.2	Decreased by 27 %
Irradiated nanocomposites		
PBAT/3% MWCNT-0 kGy	238 ± 67.6	-
PBAT/3% MWCNT-150 kGy	211 ± 35.8	Increased by 11 %
PBAT/3% MWCNT-200 kGy	190 ± 47.7	Increased by 20 %
PBAT/3% MWCNT-300 kGy	135 ± 35.4	Increased by 43 %

ε_B: Elongation at break

Similar trend of elongation at break of irradiated PBAT is observed except that at the dose of 150 kGy. This value of PBAT irradiated with 150 kGy increased by 19% in comparison to that of unirradiated PBAT. The irradiation dose of 150 kGy corresponds to PBAT branching as suggested by degree of crosslinking. Dose dependent change of elongation at break of nanocomposites due to EB irradiation induced crosslinking without changing other mechanical parameters is expected to improve the strain sensing behavior of nanocomposites.

4.4.2.2. Micromechanical Behavior

Microindentation measurements of EB irradiated PBAT/3 % MWCNT nanocomposites were carried out. The change in *HM, EIT* and h_{max} of same composites irradiated with different doses are presented in **Figure 30**. Similarly, the corresponding data of this measurements are presented in **Table 14**.
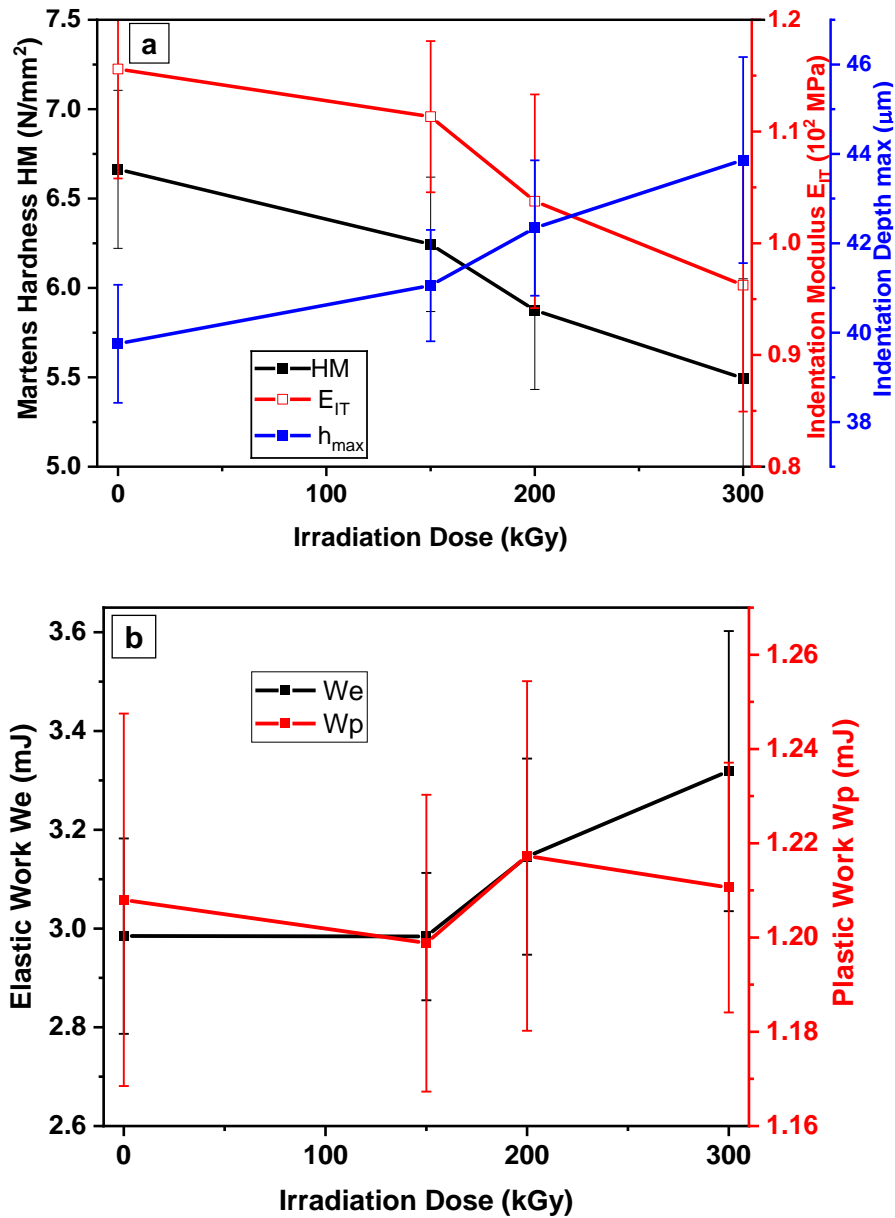
Figure 30: (a) Martens hardness (*HM*), indentation modulus (E_{IT}) and indentation depth (h_{max}) and (b) work done by elastic deformation (W_e) and plastic deformation (W_p) of EB irradiated PBAT/3% MWCNT nanocomposites as a function of irradiation dose

Table 14: Micromechanical properties of EB irradiated PBAT/3% MWCNT nanocomposites

Sample	HM (N/mm²)	E_{IT} (MPa)	h_{max} (µm)
PBAT/3% MWCNT -0 kGy	6.66 ± 0.44	115.59 ± 9.79	39.75 ± 1.25
PBAT/3% MWCNT -150 kGy	6.24 ± 0.38	111.33 ± 6.78	41.05 ± 1.32
PBAT/3% MWCNT -200 kGy	5.88 ± 0.44	103.76 ± 9.57	42.34 ± 1.51
PBAT/3% MWCNT -300 kGy	5.50 ± 0.84	96.25± 11.22	43.86 ± 2.30

HM: Martens hardness, E_{IT}: Indentation modulus, h_{max}: maximum indentation depth

Table 15: Elastic and plastic work (W_e and W_p) of deformation of EB irradiated PBAT/3% MWCNT nanocomposites and their ratio (W_e/W_p)

Sample	W_e (mJ)	W_p (mJ)	W_e/W_p
PBAT/3% MWCNT -0 kGy	2.98 ± 0.19	1.20 ± 0.04	2.47
PBAT/3% MWCNT -150 kGy	2.98 ± 0.12	1.20 ± 0.03	2.49
PBAT/3% MWCNT -200 kGy	3.14 ± 0.19	1.22 ± 0.04	2.58
PBAT/3% MWCNT -300 kGy	3.31 ± 0.28	1.21 ± 0.03	2.74

Figure 30 shows that both Martens hardness and indentation modulus of EB irradiated PBAT/3% MWCNT nanocomposites decrease with higher irradiation dose. Meanwhile, maximum indentation depth of the nanocomposites increases with increasing irradiation dose. Both Martens hardness and indentation modulus are decreased by ~17% by the irradiation of the samples with 300 kGy dose. Similarly, maximum indentation depth is increased by ~10% at this irradiation dose. These trends of change of micromechanical parameters are attributed to the EB irradiation induced polymer branching and crosslinking. This is due to the increasing relaxation of rigid polymer chains of the nanocomposites by their branching and crosslinking. Such a relaxation leads to the decrease in interfacial interaction of MWCNT and PBAT chains. On the other hand, increase in maximum indentation depth of the nanocomposites implies their increased elastic deformability which is beneficial to their strain sensing applications. Similarly, a closer view of **Figure 30b** and **Table 15** shows an increasing trend of elastic work (W_e) of PBAT/3% MWCNT nanocomposites with increasing irradiation dose, however, plastic work (W_p) of deformation remains almost the same. Such a variation of work of deformation increases W_e/ W_p ratio which is listed in **Table 15**. It suggests an increased elastic deformability of EB irradiated nanocomposites.

4.4.3. Strain Sensing Behavior

Strain sensing behavior of PBAT/3% MWCNT nanocomposites irradiated with 150, 200 and 300 kGy was investigated carrying out cyclic strain test under the same conditions as before. Results of cyclic strain tests of EB irradiated PBAT/3% MWCNT nanocomposites are presented in **Figure 31 to Figure 33**. It is observed that $\Delta R/R_0$ values of nanocomposites irradiated with 150 and 200 kGy fit well with mechanical strain up to 10% which was fitted only up to 8% strain in case of unirradiated PBAT/3% MWCNT nanocomposites as discussed in section 4.3.3. They are highlighted in **Figure 31b** and **Figure 32b** which are the closer regimes of **Figure 31a and 32a,** respectively. Meanwhile, critical strain of these nanocomposites is 3% in which electrical resistance of the nanocomposites decreases in comparison to initial resistance due to composite conditioning and relaxation effect. Critical strain value for the unirradiated nanocomposites was 1%. Increase in critical strain of irradiated nanocomposites is ascribed to the decreased interfacial affinity of CNT towards PBAT due to polymer branching and crosslinking. Crosslinking PBAT/MWCNT nanocomposites by the EB irradiation was carried out on melt-mixed nanocomposites due to which MWCNT-PBAT interfacial interaction is affected by the branching and crosslinking of polymer matrix. Such an increased critical strain is highlighted in **Figure 31c** and **Figure 32c** (closest regimes of **Figure 31a** and **Figure 32a,** respectively). These results are attributed to the effect of PBAT-branching and the crosslinking carried out by the irradiation dose of 150 and 200 KGy, respectively, which controls the viscoelastic flow of PBAT chains during mechanical deformation.
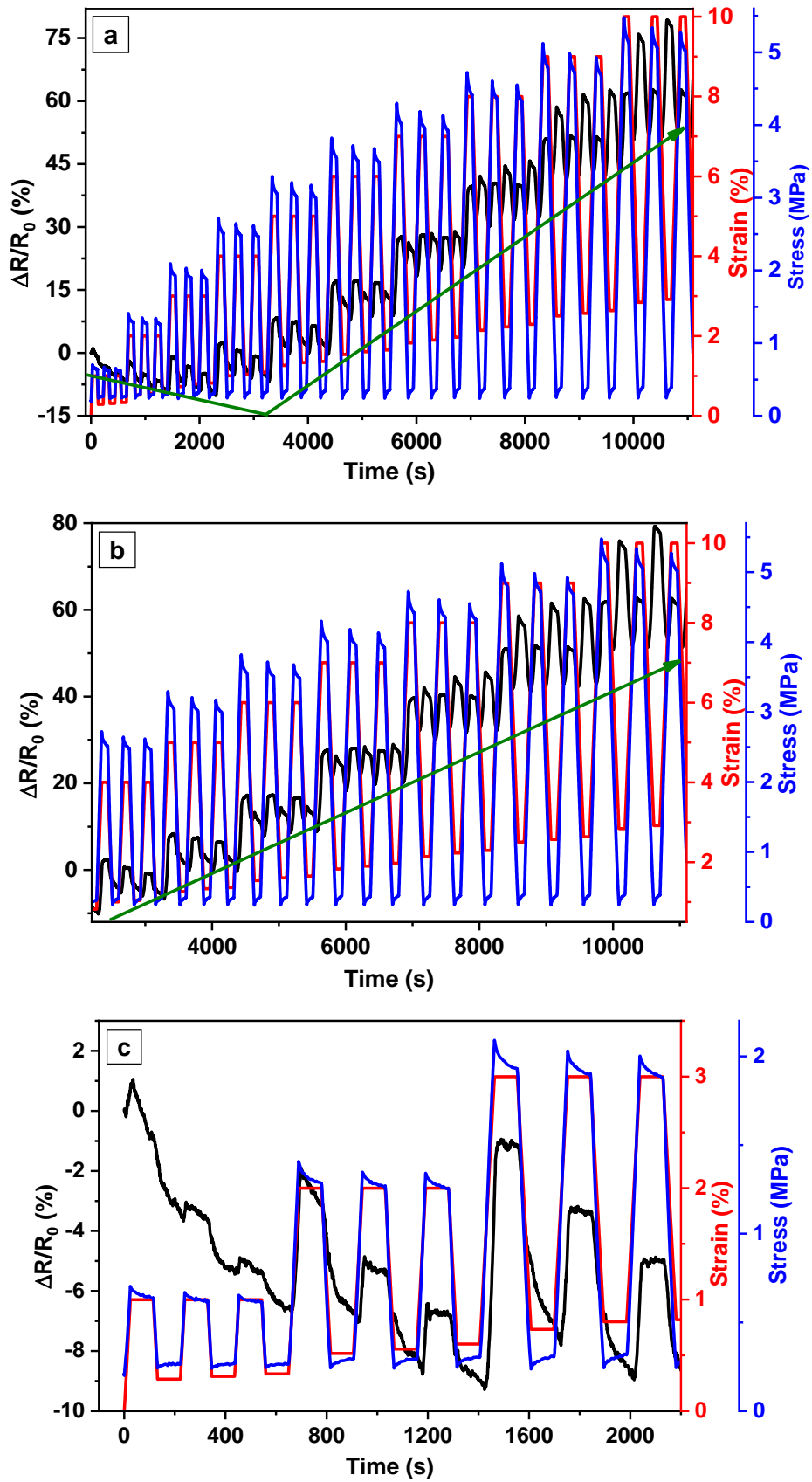
Figure 31: (a) Cyclic strain test of PBAT/3% MWCNT nanocomposites irradiated with 150 kGy (b) highlighted portion of increasing relative resistance change ($\Delta R/R_0$) fitted with strain and (c) highlighted portion of decreasing $\Delta R/R_0$ up to 3% strain
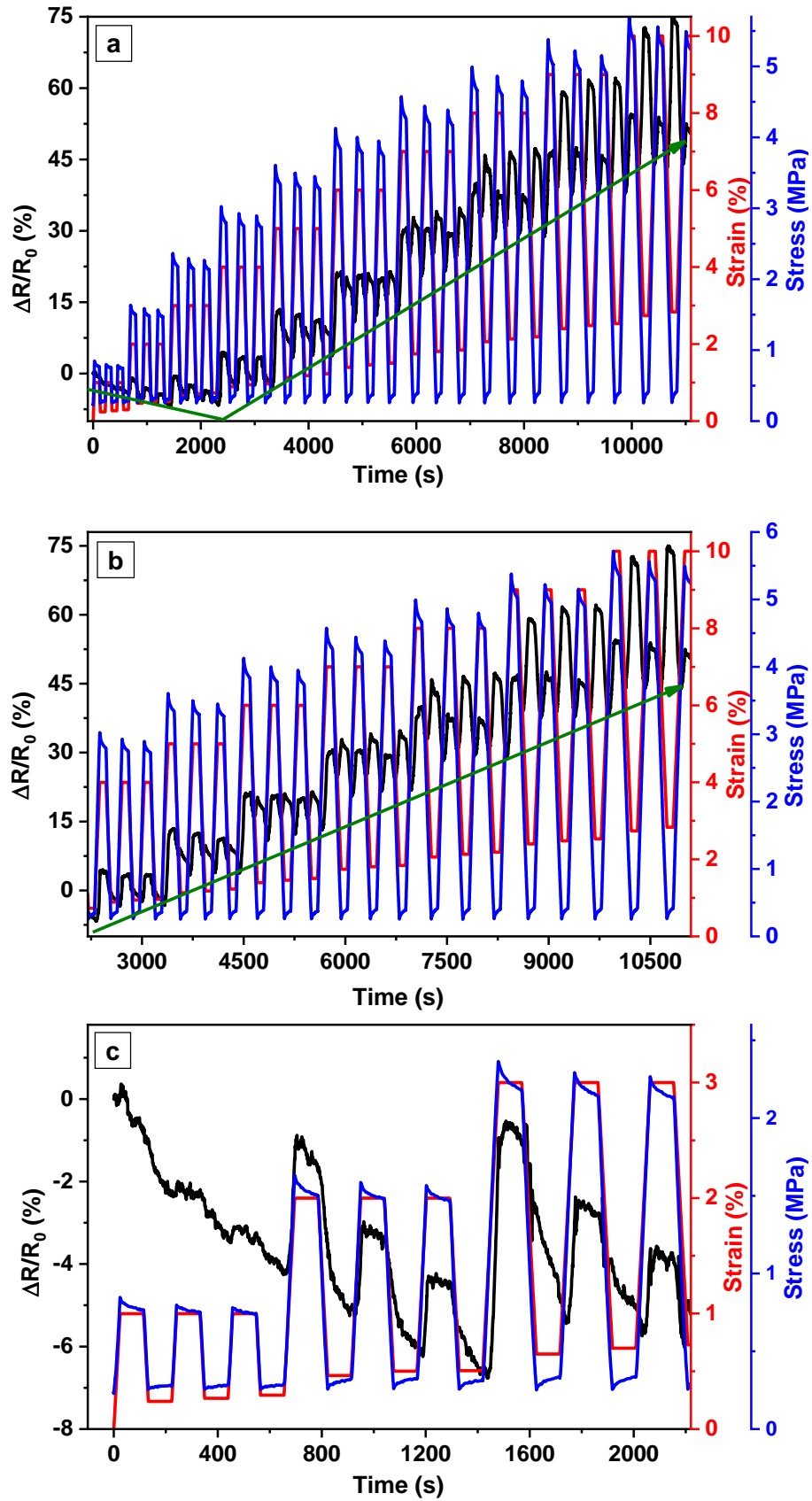
Figure 32: (a) Cyclic strain test of PBAT/3% MWCNT nanocomposites irradiated with 200 kGy (b) highlighted portion of increasing relative resistance change ($\Delta R/R_0$) fitted with strain and (c) highlighted portion of decreasing $\Delta R/R_0$ up to 3% strain

Different results are obtained from the cyclic strain test of PBAT/3% MWCNT irradiated with the dose of 300 kGy which are presented in **Figure 33**. It is observed that $\Delta R/R_0$ values have no correlation with the mechanical strain and it changes in an irregular way regardless the effect of strain loading and unloading during the experiment. It seems that electrical resistance decreased while moving from first to second cycle as that in other irradiated samples, however, it continuously decreased up to 10% strain without any correlation with the change in mechanical strain. Such a trend of $\Delta R/R_0$ values of nanocomposites even at higher strain is attributed to the formation of a 3D crosslinked PBAT network which restricted the homogeneous and reversible deformation of the conductive CNT network up on applying the mechanical strain. Higher degree of crosslinking of nanocomposites restricts the homogeneous deformation as well as destruction of percolation network with mechanical strain (Zhang *et al*., 2013).
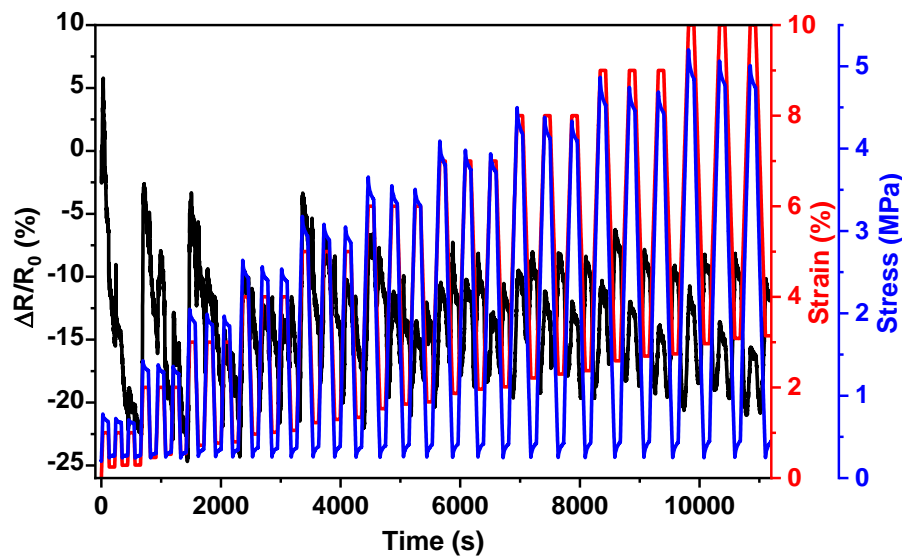
Figure 33: Cyclic strain test of PBAT/3% MWCNT nanocomposites irradiated with 300 kGy

Further cyclic strain tests of both unirradiated and irradiated (150 and 200 kGy) PBAT/3% MWCNT nanocomposites were carried out with higher number of strain loading/unloading cycles and applying a fixed value of mechanical strain. Same experimental conditions were applied for these tests also except the applied mechanical strain and number of cycles. Mechanical strain of 7% was applied in these tests with 15 loading unloading cycles. 7% strain was chosen which is just below the optimum strain value (8%) of unirradiated PBAT/3% MWCNT nanocomposites up to which $\Delta R/R_0$ values fitted well as suggested by the previous cyclic strain experiments discussed in section 4.3.3. These cyclic tests were targeted to investigate the stability and

reproducibility of piezoresistive sensitivity of nanocomposites with higher number of cycles.

Results of cyclic strain experiment of unirradiated PBAT/3% MWCNT nanocomposites applying 7% strain with 15 cycles are presented in **Figure 34 (a-c)**. It seems that resistance change decays in first few cycles (highlighted in **Figure 34b** among which the decay in the first cycle is the most significant. This behavior is common in thermoplastic elastomers which is explained in accordance with Mullin's effect. According to Mullin's effect, contact surface between filler particles will be increased due to repeated stretching and releasing of nanocomposites (Salaeh *et al*., 2020). At higher strain, polymer chains rearrange themselves which is called strain softening. It minimizes the deformation energy and physical damage of polymer matrix is controlled. After few cycles, $\Delta R/R_0$-strain curves reach a plateau after which they stabilize and all of the resistance amplitudes become similar (Xiang *et al*., 2019; R. Zhang *et al*., 2013). These results are consistent to some extent as presented in **Figure 34c**. Similar results are found reported in literature. Based on these results and the reports in literature, it is be predicted that resistance change will be more stabilized beyond 15 cycles (Sang *et al*., 2019; Xiang *et al*., 2019).

Shoulder peaks are appeared in this experiment which become dominant beyond 4% strain in PBAT/3% MWCNT and become even higher than the first peaks at higher strain as suggested by the results of cyclic strain test, discussed in section 4.3.3.

Figure 34: (a) Cyclic strain test of PBAT/3% MWCNT nanocomposites at 7% strain and 15 cycles (b) highlighted first half of the test and (c) highlighted second half of the test

Figure 35 presents the results of cyclic strain experiment of PBAT/3% MWCNT nanocomposites irradiated with the dose of 150 kGy applying 7% strain with 15 cycles. Similar results as that of unirradiated samples are suggested except that of shoulder peaks. Shoulder peaks are lowered than the first peaks which is implied by the closer view of **Figure 35b** and **35c.** It suggests a better recovery of residual electrical resistance during unloading. It should be due to the controlled mobility of PBAT chains carried out by PBAT branching at 150 kGy as suggested by the results of degree of crosslinking. This is further supported by the results of next section.
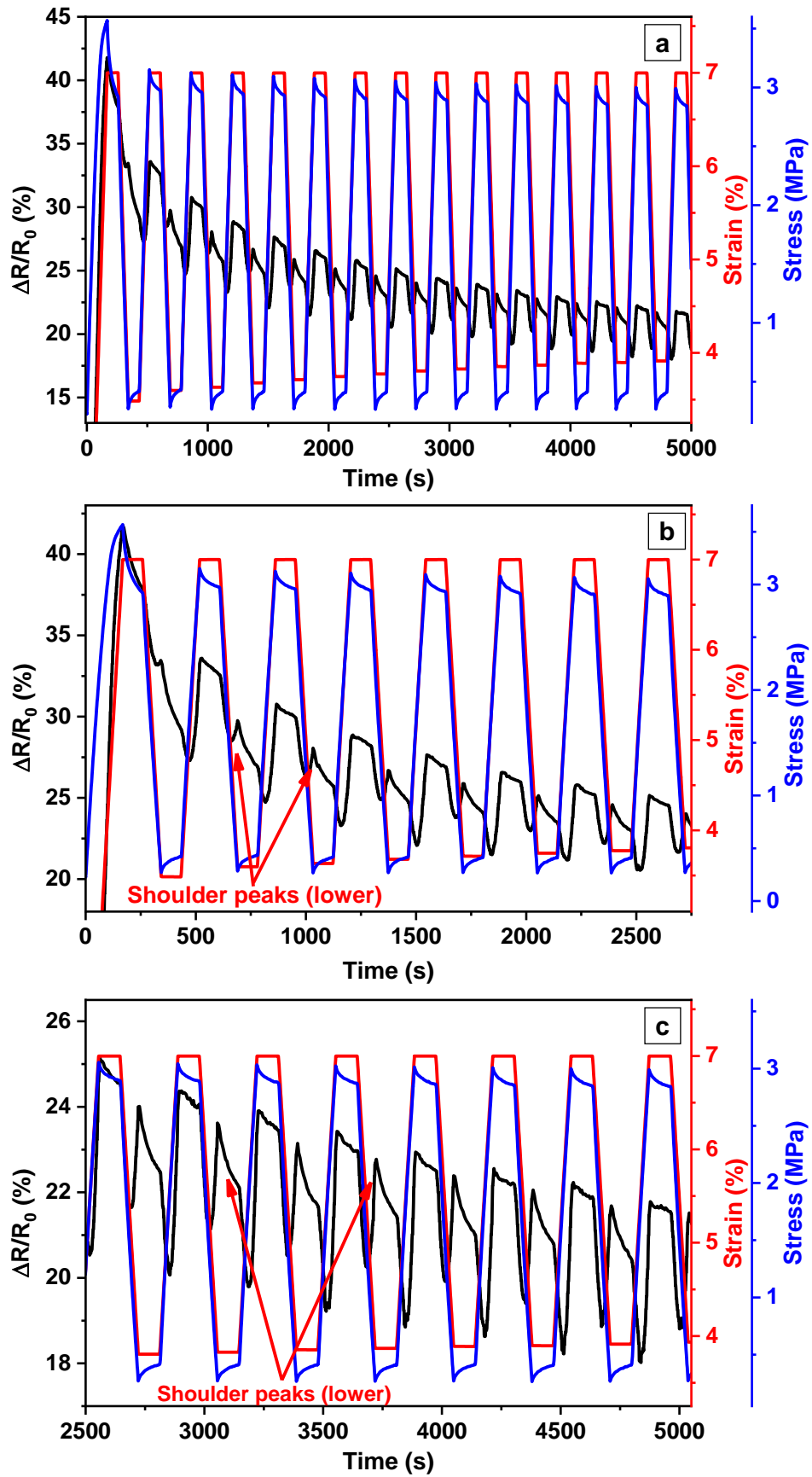
Figure 35: (a) Cyclic strain test of PBAT/3% MWCNT-150 kGy nanocomposites at 7% strain and 15 cycles (b) highlighted first half of the test and (c) highlighted second half of the test

Furthermore, results of cyclic strain experiment of PBAT/3% MWCNT irradiated with 200 kGy are presented in **Figure 36 (a-c).** Results of resistance change as a function of increasingly applied mechanical strain, similar to that of samples irradiated with 150 kGy are suggested except those with shoulder peaks. Only minor shoulder peaks are appeared in these nanocomposites. Recovery of the residual resistance during strain unloading is further improved in these composites due to higher crossliking of polymer matrix and the controlled viscoelastic flow of PBAT chains. Elasticity and the stretchability of the elastomers are enhanced by the crosslinking (Park *et al*., 2022). In this case, higher crosslinking density of PBAT (at 200 kGy) should have controlled the destruction of CNT network during deformation (Zhang *et al*., 2013) because deformation of filler network is carried out by matrix-to-filler stress transfer. Hence, minor competition between destruction of old conductive pathways and formation of new pathways is minimized. Change in electrical resistance should be carried out only by the loss of MWCNT-MWCNT contacts in the conductive network as reported in the literature (Salaeh *et al*., 2020).
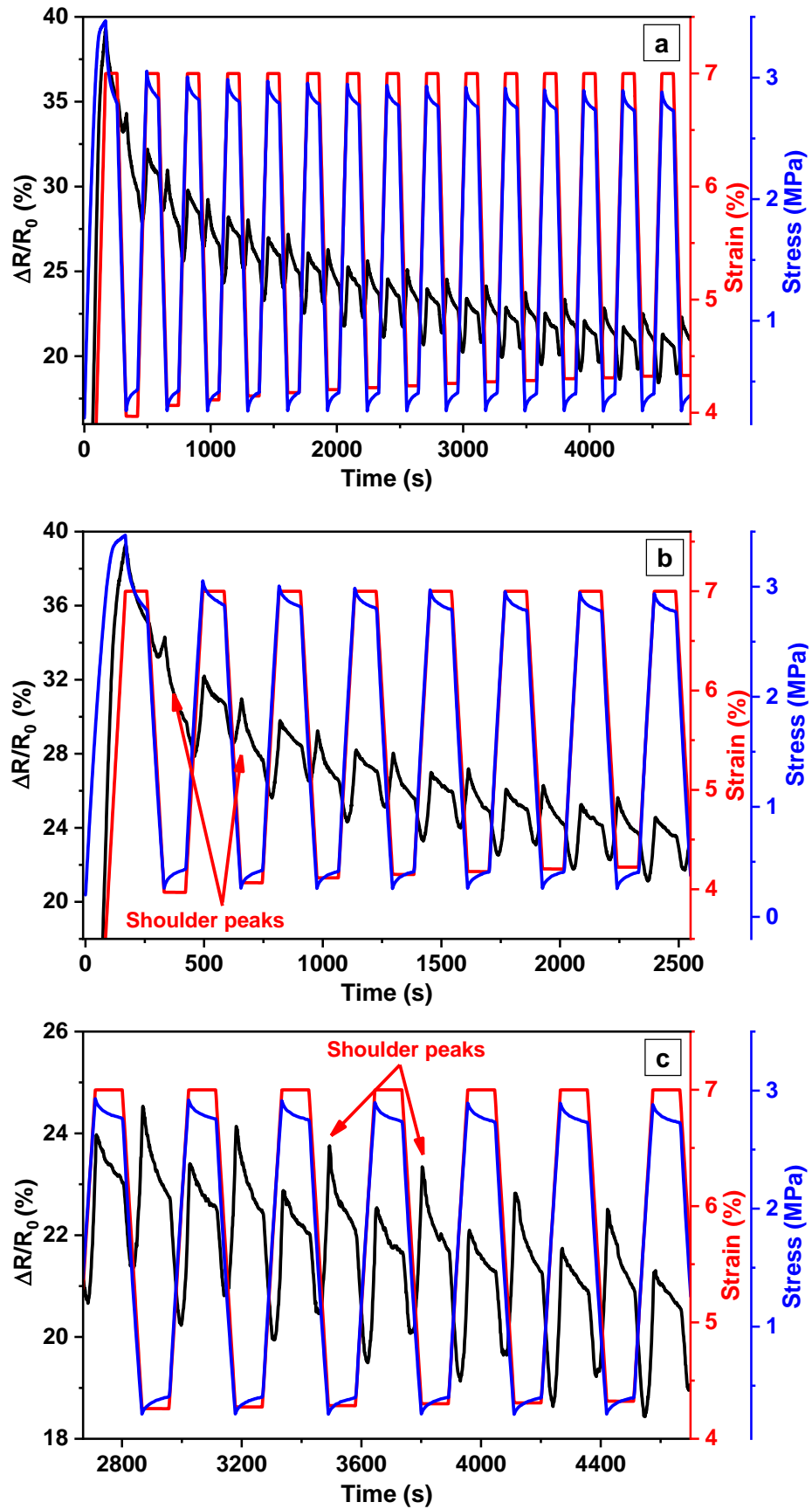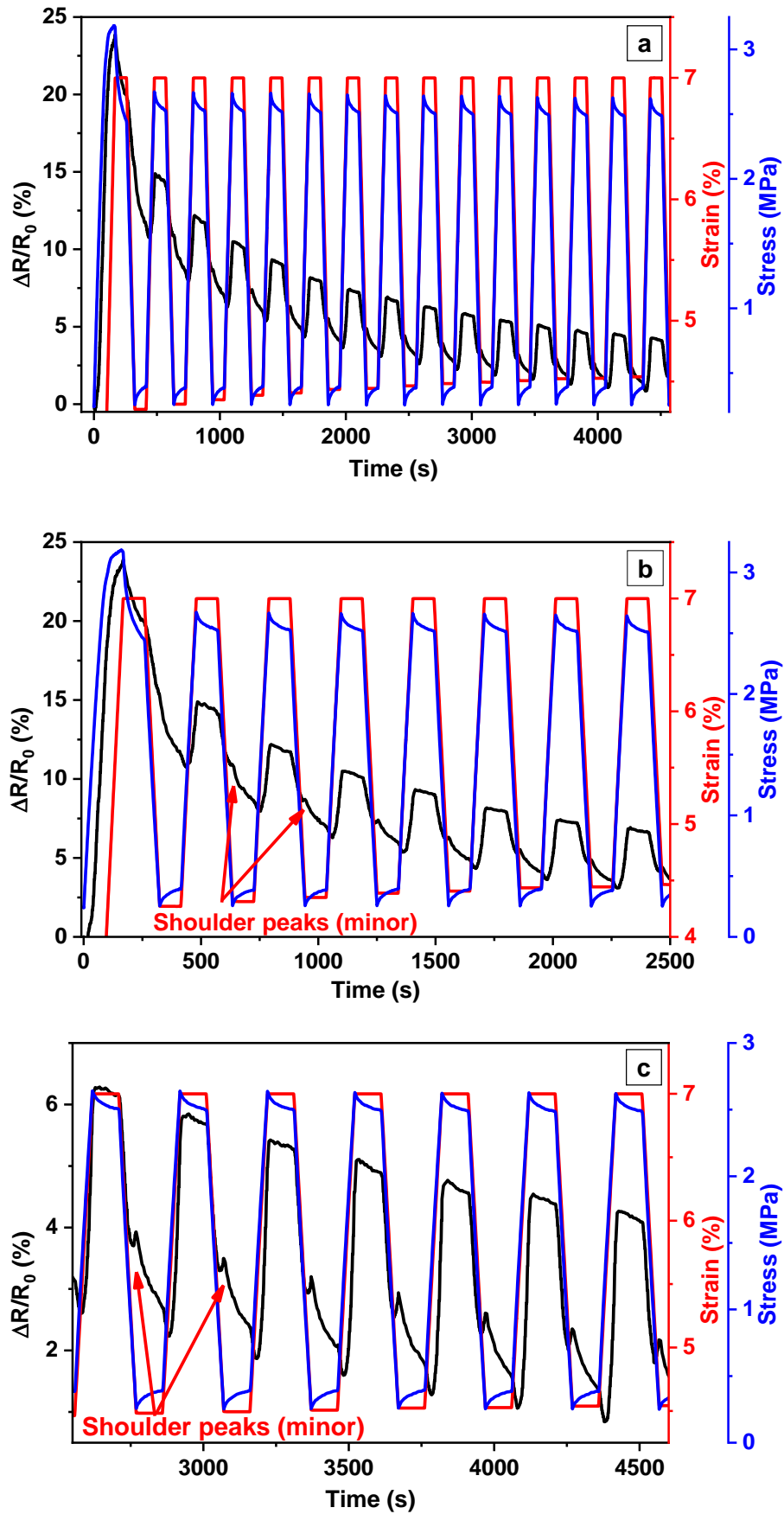
Figure 36: (a) Cyclic strain test of PBAT/3% MWCNT-200 kGy nanocomposites at 7% strain and 15 cycles (b) highlighted first half of the test and (c) highlighted second half of the test

4.4.4. Summary of Effect of EB Irradiation

➢ Dose dependent crosslinking of neat PBAT occurred only above the irradiation dose of 150 kGy. It is indicated by the reduced solubility of PBAT irradiated with 200 kGy and gel formation in its solution when dissolved in chloroform. Degree of crosslinking of 51%, 62% and 73% were determined at the irradiation dose of 200, 250 and 300 kGy, respectively.

➢ Tensile test of irradiated PBAT and PBAT/MWCNT nanocomposites confirmed the effect of crosslinking only on their elongation at break. This value of neat PBAT increased by 19% at 150 kGy. On the other hand, it is decreased by 12 and 27% at the crosslinking degree of 62 and 73%, respectively. Meanwhile, tensile modulus and tensile strength of irradiated PBAT remains unchanged. Similarly, value of elongation at break of irradiated PBAT/MWCNT nanocomposites was decreased by 11%, 20% and 43% at the dose of 150, 200 and 300 kGy, respectively. Tensile modulus and tensile strength of irradiated nanocomposites remained unaltered as that of the irradiated PBAT. It leads the nanocomposites to higher elastic deformability of the irradiated nanocomposites. This conclusion is further supported by the change in dose dependent change of micromechanical behavior of the irradiated nanocomposites. Increased maximum indentation depth, decreased Martens hardness and indentation modulus, and increasing ratio of elastic to plastic work of deformation of the irradiated PBAT/3% MWCNT nanocomposites are in the favour of this conclusion.

➢ Electron beam irradiation induced branching and crosslinking of polymer matrix enhanced the strain sensing behaviour of CPC. It is implied by the improved strain sensing behaviour of EB irradiated PBAT/3% MWCNT nanocomposites. $\Delta R/R_0$ values of these nanocomposites fitted well up to 10% mechanical strain which was only up to 8% strain for unirradiated nanocomposites. Meanwhile, critical strain value of the irradiated composites increased to 3% from 1% (unirradiated samples) due to the reduced CNT-PBAT interfacial interaction carried out by PBAT branching (at 150 kGy) and crosslinking (at 200 kGy, degree of crosslinking: 51%). However, $\Delta R/R_0$ values with no correlation with strain applied, as performed by the nanocomposites irradiated with higher dose (300 kGy, degree of crosslinking: 72%) reveals the formation of a 3D crosslinked PBAT-network. It restricts the homogeneous deformation and relaxation of conductive MWCNT-network by the mechanical strain.

➢ Results of cyclic strain test of irradiated composites with 7% strain and 15 cycles performed the lower shoulder peaks (at 150 kGy) and even the minor peaks (dose: 200 kGy). On the basis of these results, it is concluded that EB irradiation induced crosslinking of polymer matrix of CPC up to a moderate degree can be a strategy to improve the strain sensing behavior of CPC.

4.5. Thermal Properties of Nanocomposites

Thermal properties of polymeric materials greatly influence their performance during applications. Therefore, thermal properties (thermal stability, melting and crystallization behavior) of PBAT/MWCNT nanocomposites are investigated. Thermal stability of nanocomposites is investigated by thermogravimetric analysis (TGA) whereas, their thermal transitions, crystallization behavior are analysed by differential scanning calorimetry (DSC). Characteristic thermal decomposition pattern of the polymer matrix and the corresponding nanocomposites as a function of increasing temperature will be evaluated by TGA. Initial degradation temperature (T_{onset}), temperature of maximum degradation (T_{max}) and final degradation temperature (T_f) are taken into account to investigate the thermal stability of the nanocomposites. Similarly, melting behavior of materials will be investigated by the evaluation of melting temperature (T_m) and the enthalpy of melting (ΔH_m); whereas crystallization behavior will be analysed taking crystallization temperature (T_c), enthalpy of crystallization (ΔH_c) and the degree of crystallinity (X_c) into account. Corresponding TGA and DSC results of neat PBAT and PBAT/MWCNT nanocomposites (both unirradiated and EB irradiated) are discussed in this section.

4.5.1. Thermal Properties of Unirradiated Nanocomposites

Thermogravimetric Analysis (TGA): Thermogravimetric mass loss curves and corresponding first differential curves of pure PBAT and some of the PBAT/MWCNT nanocomposites (1, 2, 3, 6 and 10 wt.-% of MWCNT) are presented in **Figure 37a** and **b**, respectively. The effect of presence of MWCNT on thermal stability of PBAT/MWCNT nanocomposites are evaluated. The TGA curves are analyzed to determine the T_{onset}, T_f, and the temperature range of severe degradation of the materials, whereas differential curves are used to determine $T_{max.}$ Nanocomposites with low MWCNT content (up to 3 wt.-%) are mainly targeted for the investigation of the effect of low concentration of MWCNT and the trend of this effect at higher MWCNT concentration in comparison to polymer matrix. Similarly, the composites with higher CNT content (6 and 10 wt.-%) will be targeted to analyse the effect of higher CNT concentrations on thermal stability of the nanocomposites. The corresponding results of TGA are listed in **Table 16**.
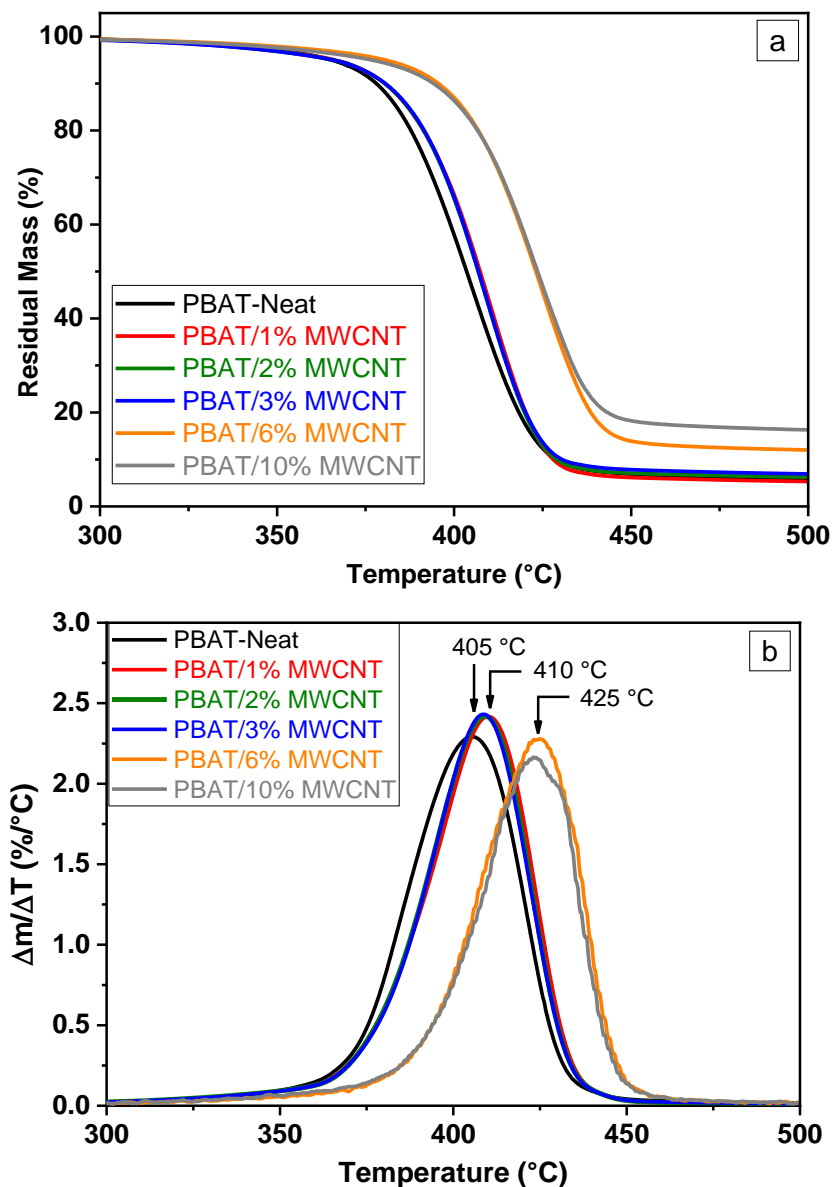
Figure 37: (a) TGA mass loss curves and (b) their first derivative curves of neat PBAT and PBAT/MWCNT nanocomposites

Figure 37a suggests a single step thermal degradation of PBAT and PBAT/MWCNT nanocomposites. Severe mass loss of PBAT occurs from 371 to 430 °C in which maximum degradation takes place at 405 °C (as suggested by DTG curve in **Figure 37b**. Initial degradation temperature (T_{onset}) of PBAT/MWCNT nanocomposites (371 °C) is increased to 374 °C (1 to 3 wt.-% MWCNT) and 388 °C (6 and 10 wt.-% MWCNT) revealing an increased thermal stability of nanocomposites by the presence of MWCNT. However, the trend of increasing thermal stability with increasing filler concentration is not clearly distinguishable among the nanocomposites with low CNT

content (1 to 3 wt.-% of MWCNT) and that between the nanocomposites with 6 and 10 wt.-% MWCNT.

The maximum thermal degradation of nanocomposites with low CNT content takes place at ~410 °C, while the nanocomposites with 6 and 10 wt.-% CNT content degrade the most at ~425 and 423 °C respectively according to the DTG curves in **Figure 37b** and the data presented in **Table 16**. Higher T_{max} values of PBAT/MWCNT nanocomposites if compared to neat PBAT (405 °C) and its increasing values with increasing MWCNT content in the nanocomposites suggest an enhanced interfacial adhesion of MWCNT in PBAT matrix (Mohanty & Nayak, 2009). Higher CNT content in the nanocomposites retards the chain mobility of polymer matrix that controls the chain unzipping during thermal degradation (Zhang *et al.*, 2019). Similarly, final degradation temperature (T_f) of nanocomposites is found to increase with increasing MWCNT content. These results also suggest an increased thermal stability of nanocomposites (Teamsinsungvon *et al.*, 2013; Xu *et al.*, 2019).

Table 16: TGA data of neat PBAT and PBAT/MWCNT nanocomposites

Samples	T_{max} (°C)	Weight loss (%)	Residue (%)
PBAT-neat	405	94.8	4.4
PBAT/1% MWCNT	410	95.2	4.7
PBAT/2% MWCNT	409	94.3	5.9
PBAT/3% MWCNT	409	93.5	6.3
PBAT/6% MWCNT	425	88.8	10.2
PBAT/10% MWCNT	423	84.6	14.1

Higher values of $T_{onset,}$ T_{max} and T_f imply an increased thermal stability of nanocomposites with the increased CNT content. Enhanced thermal stability of the nanocomposites is attributed to the high thermal stability of CNT (~2800 °C), their uniform distribution throughout the nanocomposites and good PBAT-CNT physical type of interfacial interaction (with lower interfacial tension, assuggested by FTIR spectroscopy) (Das *et al.*, 2018; Hong *et al.*, 2012; Ko *et al.*, 2009; Rosenberger *et al.*, 2020; Zhang *et al.*, 2019). CNT always have a good interfacial interaction with lower interfacial tension with the polymers comprising aromatic ring which is present in BT unit of PBAT (Ko *et al.*, 2009). The results discussed here are consistent with that reported in literature (Sirisinha & Somboon, 2011). Although thermal stability of nanocomposites is found to increase with increasing filler concentration, it can be

saturated at higher CNT concentration (at or above 10 wt.-%) because of filler non-wetting effect by the polymer melts as discussed in chapter 4.2.2.

From **Table 16**, residue of nanocomposite left at 800 °C after the complete degradation of PBAT seems to increase with increasing filler content. This is obviously due to the increasing CNT content of nanocomposites which can't be degraded by thermal treatment in the temperature range of this experiment.

Differential Scanning Calorimetry (DSC): Crystallization behavior and the corresponding thermal transitions of PBAT-neat and PBAT/MWCNT nanocomposites are analysed by DSC. DSC thermograms of first heating scan, cooling scan and second heating scan of polymer matrix and that of nanocomposites are presented in **Figure 38 (a-c)**, respectively. Similarly, thermal parameters (calculated from DSC curves) corresponding to DSC results are presented in **Table 17**.

DSC thermograms of first heating scan show three transitions of temperature, signifying glass transition temperature (T_g), first melting point (T_{m1}) and second melting point (T_{m2}) from left to right, respectively as illustrated in **Figure 38a**. Similarly, thermograms of cooling and second heating scans exhibit two temperature transitions from left to right signifying T_g and T_m, respectively. It seems that there is not a uniform trend of change of T_g with the increasing CNT concentration in nanocomposites. Its value is almost unchanged at lower CNT concentration, however, it is increased by 3 and 4°C on the addition of both 6 wt.-% and 10 wt.-% of MWCNT, respsctively. Change in T_g of polymers with the presence of MWCNT suggests a matrix-filler interfacial interaction (González Seligra *et al*., 2016).

Two melting temperatures, T_{m1} and T_{m2} exhibited by the thermograms of first heating scan correspond to the melting of crystals of soft BA unit of PBAT and the melting of co-crystals of BT and BA units of PBAT, respectively (Rosenberger *et al*., 2020). The crystals of BA unit adjust into the crystals of BT unit by the process of co-crystallization, fitting the perfect crystal structure of PBAT. Segments of adipic acid and terephthalic acid present in PBAT are of similar length by which BA unit fits into BT unit due to the process of co-crystallization. Two melting points are not shown by the second heating thermograms (González Seligra *et al*., 2016; Pietrosanto *et al*., 2020; Teamsinsungvon *et al*., 2013; Yang & Qiu, 2011). Value of T_{m1} is increased with higher MWCNT content of the nanocomposites, however, T_{m2} values in both first and second heating scans seem to be decreased with increasing MWCNT concentration. Lower value of T_{m2} corresponds to the formation of improper crystals due to the confinement

of CNT on polymer chains, controlling their mobility. This effect slows down the process of crystallization (González Seligra *et al.*, 2016). As a result, value of X_c is in decreasing order with increasing MWCNT content in the nanocomposites.
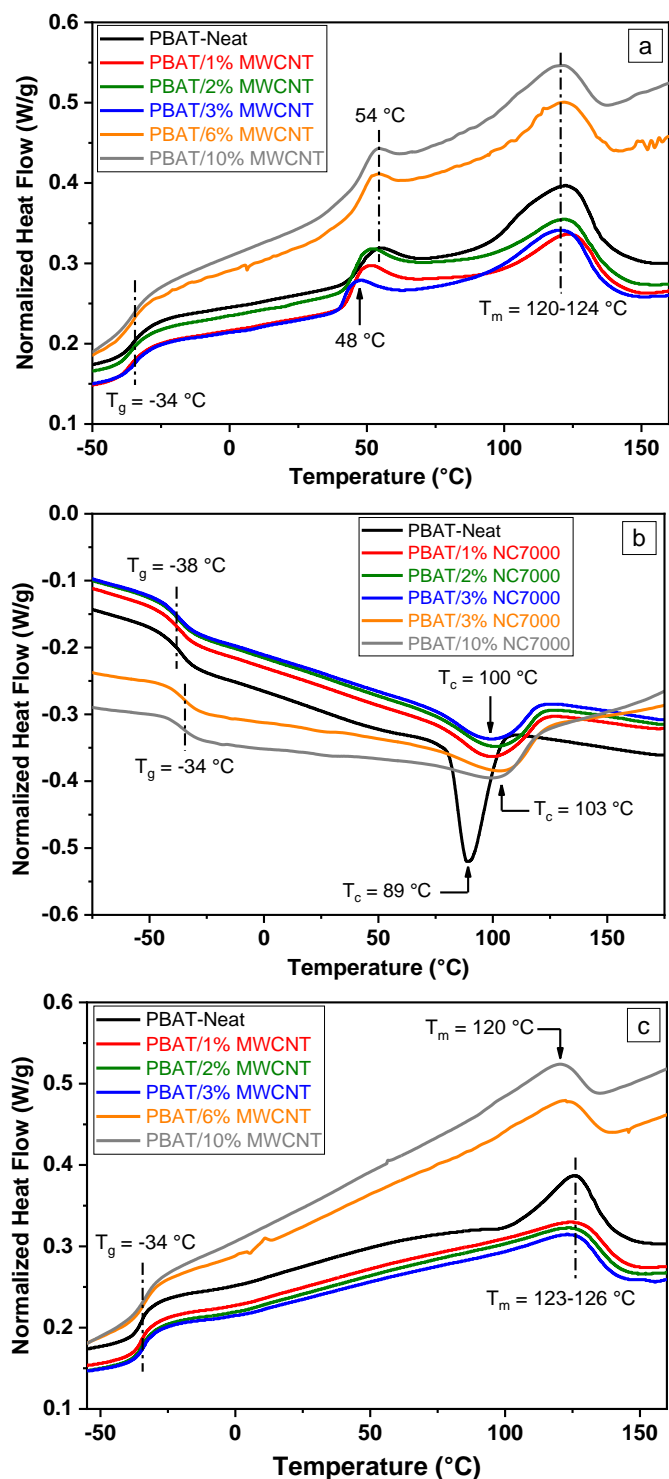
Figure 38: DSC thermograms of neat PBAT and PBAT/MWCNT nanocomposites: (a) first heating (b) cooling and (c) second heating

From **Table 17**, it seems that the values of enthalpy of fusion (ΔH_{m}) and degree of crystallization (χ_{c}) significantly decrease with increasing CNT content in the nanocomposites. It can be seen that value of χ_{c} is almost unchanged at 1 and 2 wt.-% of MWCNT. It is due to the nucleation effect (heterogeneous) of MWCNT which enhances the chain mobility at lower CNT concentration. However, mobility of polymer chains is blocked at higher CNT content (Rodrigues *et al*., 2016; Xu *et al.,* 2019) and the degree of crystallinity decreases. The value of χ_{c} is reduced to 27.1 and 21.0% on the addition of 3 and 10 wt.-% of MWCNT, respectively. Decrease in T_{m}, ΔH_{m}, X_{c} with increasing filler content implies that the extent of the process of crystallization is decreased and the less perfect crystals are formed at higher filler concentrations. At higher MWCNT content, the melt viscosity of the composites will increase which obstructs the chain mobility of PBAT leading to the formation of imperfect crystals (Fukushima *et al*., 2012; Hong *et al*., 2012; Sirisinha & Somboon, 2011). On the other hand, crystallization temperature (T_c) is significantly increased with the increasing filler concentration in nanocomposites as performed by cooling scan thermograms which facilitates the process of crystallization and the size of crystals formed enhancing the process of nucleation (Giri *et al*., 2021; Xu *et al*., 2019). Value of T_c is increased from 89 to 105 °C on the addition of 10 wt.-% MWCNT. Process of crystallization of PBAT, occurring below 105 °C is reported by Behera *et al.* (Behera *et al*., 2020).

Table 17: DSC Data of neat PBAT and PBAT/MWCNT nanocomposites

Samples	DSC first heating			DSC cooling		DSC second heating			
	T_{m} (°C)	ΔH_{m} (J g^{-1})	χ_{c} (%)	T_{c} (°C)	ΔH_{c} (J g^{-1})	T_{g} (°C)	T_{m} (°C)	ΔH_{m} (J g^{-1})	χ_{c} (%)
PBAT-Neat	122.3	38.4	33.7	89.2	28.1	−37.5	125.8	33.9	29.7
PBAT/1% MWCNT	123.5	32.0	28.3	99.8	25.7	−38.0	124.4	32.0	28.3
PBAT/2% MWCNT	121.9	39.2	35.1	99.7	24.6	−38.0	123.7	32.7	29.3
PBAT/3% MWCNT	120.4	34.6	31.3	101.3	23.3	−38.0	123.2	30.0	27.1
PBAT/6% MWCNT	120.3	30.5	28.5	106.9	26.6	−34.5	121.3	23.2	21.7
PBAT/10% MWCNT	120.2	27.3	26.6	105.0	30.2	−33.5	119.7	21.6	21.0

Increasing trend of T_c suggests that MWCNT act as heterogeneous nucleating agent which increase the crystallization sites in the PBAT/MWCNT nanocomposites and promotes the rearrangement of chains of PBAT leading to the formation of more ordered crystals (Fukushima *et al*., 2012; Mohanty & Nayak, 2009). Hence, increase in the value of T_c PBAT/MWCNT nanocomposites is in favour of the crystallization

process of PBAT regardless the trend of enthalpy of crystallization and melting; and melting temperature.

4.5.2. Thermal properties of EB Irradiated Nanocomposites

Thermogravimetric Analysis (TGA): Thermal stability of EB irradiated PBAT/MWCNT nanocomposites were investigated by TGA measurements of PBAT/3% MWCNT nanocomposites, irradiated with different doses (150, 200 and 300 kGy). TGA and DTG curves of the EB irradiated PBAT/3% MWCNT nanocomposites are presented in **Figure 39 (a, b)**, respectively. The corresponding TGA results are presented in **Table 18**. TGA and DTG curves and the corresponding results of unirradiated PBAT/3% MWCNT nanocomposites are also presented for the comparative analyses.

From Figure 39a, it seems that T_{onset} of EB irradiated composites is slightly lower than that of unirradiated composites. It decreased from 374 °C (unirradiated composites) to 370 °C (irradiated composites). In the same way, T_{max} values of unirradiated and irradiated samples are 409 °C and 402 °C, respectively. T_{max} of irradiated composites is lower even than that of neat polymer matrix which is 405 °C. Such a decrease in thermal stability and T_{max} of EB irradiated nanocomposites is attributed to the irradiation induced degradation of polymer matrix (Pietrosanto *et al*., 2020; Rzepna *et al*., 2018; Zhao *et al*., 2020). However, values of T_f of irradiated nanocomposites is found almost unchanged.
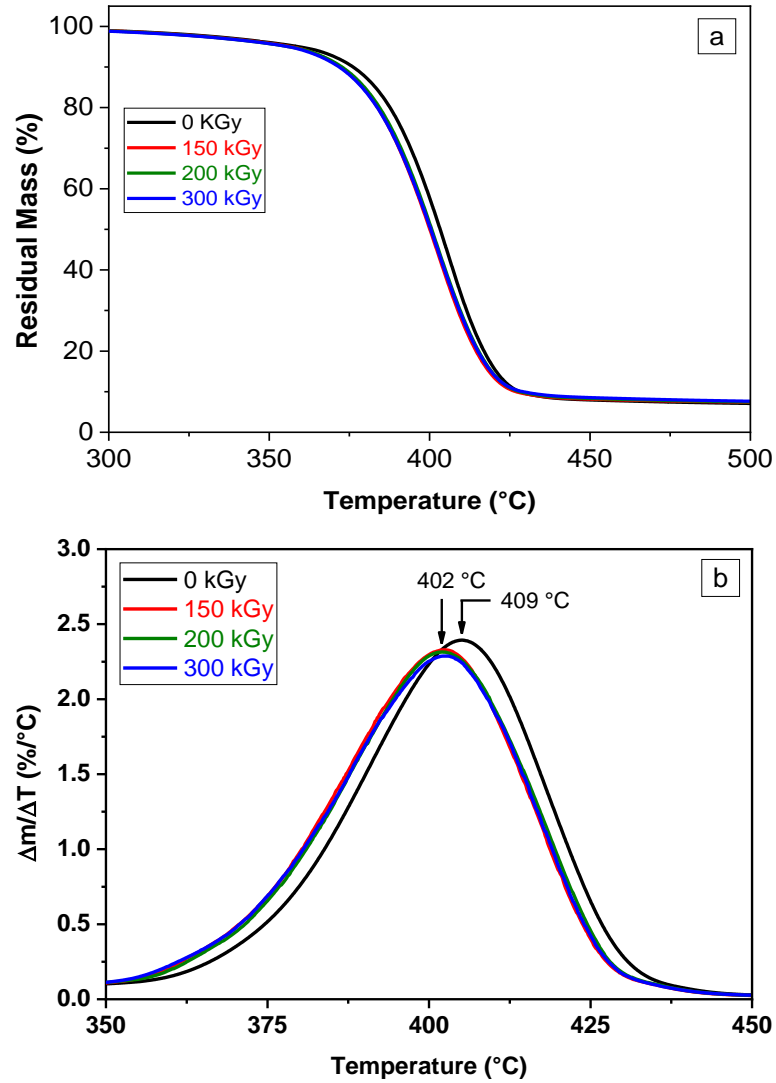
Figure 39: (a) TGA mass loss curves and their (b) first derivative curves of EB irradiated PBAT/3% MWCNT nanocomposites with different doses

Table 18: TGA Data of EB irradiated PBAT/3% MWCNT nanocomposites

Samples	T_{max} (°C)	Weight loss (%)	Residue (%)
PBAT/3% MWCNT -0 kGy	409	92.5	6.3
PBAT/3% MWCNT -150 kGy	402	94.3	5.9
PBAT/3% MWCNT -200 kGy	402	93.2	6.8
PBAT/3% MWCNT -300 kGy	403	92.8	7.0

The effect of EB irradiation on thermal stability and the variation of T_{max} seems independent of irradiation dose used in this work. Similarly, unchanged values of residue left at 800 °C (**Table 18**) implies no effect of irradiation on CNT because both unirradiated and irradiated samples contain 3 wt.-% of fillers.

Differential Scanning Calorimetry (DSC): DSC thermograms of PBAT/3% MWCNT nanocomposites irradiated with different doses (150, 200 and 300 kGy) and the corresponding DSC data are presented in **Figure 40 (a-c)**, and **Table 19**, respectively.
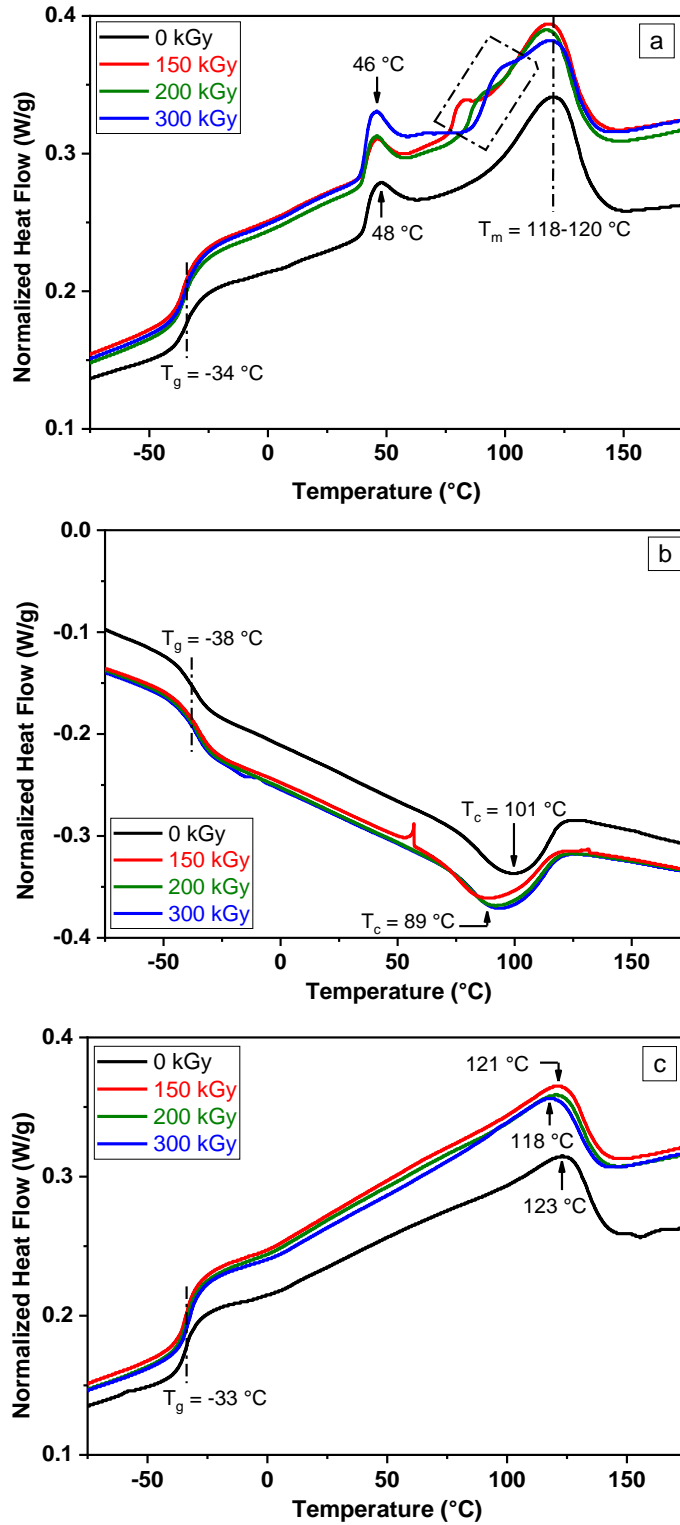
Figure 40: DSC thermograms of unirradiated and EB-irradiated PBAT/3% MWCNT nanocomposites: (a) first heating (b) cooling and (c) second heating with different dose

Table 19: DSC data of EB irradiated PBAT/3% MWCNT nanocomposites

Samples	DSC first heating			DSC cooling		DSC second heating			
	T_m (°C)	ΔH_m (J g^{-1})	χ_c (%)	T_c (°C)	ΔH_c (J/g)	T_g (°C)	T_m (°C)	ΔH_m (J g^{-1})	χ_c (%)
PBAT/3% MWCNT -0 kGy	120.4	34.6	31.2	101.3	23.3	–38.0	123.2	30.0	27.1
PBAT/3% MWCNT -150 kGy	118.5	33.4	30.2	88.9	24.7	–38.5	121.1	30.5	27.6
PBAT/3% MWCNT -200 kGy	117.5	34.8	31.5	91.9	24.6	–38.0	120.5	30.0	27.1
PBAT/3% MWCNT -300 kGy	119.0	34.4	31.1	93.7	23.3	–38.0	118.1	27.1	24.5

Table 19 suggests an overall decreasing trend of T_m, ΔH_m, T_c and χ_c of irradiated nanocomposites with increasing irradiation dose. Even the values of T_{m1} performed by the thermograms in first heating, corresponding to melting temperatures of crystals of BA units of PBAT decreases with increasing dose of irradiation. Meanwhile, χ_c values from first heating scans seem slightly increased, however, they decrease in second heating scan particularly with 300 kGy dose. Decrease in these thermal parameters of nanocomposites with same CNT content with increasing irradiation dose is attributed to the slightly declined molecular weight of polymer matrix due to material degradation (minor) carried out by EB irradiation and increase in branching density of polymer matrix in irradiated nanocomposites. Higher branching density of polymers controls the process of crystallization which is exhibited by the composites irradiated with 300 kGy (Pietrosanto *et al*., 2020; Rzepna *et al*., 2018). Despite the irradiation resistance of PBAT at lower dose, it is degraded through aliphatic ester group at higher dose (used in this work) (Rzepna *et al*., 2018; Zhao *et al.*, 2020). Decrease in degree of crystallization is also attributed to the irradiation induced polymer degradation and decrease in molecular weight, however, dose dependent degradation effect could not be distinguished between different doses which can be expected at higher doses than that is used in this work.

T_g of EB irradiated PBAT/MWCNT nanocomposites seems unchanged by the irradiation with in this dose. Increased value of T_g of EB irradiated PBAT based composites, attributed to the formation of a 3D crosslinks PBAT-network is reported in literature (Hwang *et al*., 2010), however, this is not noticed in this work.

4.5.3. Summary of Thermal Properties

➤ TGA analyses of PBAT-neat and PBAT/MWCNT nanocomposites shows the enhanced thermal stability of the nanocomposites compared to that of neat PBAT. Increased T_{onset}, T_{max} and T_f values of the nanocomposites with the increasing MWCNT concentration imply the enhanced thermal stability. High thermal stability of MWCNT, their uniform distribution in the nanocomposites during melt-mixing, good filler-matrix interaction and the affinity of MWCNT with PBAT (due to the presence of aromatic ring) may be attributed to be responsible for the improved thermal stability of the nanocomposites.

➤ Thermal stability of EB irradiated nanocomposites is found to reduce, however, up on EB irradiation, values of both T_{onset} and T_{max} are decreased and that of T_f. remained unchanged. Decrease in molecular weight of polymer matrix due to the irradiation might be the reason behind this effect.

➤ DSC analysis of nanocomposites in comparison to neat PBAT suggest an unchanged T_g and significantly increased T_c. On the other hand, values of T_m, ΔH_m, ΔH_c, and X_c decrease with increasing CNT concentration in the nanocomposites. These results imply that MWCNT act as heterogeneous nucleating agent in the nanocomposites retarding the mobility of PBAT chains. As a result, the process of crystallization will also be retarded and the less perfect crystals will be formed. However, increasing value of T_c compensates the process of PBAT crystallization increasing the crystal size and the number of crystallization sites in the nanocomposites. Meanwhile, first heating scan of DSC exhibits two melting peaks around at 48 °C and 120 °C. The first melting temperature corresponds to the melting of crystals of BA unit of PBAT formed during melt-mixing. These crystals of BA adjust into crystals of BT units later by the process of co-crystallization forming perfect PBAT crystals whose melting temperature is signified by the second peak around at 120 °C.

➤ The effect of EB irradiation can also be noticed in the DSC analysis of irradiated nanocomposites. The value of T_m, ΔH_m, T_c and χ_c of the irradiated nanocomposites, are decreased with irradiation. Decrease in χ_c is significant with the dose 300 kGy. This result of DSC is consistent with that of tensile and microindentation tests. Even the value of T_{m1} corresponding to the melting of BA crystal, possessed by first heating scans is decreases from 48 °C to 46 °C.

CHAPTER 5

5. CONCLUSIONS AND RECOMMENDATIONS FOR FUTURE WORKS

This chapter summarizes the outcome and the conclusions drawn from the entire research work. Incorporation of MWCNT into PBAT matrix imparted various physical properties in the development of morphology and microstructure of PBAT/MWCNT nanocomposites. Study of deformation behavior of the materials in correlation with their electrical properties have been the primary objective of this research work.

5.1. Conclusions

➢ Melt-mixed flexible and electrically conductive PBAT/MWCNT nanocomposites have been successfully fabricated.

➢ Different microscopic techniques such as scanning electron microscopy (SEM), transmission electron microscopy (TEM) and transmission light microscopy (TLM) altogether revealed uniform MWCNT distribution throughout the polymer matrix. Uniform surface morphology of nanocomposites with a net-like CNT-network formed by CNT-CNT connection is implied by scanning electron microscopy (SEM). A low rate of agglomeration of MWCNT and the uniform distribution of agglomerates are suggested by TEM and TLM. Agglomerate area ratio (A/A_0) in the range of 0.27 to 1.26 suggests a low MWCNT aggregation.

➢ Comparative analyses of Fourier transform infrared (FTIR) spectra of neat PBAT and PBAT/MWCNT nanocomposites reveal a physical type of binding force between polymer matrix and filler. The interfacial adhesion of filler onto the matrix is responsible for the formation of nanocomposite microstructure.

➢ Increasing slope of tensile stress-strain curves with higher concentration of MWCNT in nanocomposites implies the mechanical reinforcement of nanocomposites by MWCNT. It is further supported by the elevated Martens hardness (HM) and indentation modulus (E_{IT}), and lowered maximum indentation depth (h_{max}) of nanocomposites. Formation of micro-voids and cracks in the nanocomposites at higher filler concentration is revealed by the decreasing ratio of elastic to plastic work of deformation i.e. 3.25 (neat PBAT) to 2.13 (PBAT/5% MWCNT nanocomposites).

- Achievement of comparatively low percolation threshold (between 0.5 to 1 wt.-% of MWCNT) is due to uniform filler dispersion, low rate of agglomeration. Relative resistance change ($\Delta R/R_0$), increased in a non-linear and exponential-like manner as a function of mechanical strain during tensile stretching of nanocomposites confirms their piezoresitivity. Range of volume resistivity (6.90×10^5 Ω.cm to 1.24×10^1 Ω.cm) of electrically conductive PBAT/MWCNT nanocomposites and their piezoresitivity reveal their potential of strain sensing applications. Fitting of $\Delta R/R_0$ maxima at low mechanical strain (2 to 8%) in cyclic strain test confirms their low-strain sensing potential. Moreover, improved fitting of $\Delta R/R_0$ maxima with strain (up to 10%) with minor shoulder peaks during cyclic strain test of PBAT/MWCNT nanocomposites, crosslinked by electron beam (EB) irradiation suggests EB irradiation induced crosslinking as a strategy to improve their elastic properties leading to improved strain sensing behavior. Meanwhile, resistance change of nanocomposites irradiated with the highest dose (300 kGy) in an irregular way performing no fitting of resistance maxima with mechanical strain suggest the application of this method only up to a moderate dose of irradiation.

- Enhanced thermal stability of PBAT/MWCNT nanocomposites with the incorporation of MWCNT into PBAT is revealed by thermogravimetric analysis (TGA). A good MWCNT-PBAT interfacial interaction and uniform dispersion in the nanocomposites are responsible for enhanced thermal stability. Differential scanning calorimetry (DSC) studies of PBAT/MWCNT nanocomposites suggest an unchanged glass transition temperature (T_g), increased crystallization temperature (T_c), decreased melting temperature (T_m), enthalpy of melting (ΔH_m) and enthalpy of crystallization (ΔH_c). As a consequence, decreased crystallinity (χ_c) is achieved signifying that MWCNT act as a heterogeneous nucleating agent retarding the polymer crystallization. Furthermore, slightly decreased thermal stability of EB irradiated nanocomposites (with same filler concentration) implies the minor degradation of polymer matrix by EB irradiation. Reduced crystallinity (χ_c) of irradiated nanocomposites is attributed to the retarded chain mobility of PBAT by the crosslinks

5.2. Recommendations for Future Works

Based on the above listed findings and conclusions, following recommendations are put forward for future works.

➤ Investigation of strain sensing behavior of PBAT/MWCNT nanocomposites applying higher mechanical strain (beyond 10%) and reproducibility of change in electrical resistance with maximum number of cycles would be worthy.

➤ Exploration of more strategic methods to improve the elastic properties and strain sensing performance of PBAT/MWCNT nanocomposites to prepare biodegradable strain sensors addressing the existing plastic waste problem.

➤ Investigation of strain sensing behavior of PBAT/MWCNT nanocomposites using PBAT with varied molar ratio of BA and BT units to investigate the variation in elastic properties and the rate of biodegradation.

CHAPTER 6

6. SUMMARY

As per the aim of fabrication of biodegradable CPC and investigate their piezoresistivity and strain sensing behavior, PBAT/MWCNT nanocomposites were prepared by the method of microcompounding followed by compression moulding. PBAT was taken as a biodegradable, flexible and stretchable polymer matrix whereas MWCNT were taken as conductive filler. Investigation of morphology, structure, deformation behavior, electrical conductivity, thermal stability and crystallization behavior of the nanocomposites was carried out. Deformation behavior of nanocomposites was correlated with their electrical properties targeting their piezoresistive strain sensing behavior. Low-strain sensing capacity of PBAT/MWCNT nanocomposites opened the door to explore for a strategic method to enhance their strain sensing capacity. Crosslinking the PBAT/MWCNT nanocomposites by EB irradiation was employed as a strategy to improve the elastic deformability (essential for strain sensing) of the nanocomposites. This strategy was found applicable up to a moderate dose of irradiation.

Chapter 1 introduces an overall research work, provides an overview of related works and draws a research gap from the survey of reported works. It includes the aim of the research work which is divided into general objective and the specific objectives. The particular works conducted to meet the objectives of the entire research project are included by the specific objectives. Similarly, it includes the research contribution, and the scope and limitations of the studies.

Chapter 2 includes a critical review of related works reported in literature. Biodegradable and electrically conductive polymer composites (CPC), their electrical conductivity and percolation theory are explained. As a research gap, this chapter mentions the necessity of investigation of piezoresistive strain sensing behavior of PBAT based biodegradable CPC. It also explains about the method of quantification of piezoresitive sensitivity of flexible and stretchable CPC. Furthermore, it puts forward electron beam (EB) irradiation, as a strategic method of crosslinking CPC to enhance their elastic deformability, summarizes the related works of PBAT, PLA/PBAT and the corresponding composites reported in literature.

Chapter 3 lists out the materials used with their physical properties and the methods employed for sample preparation. Similarly, it involves the conditions employed for the preparation of samples, tools and techniques adopted for their characterization, laboratory manuals, corresponding instruments and the conditions of measurements.

Chapter 4 of this thesis presents the overall results of entire research work, and their analyses and interpretation. The morphological and structural investigation of the nanocomposites were carried out employing different microscopic techniques and FTIR spectroscopy, respectively. Microscopic studies attested uniform filler dispersion and an interconnected MWCNT-network throughout the polymer matrix whereas a physical filler-matrix binding force with a good interfacial interaction was revealed by FTIR spectroscopy. Deformation behavior of the nanocomposites in correlation with the change in electrical resistance during tensile stretching and cyclic strain test confirmed their piezoresistive properties and strain sensing behavior, respectively. Low-strain sensing potential of nanocomposites was improved by crosslinking the polymer matrix by electron beam irradiation in order to improve their elastic properties. Increased thermal stability of nanocomposites with the presence of MWCNT is revealed by TGA whereas decreased crystallinity and the formation of less perfect crystals of polymer was attested by DSC. Similarly, slightly decreased thermal stability with lower crystallinity of EB irradiated nanocomposites was attested.

Chapter 5 of this thesis includes the general conclusions drawn from the overall research work in connection to the general and specific objectives. Recommends for new possible explorations after carrying out this work are listed. PBAT is concluded to be an efficient polymer matrix to develop flexible, biodegradable and biocompatible strain sensors. Moreover, EB irradiation (up to a moderate dose) induced crosslinking is conclusively proposed as a strategic method to enhance elastic deformability and strain sensing behavior of CPC.

Chapter 6 summarizes the content of all chapters of this thesis in brief.

REFERENCES

Adhikari, R., Bhandari, N. L., Causin, V., Le, H. H., Radusch, H.-J., Michler, G. H., & Saiter, J. M. (2012). Study of Morphology, Mechanical Properties, and Thermal Behavior of Green Aliphatic-Aromatic Copolyester/Bamboo Flour Composites. *Polymer Engineering & Science*, *52*(11): 2296–2303.
https://doi.org/10.1002/pen.23335

Al-Itry, R., Lamnawar, K., & Maazouz, A. (2012). Improvement of Thermal Stability, Rheological and Mechanical Properties of PLA, PBAT and Their Blends by Reactive Extrusion with functionalized Epoxy. *Polymer Degradation and Stability*, *97*(10): 1898–1914.
https://doi.org/10.1016/j.polymdegradstab.2012.06.028

Al-Itry, R., Lamnawar, K., Maazouz, A., Billon, N., & Combeaud, C. (2015). Effect of the Simultaneous Biaxial Stretching on the Structural and Mechanical Properties of PLA, PBAT and Their Blends at Rubbery State. *European Polymer Journal*, *68*(May): 288–301. https://doi.org/10.1016/j.eurpolymj.2015.05.001

Alamusi, Hu, N., Fukunaga, H., Atobe, S., Liu, Y., & Li, J. (2011). Piezoresistive Strain Sensors Made from Carbon Nanotubes Based Polymer Nanocomposites. *Sensors*, *11*(11): 10691–10723. https://doi.org/10.3390/s111110691

Almahri, S., Schneider, J., Schiffer, A., & Kumar, S. (2022). Piezoresistive Sensing Performance of Multifunctional MWCNT/HDPE Auxetic Structures Enabled by Additive Manufacturing. *Polymer Testing*, *114*(June): 107687.
https://doi.org/10.1016/j.polymertesting.2022.107687

Amjadi, M., Pichitpajongkit, A., Lee, S., Ryu, S., & Park, I. (2014). Highly Stretchable and Sensitive Strain Sensor Based on Silver Nanowire-Elastomer Nanocomposite. *ACS Nano*, *8*(5): 5154–5163. https://doi.org/10.1021/nn501204t

Amjadi, M., Yoon, Y. J., & Park, I. (2015). Ultra-stretchable and Skin-mountable Strain Sensors Using Carbon Nanotubes-Ecoflex Nanocomposites. *Nanotechnology*, *26*(37): 375501. https://doi.org/10.1088/0957-4484/26/37/375501

Baltá Calleja, F. J., Bayer, R. K., & Ezquerra, T. A. (1988). Electrical Conductivity of Polyethylene-Carbon-Fibre Composites Mixed with Carbon Black. *Journal of Materials Science*, *23*(4): 1411–1415. https://doi.org/10.1007/BF01154609

Barron, A., & Sparks, T. D. (2020). Commercial Marine-Degradable Polymers for Flexible Packaging. *IScience*, *23*(8): 101353. https://doi.org/10.1016/j.isci.2020.101353

Behera, K., Veluri, S., Chang, Y. H., Yadav, M., & Chiu, F. C. (2020). Nanofillers-Induced Modifications in Microstructure and Properties of PBAT/PP Blend: Enhanced Rigidity, Heat Resistance, and Electrical Conductivity. *Polymer*, *203*(June): 122758. https://doi.org/10.1016/j.polymer.2020.122758

Bhandari, N. L. (2014). *Morphology and Deformation Behaviour of Natural Fibers-Thermoplastics Composites* (Unpublished doctoral dissertation). Central Department of Chemistry, Institute of Science and Technology, Tribhuvan University, Kathmandu, Nepal.

Bhandari, N. L., Thomas, S., Das, C. K., Saiter, J. M., Micher, G. H., Pandey, D. P., & Adhikari, R. (2013). Morphology and Some Physical Properties of Eco-friendly Bamboo Flour Reinforced Plastics Composites. *The Journal of University Grants Commission*, *2*(1): 38–49.

Bhawal, P., Ganguly, S., Das, T. K., Mondal, S., Nayak, L., & Das, N. C. (2019). A comparative Study of Physico-mechanical and Electrical Properties of Polymer-carbon Nanofiber in Wet and Melt Mixing Methods. *Materials Science and Engineering B: Solid-State Materials for Advanced Technology*, *245*(May): 95–106. https://doi.org/10.1016/j.mseb.2019.05.020

Bokobza, L. (2007). Multiwall Carbon Nanotube Elastomeric Composites: A Review. *Polymer*, *48*(17): 4907–4920. https://doi.org/10.1016/j.polymer.2007.06.046

Burillo, G., Tenorio, L., Bucio, E., Adem, E., & Lopez, G. P. (2007). Electron beam irradiation effects on poly(ethylene terephthalate). *Radiation Physics and Chemistry*, *76*(11–12): 1728–1731.
https://doi.org/10.1016/j.radphyschem.2007.02.097

Calderaro, M. P., Pinheiro, I. F., de Holanda Saboya Souza, D., Clepf Pagotto, C., & Morales, A. R. (2021). PBAT/hybrid Nanofillers Composites—Part 2: Morphological, Thermal and Rheological Properties. *Journal of Applied Polymer Science*, *138*(20): https://doi.org/10.1002/app.50414

Canavese, G., Lombardi, M., Stassi, S., & Pirri, C. F. (2012). Comprehensive Characterization of Large Piezoresistive Variation of Ni-PDMS Composites. *Applied Mechanics and Materials*, *110*(*116*): 1336–1344.
https://doi.org/10.4028/www.scientific.net/AMM.110-116.1336

Canavese, G., Stassi, S., Fallauto, C., Corbellini, S., Cauda, V., Camarchia, V., Pirola, M., & Pirri, C. F. (2014). Piezoresistive Flexible Composite for Robotic Tactile Applications. *Sensors and Actuators, A: Physical*, *208*: 1–9.
https://doi.org/10.1016/j.sna.2013.11.018

Cetin, M. S., & Karahan Toprakci, H. A. (2021). Flexible Electronics from Hybrid Nanocomposites and Their Application as Piezoresistive Strain Sensors. *Composites Part B: Engineering*, *224*(August): 109199.
https://doi.org/10.1016/j.compositesb.2021.109199

Chaudhari, C. V., Dubey, K. A., Bhardwaj, Y. K., & Sabharwal, S. (2012). Radiation Processed Styrene-butadiene Rubber/Ethylene-propylene Diene Rubber/Multiple-walled Carbon Nanotubes Nanocomposites: Effect of MWNT Addition on Solvent Permeability Behavior. *Journal of Macromolecular Science, Part B: Physics*, *51*(5): 839–859. https://doi.org/10.1080/00222348.2011.610228

Chen, J., Zhu, Y., Huang, J., Zhang, J., Pan, D., Zhou, J., Ryu, J. E., Umar, A., & Guo, Z. (2021). Advances in Responsively Conductive Polymer Composites and Sensing Applications. *Polymer Reviews*, *61*(1): 157–193. https://doi.org/10.1080/15583724.2020.1734818

Chen, L., Chen, G., & Lu, L. (2007). Piezoresistive Behavior Study on Finger-sensing Silicone Rubber/Graphite Nanosheet Nanocomposites. *Advanced Functional Materials*, *17*(6): 898–904. https://doi.org/10.1002/adfm.200600519

Chivrac, F., Kadlecová, Z., Pollet, E., & Avérous, L. (2006). Aromatic Copolyester-based Nano-biocomposites: Elaboration, Structural Characterization and Properties. *Journal of Polymers and the Environment*, *14*(4): 393–401. https://doi.org/10.1007/s10924-006-0033-4

Chodák, I., Omastová, M., & Pionteck, J. (2001). Relation Between Electrical and Mechanical Properties of Conducting Polymer Composites. *Journal of Applied Polymer Science*, *82*(8): 1903–1906. https://doi.org/10.1002/app.2035

Choi, J. H., Jung, C. H., Hwang, I. T., & Choi, J. H. (2013). Preparation and Characterization of Crosslinked Poly(Butylene Adipate-*co*-Terephthalate)/Polyhedral Oligomeric Silsesquioxane Nanocomposite by Electron Beam Irradiation. *Radiation Physics and Chemistry*, *82*(1): 100–105. https://doi.org/10.1016/j.radphyschem.2012.09.005

Chongcharoenchaikul, T., Miyaji, K., Junkong, P., Poompradub, S., & Ikeda, Y. (2022). Effects of Organic Components in Cuttlebone on the Morphological and Mechanical Properties of Peroxide Cross-linked Cuttlebone/Natural Rubber Composites. *RSC Advances*, *12*(22): 13557–13565. https://doi.org/10.1039/d2ra01885c

Christ, J. F., Aliheidari, N., Ameli, A., & Pötschke, P. (2017). 3D Printed Highly Elastic Strain Sensors of Multiwalled Carbon Nanotube/Thermoplastic Polyurethane Nanocomposites. *Materials and Design*, *131*: 394–401. https://doi.org/10.1016/j.matdes.2017.06.011

Ciselli, P., Lu, L., Busfield, J. J. C., & Peijs, T. (2010). Piezoresistive Polymer Composites Based on EPDM and MWNTs for Strain Sensing Applications. *E-Polymers*, *014:* 1–13. https://doi.org/10.1515/epoly.2010.10.1.125

Clough, R. L. (2001). High-energy Radiation and Polymers: A Review of Commercial Processes and Emerging Applications. *Nuclear Instruments and Methods in Physics Research, Section B: Beam Interactions with Materials and Atoms*, *185*(1–4): 8–33. https://doi.org/10.1016/S0168-583X(01)00966-1

Costa, P., Nunes-Pereira, J., Oliveira, J., Silva, J., Moreira, J. A., Carabineiro, S. A. C., Buijnsters, J. G., & Lanceros-Mendez, S. (2017). High-performance Graphene-Based Carbon Nanofiller/Polymer Composites for Piezoresistive Sensor Applications. *Composites Science and Technology*, *153*: 241–252. https://doi.org/10.1016/j.compscitech.2017.11.001

Cranston, E., Kawada, J., Raymond, S., Morin, F. G., & Marchessault, R. H. (2003). Cocrystallization Model for Synthetic Biodegradable Poly(Butylene Adipate-*co*-Butylene Terephthalate). *Biomacromolecules*, *4*(4): 995–999. https://doi.org/10.1021/bm034089n

Cravanzola, S., Haznedar, G., Scarano, D., Zecchina, A., & Cesano, F. (2013). Carbon-Based Piezoresistive Polymer Composites: Structure and Electrical Properties. *Carbon*, *62*: 270–277. https://doi.org/10.1016/j.carbon.2013.05.064

Das, A., Adhikari, J., & Saha, P. (2018). Electrospun Polymeric Nanocarbon Nanomats for Tissue Engineering. *In Nanocarbon and its Composites: Preparation, Properties and Applications*. Elsevier Ltd. https://doi.org/10.1016/B978-0-08-102509-3.00004-3

Deshmukh, K., Ahamed, M. B., Deshmukh, R. R., Pasha, S. K. K., Sadasivuni, K. K., Polu, A. R., Ponnamma, D., AlMaadeed, M. A. A., & Chidambaram, K. (2017). Newly developed Biodegradable Polymer Nanocomposites of Cellulose Acetate and Al_2O_3 Nanoparticles with Enhanced Dielectric Performance for Embedded Passive Applications. *Journal of Materials Science: Materials in Electronics*, *28*(1): 973–986. https://doi.org/10.1007/s10854-016-5616-9

Dhakal, K. N., Khanal, S., Krause, B., Lach, R., Grellmann, W., Le, H. H., Das, A., Wießner, S., Heinrich, G., Pionteck, J., & Adhikari, R. (2022). Electrically Conductive and Piezoresistive Polymer Nanocomposites Using Multiwalled Carbon Nanotubes in a Flexible Copolyester: Spectroscopic, Morphological, Mechanical and Electrical Properties. *Nano-Structures and Nano-Objects*, *29*: 100806. https://doi.org/10.1016/j.nanoso.2021.100806

Dhakal, K. N., Krause, B., Lach, R., Wutzler, A., Grellmann, W., Le, H. H., Das, A., Wießner, S., Heinrich, G., & Adhikari, R. (2022). Electrically Conductive Nanocomposites Based on Poly(Lactic Acid)/Flexible Copolyester Blends with Multiwalled Carbon Nanotubes. *Journal of Applied Polymer Science*, *139*(4): 1–12. https://doi.org/10.1002/app.51554

Dil, E. J., Arjmand, M., Navas, I. O., Sundararaj, U., & Favis, B. D. (2020). Interface Bridging of Multiwalled Carbon Nanotubes in Polylactic Acid/Poly(Butylene Adipate-*co*-Terephthalate): Morphology, Rheology, and electrical Conductivity. *Macromolecules*, *53*(22): 10267–10277. https://doi.org/10.1021/acs.macromol.0c01525

Ding, K., Wei, N., Zhou, Y., Wang, Y., Wu, D., Liu, H., Yu, H., Zhou, C., Chen, J., & Chen, C. (2016). Viscoelastic Behavior and Model Simulations of Poly(Butylene Adipate-*co*-Terephthalate) Biocomposites with Carbon Nanotubes: Hierarchical Structures and Relaxation. *Journal of Composite Materials*, *50*(13): 1805–1816. https://doi.org/10.1177/0021998315596592

Duan, L., Spoerk, M., Wieme, T., Cornillie, P., Xia, H., Zhang, J., Cardon, L., & D'hooge, D. R. (2019). Designing Formulation Variables of Extrusion-based Manufacturing of Carbon Black Conductive Polymer Composites for Piezoresistive Sensing. *Composites Science and Technology*, *171*(December 2018): 78–85. https://doi.org/10.1016/j.compscitech.2018.12.009

Dubey, K. A., Mondal, R. K., Grover, V., Bhardwaj, Y. K., & Tyagi, A. K. (2015). Development of a Novel Strain Sensor Based on Fluorocarbon-elastomeric Nanocomposites: Effect of Network Density on the Electromechanical Properties. *Sensors and Actuators, A: Physical*, **221**: 33–40. https://doi.org/10.1016/j.sna.2014.10.036

Dubey, K. A., Mondal, R. K., Kumar, J., Melo, J. S., & Bhardwaj, Y. K. (2020). Enhanced Electromechanics of Morphology-immobilized Co-continuous Polymer Blend/Carbon Nanotube High-range Piezoresistive Sensor. *Chemical Engineering Journal*, **389**: 124112. https://doi.org/10.1016/j.cej.2020.124112

Dubey, N., Kushwaha, C. S., & Shukla, S. K. (2020). A Review on Electrically Conducting Polymer Bionanocomposites for Biomedical and Other Applications. *International Journal of Polymeric Materials and Polymeric Biomaterials*, **69**(11): 709–727. https://doi.org/10.1080/00914037.2019.1605513

Feig, V. R., Tran, H., & Bao, Z. (2018). Biodegradable Polymeric Materials in Degradable Electronic Devices. *ACS Central Science*, **4**(3): 337–348. https://doi.org/10.1021/acscentsci.7b00595

Ferreira, A., Martínez, M. T., Ansón-Casaos, A., Gómez-Pineda, L. E., Vaz, F., & Lanceros-Mendez, S. (2013). Relationship Between Electromechanical Response and Percolation Threshold in Carbon Nanotube/Poly(Vinylidene Fluoride) Composites. *Carbon*, **61**: 568–576. https://doi.org/10.1016/j.carbon.2013.05.038

Ferreira, F. V., Cividanes, L. S., Gouveia, R. F., & Lona, L. M. F. (2019). An Overview on Properties and Applications of Poly(Butylene Adipate-*co*-Terephthalate)– PBAT Based Composites. *Polymer Engineering and Science*, **59**(s2): E7–E15. https://doi.org/10.1002/pen.24770

Folorunso, O., Hamam, Y., Sadiku, R., Ray, S. S., & Joseph, A. G. (2019). Parametric Analysis of Electrical Conductivity of Polymer-composites. *Polymers*, **11**(8): 1–20. https://doi.org/10.3390/polym11081250

Foulger, S. H. (1999). Electrical Properties of Composites in the Vicinity of the Percolation Threshold. *Journal of Applied Polymer Science*, *72*(12): 1573–1582. https://doi.org/10.1002/(SICI)1097-4628(19990620)72:12<1573::AID-APP10>3.0.CO;2-6

Fukushima, K., Wu, M. H., Bocchini, S., Rasyida, A., & Yang, M. C. (2012). PBAT Based Nanocomposites for Medical and Industrial Applications. *Materials Science and Engineering C*, *32*(6): 1331–1351. https://doi.org/10.1016/j.msec.2012.04.005

Gan, Z., Kuwabara, K., Yamamoto, M., Abe, H., & Doi, Y. (2004). Solid-state Structures and Thermal Properties of Aliphatic-aromatic Poly(Butylene Adipate-*co*-Butylene Terephthalate) Copolyesters. *Polymer Degradation and Stability*, *83*(2): 289–300. https://doi.org/10.1016/S0141-3910(03)00274-X

Gao, C., Jin, Y. Z., Kong, H., Whitby, R. L. D., Acquah, S. F. A., Chen, G. Y., Qian, H., Hartschuh, A., Silva, S. R. P., Henley, S., Fearon, P., Kroto, H. W., & Walton, D. R. M. (2005). Polyurea-functionalized Multiwalled Carbon Nanotubes: Synthesis, Morphology, and Raman Spectroscopy. *Journal of Physical Chemistry B*, *109*(24): 11925–11932. https://doi.org/10.1021/jp051642h

Gau, C., Ko, H. S., & Chen, H. T. (2009). Piezoresistive Characteristics of MWNT Nanocomposites and Fabrication as a Polymer Pressure Sensor. *Nanotechnology*, *20*(18): https://doi.org/10.1088/0957-4484/20/18/185503

Ge, F. F., Tsou, C. H., Yuan, S., De Guzman, M. R., Zeng, C. Y., Li, J., Jia, C. F., Cheng, B. Y., Yang, P. C., & Gao, C. (2021). Barrier Performance and Biodegradability of Antibacterial Poly(Butylene Adipate-*co*-Terephthalate) Nanocomposites Reinforced with a New MWCNT-ZnO Nanomaterial. *Nanotechnology*, *32*(48): https://doi.org/10.1088/1361-6528/ac1b52

Georgopoulou, A., & Clemens, F. (2020). Piezoresistive Elastomer-Based Composite Strain Sensors and Their Applications. *ACS Applied Electronic Materials*, *2*(7): 1826–1842. https://doi.org/10.1021/acsaelm.0c00278

Georgousis, G., Kontou, E., Kyritsis, A., Pissis, P., Mičušík, M., & Omastová, M. (2018). Piezoresistivity of Conductive Polymer Nanocomposites: Experiment and Modeling. *Journal of Reinforced Plastics and Composites*, *37*(17): 1085–1098. https://doi.org/10.1177/0731684418783051

Georgousis, G., Pandis, C., Chatzimanolis-Moustakas, C., Kyritsis, A., Kontou, E., Pissis, P., Krajči, J., Chodák, I., Tabačiarová, J., Mičušík, M., & Omastová, M. (2015). Study of the reinforcing Mechanism and Strain Sensing in a Carbon Black Filled Elastomer. *Composites Part B: Engineering*, *80*: 20–26. https://doi.org/10.1016/j.compositesb.2015.05.021

Georgousis, G., Pandis, C., Kalamiotis, A., Georgiopoulos, P., Kyritsis, A., Kontou, E., Pissis, P., Micusik, M., Czanikova, K., Kulicek, J., & Omastova, M. (2015). Strain Sensing in Polymer/Carbon Nanotube Composites by Electrical Resistance Measurement. *Composites Part B: Engineering*, *68*: 162–169. https://doi.org/10.1016/j.compositesb.2014.08.027

Georgousis, G., Roumpos, K., Kontou, E., Kyritsis, A., Pissis, P., Koutsoumpis, S., Mičušík, M., & Omastová, M. (2017). Strain and Damage Monitoring in SBR Nanocomposites under Cyclic Loading. *Composites Part B: Engineering*, *131:* 50–61. https://doi.org/10.1016/j.compositesb.2017.08.006

Giri, J., Lach, R., Grellmann, W., Susan, M. A. B. H., Saiter, J. M., Henning, S., Katiyar, V., & Adhikari, R. (2019). Compostable Composites of Wheat Stalk Micro- and Nanocrystalline Cellulose and Poly(Butylene Adipate-*co*-Terephthalate): Surface Properties and Degradation Behavior. *Journal of Applied Polymer Science*, *136*(43): 1–11. https://doi.org/10.1002/app.48149

Giri, J., Lach, R., Le, H. H., Grellmann, W., Saiter, J. M., Henning, S., Radusch, H. J., & Adhikari, R. (2021). Structural, Thermal and Mechanical Properties of Composites of Poly(Butylene Adipate-*co*-Terephthalate) with Wheat Straw Microcrystalline Cellulose. *Polymer Bulletin*, *78*(9): 4779–4795. https://doi.org/10.1007/s00289-020-03339-5

Gong, S., & Zhu, Z. H. (2014). On the Mechanism of Piezoresistivity of Carbon Nanotube Polymer Composites. *Polymer*, *55*(16): 4136–4149. https://doi.org/10.1016/j.polymer.2014.06.024

González Seligra, P., Eloy Moura, L., Famá, L., Druzian, J. I., & Goyanes, S. (2016). Influence of Incorporation of Starch Nanoparticles in PBAT/TPS Composite Films. *Polymer International*, *65*(8): 938–945. https://doi.org/10.1002/pi.5127

Guo, D., Pan, X., & He, H. (2019). A Simple and Cost-effective Method for Improving the Sensitivity of Flexible Strain Sensors Based on Conductive Polymer Composites. *Sensors and Actuators, A: Physical*, *298*: 11608. https://doi.org/10.1016/j.sna.2019.111608

Guo, Y., Chen, S., Sun, L., Yang, L., Zhang, L., Lou, J., & You, Z. (2021). Degradable and Fully Recyclable Dynamic Thermoset Elastomer for 3D-Printed Wearable Electronics. *Advanced Functional Materials*, *31*(9): 1–7. https://doi.org/10.1002/adfm.202009799

Guo, Y., Zuo, X., Xue, Y., Tang, J., Gouzman, M., Fang, Y., Zhou, Y., Wang, L., Yu, Y., & Rafailovich, M. H. (2020a). Engineering Thermally and Electrically Conductive Biodegradable Polymer Nanocomposites. *Composites Part B: Engineering*, *189*: 1–20. https://doi.org/10.1016/j.compositesb.2020.107905

Guo, Y., Zuo, X., Xue, Y., Tang, J., Gouzman, M., Fang, Y., Zhou, Y., Wang, L., Yu, Y., & Rafailovich, M. H. (2020b). Engineering Thermally and Electrically Conductive Biodegradable Polymer Nanocomposites. *Composites Part B: Engineering*, *189*: 107905. https://doi.org/10.1016/j.compositesb.2020.107905

Gusmão, A. P., Rosenberger, A. G., Muniz, E. C., Dragunski, D. C., & Caetano, J. (2021). Characterization of Microfibers of Carbon Nanotubes Obtained by Electrospinning for Use in Electrochemical Sensor. *Journal of Polymers and the Environment*, *29*(5): 1551–1565. https://doi.org/10.1007/s10924-020-01964-9

Haji-Saeid, M., Sampa, M. H. O., & Chmielewski, A. G. (2007). Radiation treatment for sterilization of packaging materials. *Radiation Physics and Chemistry*, *76*(8–9): 1535–1541. https://doi.org/10.1016/j.radphyschem.2007.02.068

Han, W. B., Yang, S. M., Rajaram, K., & Hwang, S. W. (2022). Materials and Fabrication Strategies for Biocompatible and Biodegradable Conductive Polymer Composites toward Bio-Integrated Electronic Systems. *Advanced Sustainable Systems*, *6*(2): 1–17. https://doi.org/10.1002/adsu.202100075

Hong, S. Y., Ko, S. W., Choi, H. J., & Lee, J. H. (2012). Multi-walled Carbon Nanotube/Biodegradable Poly(Butylene Adipate-*co*-Butylene Terephthalate) Nanocomposites and Their Physical Characteristics. *Journal of Macromolecular Science, Part B: Physics*, *51*(1): 125–133. https://doi.org/10.1080/00222348.2011.583199

Hwang, I. T., Jung, C. H., Kuk, I. S., Choi, J. H., & Nho, Y. C. (2010). Electron Beam-induced Crosslinking of Poly(Butylene Adipate-*co*-Terephthalate). *Nuclear Instruments and Methods in Physics Research, Section B: Beam Interactions with Materials and Atoms*, *268*(21): 3386–3389. https://doi.org/10.1016/j.nimb.2010.08.010

Hwang, S. H., Park, H. W., & Park, Y. Bin. (2013). Piezoresistive Behavior and Multi-directional Strain Sensing Ability of Carbon Nanotube-graphene Nanoplatelet Hybrid Sheets. *Smart Materials and Structures*, *22*(1): 015013. https://doi.org/10.1088/0964-1726/22/1/015013

Irimia-Vladu, M., Głowacki, E. D., Voss, G., Bauer, S., & Sariciftci, N. S. (2012). Green and Biodegradable Electronics. *Materials Today*, *15*(7–8): 340–346. https://doi.org/10.1016/S1369-7021(12)70139-6

Iuliano, A., Nowacka, M., Rybak, K., & Rzepna, M. (2020). The Effects of Electron Beam Radiation on Material Properties and Degradation of Commercial PBAT/PLA Blend. *Journal of Applied Polymer Science*, *137*(11): 1–10. https://doi.org/10.1002/app.48462

Jalali Dil, E., Virgilio, N., & Favis, B. D. (2016). The Effect of the Interfacial Assembly of Nano-silica in poly(Lactic Acid)/Poly(Butylene Adipate-*co*-Terephthalate) Blends on Morphology, Rheology and Mechanical Properties. *European Polymer Journal*, *85*: 635–646. https://doi.org/10.1016/j.eurpolymj.2016.07.022

Ji, M., Deng, H., Yan, D., Li, X., Duan, L., & Fu, Q. (2014). Selective Localization of Multi-walled Carbon Nanotubes in Thermoplastic Elastomer Blends: An Effective Method for Tunable Resistivity-Strain Sensing Behavior. *Composites Science and Technology*, *92*: 16–26. https://doi.org/10.1016/j.compscitech.2013.11.018

Jian, J., Xiangbin, Z., & Xianbo, H. (2020). An Overview on synthesis, Properties and Applications of Poly(Butylene Adipate-*co*-Terephthalate)–PBAT. *Advanced Industrial and Engineering Polymer Research*, *3*(1): 19–26. https://doi.org/10.1016/j.aiepr.2020.01.001

Jin, J., Lin, Y., Song, M., Gui, C., & Leesirisan, S. (2013). Enhancing the Electrical Conductivity of Polymer Composites. *European Polymer Journal*, *49*(5): 1066–1072. https://doi.org/10.1016/j.eurpolymj.2013.01.014

Kai-Ke. (2016). *Piezoresistive Behavior of Carbon Nanotube based Poly (vinylidene fluoride) Nanocomposites towards Strain Sensing Applications* (Unpublished doctoral dissertation). Faculty of Mathematics and Natural Sciences, Technical University Dresden, Germany.

Kaur, G., Adhikari, R., Cass, P., Bown, M., & Gunatillake, P. (2015). Electrically Conductive Polymers and Composites for Biomedical Applications. *RSC Advances*, *5*(47): 37553–37567. https://doi.org/10.1039/c5ra01851j

Ke, K., Pötschke, P., Gao, S., & Voit, B. (2017). An Ionic Liquid as Interface Linker for Tuning Piezoresistive Sensitivity and Toughness in Poly(vinylidene fluoride)/Carbon Nanotube Composites. *ACS Applied Materials and Interfaces*, *9*(6): 5437–5446. https://doi.org/10.1021/acsami.6b13454

Ke, K., Pötschke, P., Wiegand, N., Krause, B., & Voit, B. (2016). Tuning the Network Structure in Poly(vinylidene fluoride)/Carbon Nanotube Nanocomposites Using Carbon Black: Toward Improvements of Conductivity and Piezoresistive Sensitivity. *ACS Applied Materials and Interfaces*, *8*(22): 14190–14199. https://doi.org/10.1021/acsami.6b03451

Ke, K., Wang, Y., Liu, X. Q., Cao, J., Luo, Y., Yang, W., Xie, B. H., & Yang, M. B. (2012). A Comparison of Melt and Solution Mixing on the Dispersion of Carbon Nanotubes in a Poly(Vinylidene Fluoride) Matrix. *Composites Part B: Engineering*, *43*(3): 1425–1432. https://doi.org/10.1016/j.compositesb.2011.09.007

Khatiwada, S. P., Gohs, U., Lach, R., Heinrich, G., & Adhikari, R. (2019). A new way of toughening of thermoset by dual-cured thermoplastic/thermosetting blend. Materials, *12*(3): 548. doi:10.3390/ma12030548

Knite, M., Tupureina, V., Fuith, A., Zavickis, J., & Teteris, V. (2007). Polyisoprene-Multi-wall Carbon Nanotube Composites for Sensing Strain. *Materials Science and Engineering C*, *27*(5-8 SPEC. ISS.): 1125–1128. https://doi.org/10.1016/j.msec.2006.08.016

Ko, S. W., Hong, M. K., Park, B. J., Gupta, R. K., Choi, H. J., & Bhattacharya, S. N. (2009). Morphological and Rheological Characterization of Multi-walled Carbon Nanotube/PLA/PBAT Blend Nanocomposites. *Polymer Bulletin*, *63*(1): 125–134. https://doi.org/10.1007/s00289-009-0072-9

Kobayashi, A., Oshima, A., Okubo, S., Tsubokura, H., Takahashi, T., Oyama, T. G., Tagawa, S., & Washio, M. (2013). Thermal and Radiation Process for Nano-/Micro-fabrication of Crosslinked PTFE. *Nuclear Instruments and Methods in Physics Research, Section B: Beam Interactions with Materials and Atoms*, *295*: 76–80. https://doi.org/10.1016/j.nimb.2012.11.002

Krause, B., Rzeczkowski, P., & Pötschke, P. (2019). Thermal Conductivity and Electrical Resistivity of Melt-mixed Polypropylene Composites Containing Mixtures of Carbon-based Fillers. *Polymers*, *11*(6): https://doi.org/10.3390/POLYM11061073

Kuan, C. F., Kuan, H. C., Ma, C. C. M., & Chen, C. H. (2008). Mechanical and Electrical Properties of Multi-wall Carbon Nanotube/Poly(Lactic Acid) Composites. *Journal of Physics and Chemistry of Solids*, *69*(5–6): 1395–1398. https://doi.org/10.1016/j.jpcs.2007.10.060

Kumar, B., Castro, M., & Feller, J. F. (2012). Poly(Lactic Acid)-Multi-wall Carbon Nanotube Conductive Biopolymer Nanocomposite Vapour Sensors. *Sensors and Actuators, B: Chemical*, *161*(1): 621–628. https://doi.org/10.1016/j.snb.2011.10.077

Kumar, S., Gupta, T. K., & Varadarajan, K. M. (2019). Strong, Stretchable and Ultrasensitive MWCNT/TPU Nanocomposites for Piezoresistive Strain Sensing. *Composites Part B: Engineering*, *177*: 107285. https://doi.org/10.1016/j.compositesb.2019.107285

Kumbay Yildiz, S., Mutlu, R., & Alici, G. (2016). Fabrication and Characterisation of Highly Stretchable Elastomeric Strain Sensors for Prosthetic Hand Applications. *Sensors and Actuators, A: Physical*, *247*: 514–521. https://doi.org/10.1016/j.sna.2016.06.037

La Mantia, F. P., Botta, L., Mistretta, M. C., Fiore, A. Di, & Titone, V. (2020). Recycling of a Biodegradable Polymer Blend. *Polymers*, *12*(10): 1–12. https://doi.org/10.3390/polym12102297

Lappan, U., Geißler, U., Häußler, L., Jehnichen, D., Pompe, G., & Lunkwitz, K. (2001). Radiation-induced Branching and Crosslinking of Poly(Tetrafluoroethylene) (PTFE). *Nuclear Instruments and Methods in Physics Research, Section B: Beam Interactions with Materials and Atoms*, *185*(1–4): 178–183. https://doi.org/10.1016/S0168-583X(01)00751-0

Last, B. J., & Thouless, D. J. (1971). Percolation Theory and Electrical Conductivity. *Physical Review Letters*, *27*(25): 1719–1721. https://doi.org/10.1103/PhysRevLett.27.1719

Lee, S. W., Park, J. J., Park, B. H., Mun, S. C., Park, Y. T., Liao, K., Seo, T. S., Hyun, W. J., & Park, O. O. (2017). Enhanced Sensitivity of Patterned Graphene Strain Sensors Used for Monitoring Subtle Human Body Motions. *ACS Applied Materials and Interfaces*, *9*(12): 11176–11183. https://doi.org/10.1021/acsami.7b01551

Li, G., Shankar, S., Rhim, J. W., & Oh, B. Y. (2015). Effects of Preparation Method on Properties of Poly(Butylene Adipate-*co*-Terephthalate) Films. *Food Science and Biotechnology*, *24*(5): 1679–1685. https://doi.org/10.1007/s10068-015-0218-5

Liao, X., Zhang, Z., Kang, Z., Gao, F., Liao, Q., & Zhang, Y. (2017). Ultrasensitive and Stretchable Resistive Strain Sensors Designed for Wearable Electronics. *Materials Horizons*, *4*(3): 502–510. https://doi.org/10.1039/c7mh00071e

Liu, B., Guan, T., Wu, G., Fu, Y., & Weng, Y. (2022). Biodegradation Behavior of Degradable Mulch with Poly (Butylene Adipate-co-Terephthalate) (PBAT) and Poly (Butylene Succinate) (PBS) in Simulation Marine Environment. *Polymers*, *14*(8): 1515. https://doi.org/10.3390/polym14081515

Liu, H., Dong, M., Huang, W., Gao, J., Dai, K., Guo, J., Zheng, G., Liu, C., Shen, C., & Guo, Z. (2017). Lightweight Conductive Graphene/Thermoplastic Polyurethane Foams with Ultrahigh Compressibility for Piezoresistive Sensing. *Journal of Materials Chemistry C*, *5*(1): 73–83. https://doi.org/10.1039/c6tc03713e

Liu, H., Jian, R., Chen, H., Tian, X., Sun, C., Zhu, J., Yang, Z., Sun, J., & Wang, C. (2019). Application of Biodegradable and Biocompatible Nanocomposites in Electronics: Current Status and Future Directions. *Nanomaterials*, *9*(7): 950 https://doi.org/10.3390/nano9070950

Liu, H., Li, Q., Zhang, S., Yin, R., Liu, X., He, Y., Dai, K., Shan, C., Guo, J., Liu, C., Shen, C., Wang, X., Wang, N., Wang, Z., Wei, R., & Guo, Z. (2018). Electrically Conductive Polymer Composites for Smart Flexible Strain Sensors: A Critical Review. *Journal of Materials Chemistry C*, *6*(45): 12121–12141. https://doi.org/10.1039/C8TC04079F

Liu, H., Li, Y., Dai, K., Zheng, G., Liu, C., Shen, C., Yan, X., Guo, J., & Guo, Z. (2015). Electrically Conductive Thermoplastic Elastomer Nanocomposites at Ultralow Graphene Loading Levels for Strain Sensor Applications. *Journal of Materials Chemistry C*, *4*(1): 157–166. https://doi.org/10.1039/c5tc02751a

Liu, X., Guo, R., Lin, Z., Yang, Y., Xia, H., & Yao, Z. (2021). Resistance-strain Sensitive Rubber Composites Filled by Multiwalled Carbon Nanotubes for Structural Deformation Monitoring. *Nanomaterials and Nanotechnology*, *11*: 1–13. https://doi.org/10.1177/18479804211011384

Ma, C., Zhou, R., & Xie, L. (2022). Recent Advances in Flexible Pressure/Strain Sensors Using Carbon Nanotubes. *International Journal of Agricultural and Biological Engineering*, *15*(2): 1–12. https://doi.org/10.25165/j.ijabe.20221502.7364

MacDiarmid, A. G. (2001). "Synthetic Metals": A Novel Role for Organic Polymers. *Current Applied Physics*, *1*(4–5): 269–279. https://doi.org/10.1016/S1567-1739(01)00051-7

Madera-Santana, T. J., Meléndrez, R., González-García, G., Quintana-Owen, P., & Pillai, S. D. (2016). Effect of Gamma Irradiation on Physicochemical Properties of Commercial Poly(Lactic Acid) Clamshell for food Packaging. *Radiation Physics and Chemistry*, *123*: 6–13. https://doi.org/10.1016/j.radphyschem.2016.02.001

Malinowski, R., Moraczewski, K., & Raszkowska-Kaczor, A. (2020). Studies on the Uncrosslinked Fraction of PLA/PBAT Blends Modified by Electron Radiation. *Materials*, *13*(5): 1–16. https://doi.org/10.3390/ma13051068

Mehmood, A., Mubarak, N. M., Khalid, M., Walvekar, R., Abdullah, E. C., Siddiqui, M. T. H., Baloch, H. A., Nizamuddin, S., & Mazari, S. (2020). Graphene Based Nanomaterials for Strain Sensor Application—A Review. *Journal of Environmental Chemical Engineering*, *8*(3): 103743. https://doi.org/10.1016/j.jece.2020.103743

Mičušík, M., Omastová, M., Pionteck, J., Pandis, C., Logakis, E., & Pissis, P. (2011). Influence of Surface Treatment of Multiwall Carbon Nanotubes on the Properties of Polypropylene/Carbon Nanotubes Nanocomposites. *Polymers for Advanced Technologies*, *22*(1): 38–47. https://doi.org/10.1002/pat.1745

Mochane, M. J., Sefadi, J. S., Motsoeneng, T. S., Mokoena, T. E., Mofokeng, T. G., & Mokhena, T. C. (2020). The Effect of Filler Localization on the Properties of Biopolymer Blends, Recent Advances: A Review. *Polymer Composites*, *41*(7): 2958–2979. https://doi.org/10.1002/pc.25590

Mohanty, S., & Nayak, S. K. (2009). Starch Based Biodegradable PBAT Nanocomposites: Effect of Starch Modification on Mechanical, Thermal, Morphological and Biodegradability Behavior. *International Journal of Plastics Technology*, *13*(2): 163–185. https://doi.org/10.1007/s12588-009-0013-3

Narongthong, J., Das, A., Le, H. H., Wießner, S., & Sirisinha, C. (2018). An Efficient Highly Flexible Strain Sensor: Enhanced Electrical Conductivity, Piezoresistivity and Flexibility of a Strongly Piezoresistive Composite Based on Conductive Carbon Black and an Ionic Liquid. *Composites Part A: Applied Science and Manufacturing*, *113*(August), 330–338. https://doi.org/10.1016/j.compositesa.2018.08.004

Natarajan, T. S., Eshwaran, S. B., Stöckelhuber, K. W., Wießner, S., Pötschke, P., Heinrich, G., & Das, A. (2017). Strong Strain Sensing Performance of Natural Rubber Nanocomposites. *ACS Applied Materials and Interfaces*, *9*(5): 4860–4872. https://doi.org/10.1021/acsami.6b13074

Niu, D., Jiang, W., Ye, G., Wang, K., Yin, L., Shi, Y., Chen, B., Luo, F., & Liu, H. (2018). Graphene-elastomer Nanocomposites Based Flexible Piezoresistive Sensors for Strain and Pressure Detection. *Materials Research Bulletin*, *102*: 92–99. https://doi.org/10.1016/j.materresbull.2018.02.005

Pang, H., Xu, L., Yan, D. X., & Li, Z. M. (2014). Conductive polymer Composites with Segregated Structures. *Progress in Polymer Science*, *39*(11): 1908–1933. https://doi.org/10.1016/j.progpolymsci.2014.07.007

Papageorgiou, D. G., Li, Z., Liu, M., Kinloch, I. A., & Young, R. J. (2020). Mechanisms of Mechanical Reinforcement by Graphene and Carbon Nanotubes in Polymer Nanocomposites. *Nanoscale*, *12*(4): 2228–2267. https://doi.org/10.1039/c9nr06952f

Park, C., Kim, M. S., Kim, H. H., Sunwoo, S.-H., Jung, D. J., Choi, M. K., & Kim, D.-H. (2022). Stretchable Conductive Nanocomposites and Their Applications in Wearable Devices. *Applied Physics Reviews*, *9*(2), 021312. https://doi.org/10.1063/5.0093261

Park, S. J., Kim, J., Chu, M., & Khine, M. (2016). Highly Flexible Wrinkled Carbon Nanotube Thin Film Strain Sensor to Monitor Human Movement. *Advanced Materials Technologies*, *1*(5): 1–8. https://doi.org/10.1002/admt.201600053

Pietrosanto, A., Scarfato, P., & Maio, L. Di. (2020). Development of Eco-sustainable PBAT Based Blown Packaging Applications. *Materials*, *13*: 5395.

Pinheiro, I. F., Ferreira, F. V., Souza, D. H. S., Gouveia, R. F., Lona, L. M. F., Morales, A. R., & Mei, L. H. I. (2017). Mechanical, Rheological and Degradation Properties of PBAT Nanocomposites Reinforced by Functionalized Cellulose Nanocrystals. *European Polymer Journal*, *97*: 356–365. https://doi.org/10.1016/j.eurpolymj.2017.10.026

Pissis, P., Georgousis, G., Pandis, C., Georgiopoulos, P., Kyritsis, A., Kontou, E., Micusik, M., Czanikova, K., & Omastova, M. (2015). Strain and Damage Sensing in Polymer Composites and Nanocomposites with Conducting Fillers. *Procedia Engineering*, *114*: 590–597. https://doi.org/10.1016/j.proeng.2015.08.109

Pokhrel, S., Lach, R., Le, H. H., Wutzler, A., Grellmann, W., Radusch, H. J., Dhakal, R. P., Esposito, A., Henning, S., Yadav, P. N., Saiter, J. M., Heinrich, G., & Adhikari, R. (2016). Fabrication and Characterization of Completely Biodegradable Copolyester–Chitosan Blends: I. Spectroscopic and Thermal Characterization. *Macromolecular Symposia*, *366*(1): 23–34. https://doi.org/10.1002/masy.201650043

Pokhrel, S., Sigdel, A., Lach, R., Slouf, M., Sirc, J., Katiyar, V., Bhattarai, D. R., & Adhikari, R. (2021). Starch-based Biodegradable Film with Poly(Butylene Adipate-*co*-Terephthalate): Preparation, Morphology, Thermal and Biodegradation Properties. *Journal of Macromolecular Science, Part A: Pure and Applied Chemistry*, *58*(9): 610–621. https://doi.org/10.1080/10601325.2021.1920838

Ponnamma, D., Sadasivuni, K. K., Grohens, Y., Guo, Q., & Thomas, S. (2014). Carbon Nanotube Based Elastomer Composites-An Approach Towards Multifunctional Materials. *Journal of Materials Chemistry C*, *2*(40): 8446–8485. https://doi.org/10.1039/c4tc01037j

Qazi, R. A., Khan, M. S., Shah, L. A., Ullah, R., Kausar, A., & Khattak, R. (2020). Eco-friendly Electronics, Based on Nanocomposites of Biopolyester Reinforced with Carbon Nanotubes: A Review. *Polymer-Plastics Technology and Materials*, *59*(9): 928–951. https://doi.org/10.1080/25740881.2020.1719137

Qu, S., & Wong, S. (2007). Piezoresistive Behavior of Polymer Reinforced by Expanded Graphite. *Composites Science and Technology*, *67*(2): 231–237. https://doi.org/10.1016/j.compscitech.2006.08.008

Rahaman, M., Aldalbahi, A., Nayak, L., & Giri, R. (2019). *Electrical Conductivity of Polymer–Carbon Composites: Effects of Different Factors*. Springer Series on Polymer and Composite Materials. https://doi.org/10.1007/978-981-13-2688-2_5

Rodrigues, B. V. M., Silva, A. S., Melo, G. F. S., Vasconscellos, L. M. R., Marciano, F. R., & Lobo, A. O. (2016). Influence of Low Contents of Superhydrophilic MWCNT on the Properties and Cell Viability of Electrospun Poly (Butylene Adipate-*co*-Terephthalate) Fibers. *Materials Science and Engineering C*, *59*: 782–791. https://doi.org/10.1016/j.msec.2015.10.075

Rosenberger, A. G., Dragunski, D. C., Muniz, E. C., Módenes, A. N., Alves, H. J., Tarley, C. R. T., Machado, S. A. S., & Caetano, J. (2020). Electrospinning in the Preparation of an Electrochemical Sensor Based on Carbon Nanotubes. *Journal of Molecular Liquids*, *298*(xxxx): 112068. https://doi.org/10.1016/j.molliq.2019.112068

Ryu, S., Lee, P., Chou, J. B., Xu, R., Zhao, R., Hart, A. J., & Kim, S. G. (2015). Extremely Elastic Wearable Carbon Nanotube Fiber Strain Sensor for Monitoring of Human Motion. *ACS Nano*, *9*(6): 5929–5936. https://doi.org/10.1021/acsnano.5b00599

Rzepna, M., Przybytniak, G., & Sadło, J. (2018). Radiation Degradation and Stability of PBAT: Copolymer of Aromatic and Aliphatic Esters. *Journal of Applied Polymer Science*, *135*(37): 1–8. https://doi.org/10.1002/app.46682

Salaeh, S., Das, A., Stöckelhuber, K. W., & Wießner, S. (2020). Fabrication of a Strain Sensor from a Thermoplastic Vulcanizate with an Embedded Interconnected Conducting Filler Network. *Composites Part A: Applied Science and Manufacturing*, *130*(January): 105763. https://doi.org/10.1016/j.compositesa.2020.105763

Salehiyan, R., Nofar, M., Malkappa, K., & Ray, S. S. (2020). Effect of Nanofillers Characteristics and Their Selective Localization on Morphology Development and Rheological Properties of Melt-processed Polylactide/Poly(Butylene Adipate-*co*-Terephthalate) Blend Composites. *Polymer Engineering and Science*, *60*(11), 2749–2760. https://doi.org/10.1002/pen.25505

Salvetat-Delmotte, J. P., & Rubio, A. (2002). Mechanical properties of Carbon Nanotubes: A fiber Digest for Beginners. *Carbon*, *40*(10): 1729–1734. https://doi.org/10.1016/S0008-6223(02)00012-X

Salvetat, J.-P., Bonard, J.-M., Thomson, N. H., Kulik, A. j., Forro, L., Benoit, W., & Zuppioroli, L. (1999). Mechanical Properties of Carbon Nanotubes. *Appl. Phys. A*, *69*: 255–260. https://doi.org/10.1007/s003399900114

Sang, Z., Ke, K., & Manas-Zloczower, I. (2019). Effect of Carbon Nanotube Morphology on Properties in Thermoplastic Elastomer Composites for Strain Sensors. *Composites Part A: Applied Science and Manufacturing*, *121*: 207–212. https://doi.org/10.1016/j.compositesa.2019.03.007

Sarul, D. S., Arslan, D., Vatansever, E., Kahraman, Y., Durmus, A., Salehiyan, R., & Nofar, M. (2021). Preparation and Characterization of PLA/PBAT/CNC Blend Nanocomposites. *Colloid and Polymer Science*, *299*(6): 987–998. https://doi.org/10.1007/s00396-021-04822-9

Selvan, N. T., Eshwaran, S. B., Das, A., Stöckelhuber, K. W., Wießner, S., Pötschke, P., Nando, G. B., Chervanyov, A. I., & Heinrich, G. (2016). Piezoresistive Natural Rubber-multiwall Carbon Nanotube Nanocomposite for Sensor Applications. *Sensors and Actuators A: Physical*, *239*(1): 102–113. https://doi.org/10.1016/j.sna.2016.01.004

Shintake, J., Piskarev, E., Jeong, S. H., & Floreano, D. (2018). Ultrastretchable Strain Sensors Using Carbon Black-filled Elastomer Composites and Comparison of Capacitive Versus Resistive Sensors. *Advanced Materials Technologies*, *3*(3): 1–8. https://doi.org/10.1002/admt.201700284

Signori, F., Coltelli, M. B., & Bronco, S. (2009). Thermal Degradation of Poly(Lactic Acid) (PLA) and Poly(Butylene Adipate-*co*-Terephthalate) (PBAT) and Their Blends upon Melt Processing. *Polymer Degradation and Stability*, *94*(1): 74–82. https://doi.org/10.1016/j.polymdegradstab.2008.10.004

Silva, A. P. B., Montagna, L. S., Passador, F. R., Rezende, M. C., & Lemes, A. P. (2021). Biodegradable nanocomposites Based on PLA/PHBV Blend Reinforced with Carbon Nanotubes with Potential for Electrical and Electromagnetic Applications. *Express Polymer Letters*, *15*(10): 987–1003. https://doi.org/10.3144/expresspolymlett.2021.79

Sirisinha, K., & Somboon, W. (2011). Melt Characteristics, Mechanical, and Thermal Properties of Blown Film from Modified Blends of Poly(Butylene Adipate-*co*-Terephthalate) and Poly(Lactide). *Journal of Applied Polymer Science*, *116*(5): n/a-n/a. https://doi.org/10.1002/app.35604

Siyamak, S., Ibrahim, N. A., Abdolmohammadi, S., Yunus, W. M. Z. B. W., & Rahman, M. Z. A. B. (2012). Enhancement of Mechanical and Thermal Properties of Oil Palm Empty Fruit Bunch Fiber Poly(Butylene Adipate-*co*-Terephtalate) Biocomposites by Matrix Esterification using Succinic Anhydride. *Molecules*, *17*(2): 1969–1991. https://doi.org/10.3390/molecules17021969

Soares, B. G., Cordeiro, E., Maia, J., Pereira, E. C. L., & Silva, A. A. (2020). The Effect of the Noncovalent Functionalization of CNT by ionic Liquid on Electrical Conductivity and Electromagnetic Interference Shielding Effectiveness of Semi-Biodegradable Polypropylene/Poly(Lactic Acid) Composites. *Polymer Composites*, *41*(1): 82–93. https://doi.org/10.1002/pc.25347

Staudinger, U., Jakisch, L., & Hilbig, L. (2020). Dispersion and Localization Behavior of Modified MWCNTs in Immiscible Polymer Blends of Polystyrene and Polybutadiene and in Corresponding Nanostructured Block Copolymers. *Journal of Composites Science*, *4*(2): 40. https://doi.org/10.3390/jcs4020040

Staudinger, U., Satapathy, B. K., & Jehnichen, D. (2019). Nanofiller Dispersion, Morphology, Mechanical Behavior, and Electrical Properties of Nanostructured Styrene-Butadiene-Based Triblock Copolymer/CNT Composites. *Polymers*, *11*(11): 1831. https://doi.org/10.3390/polym11111831

Stübler, N., Fritzsche, J., & Klüppel, M. (2011). Mechanical and electrical Analysis of Carbon Black Networking in Elastomers under Strain. *Polymer Engineering & Science*, *51*(6): 1206–1217. https://doi.org/10.1002/pen.21888

Tang, X., Pötschke, P., Pionteck, J., Li, Y., Formanek, P., & Voit, B. (2020). Tuning the Piezoresistive Behavior of Poly(Vinylidene Fluoride)/Carbon Nanotube Composites using Poly(Methyl Methacrylate). *ACS Applied Materials and Interfaces*, *12*(38): 43125–43137. https://doi.org/10.1021/acsami.0c11610

Tang, Y., Zhao, Z., Hu, H., Liu, Y., Wang, X., Zhou, S., & Qiu, J. (2015). Highly Stretchable and Ultrasensitive Strain Sensor Based on Reduced Graphene Oxide Microtubes-Elastomer Composite. *ACS Applied Materials and Interfaces*, *7*(49): 27432–27439. https://doi.org/10.1021/acsami.5b09314

Teamsinsungvon, A., Ruksakulpiwat, Y., & Jarukumjorn, K. (2013). Preparation and Characterization of Poly(Lactic Acid)/Poly(Butylene Adipate-*co*-Terepthalate) Blends and Their Composite. *Polymer - Plastics Technology and Engineering*, *52*(13): 1362–1367. https://doi.org/10.1080/03602559.2013.820746

Tran, H., Feig, V. R., Liu, K., Wu, H. C., Chen, R., Xu, J., Deisseroth, K., & Bao, Z. (2019). Stretchable and Fully Degradable Semiconductors for Transient Electronics. *ACS Central Science*, *5*(11): 1884–1891. https://doi.org/10.1021/acscentsci.9b00850

Urquijo, J., Aranburu, N., Dagréou, S., Guerrica-Echevarría, G., & Eguiazábal, J. I. (2017). CNT-induced Morphology and Its Effect on Properties in PLA/PBAT-Based Nanocomposites. *European Polymer Journal*, *93*(May): 545–555. https://doi.org/10.1016/j.eurpolymj.2017.06.035

Vidhate, S., Chung, J., Vaidyanathan, V., & D'Souza, N. (2009). Time Dependent Piezoresistive Behavior of Polyvinylidene Fluoride/Carbon Nanotube Conductive Composite. *Materials Letters*, *63*(21): 1771–1773. https://doi.org/10.1016/j.matlet.2009.05.029

Vilcakova, J., Saha, P., & Quadrat, O. (2002). Electrical Conductivity of Carbon Fibres/Polyester Resin Composites in the Percolation Threshold Region. *European Polymer Journal*, *38*(12): 2343–2347. https://doi.org/10.1016/S0014-3057(02)00145-3

Wang, S., Ning, H., Hu, N., Liu, Y., Liu, F., Zou, R., Huang, K., Wu, X., Weng, S., & Alamusi. (2020). Environmentally-friendly and Multifunctional Graphene-Silk Fabric Strain Sensor for Human-Motion Detection. *Advanced Materials Interfaces*, *7*(1): 1–8. https://doi.org/10.1002/admi.201901507

Weber, M., & Kamal, M. R. (1997). Estimation of the Volume Resistivity of Conductive Fiber Composites by Two New Models. *Annual Technical Conference - ANTEC, Conference Proceedings*, *2*(6): 2357–2361. https://doi.org/10.1016/b978-188420777-8.50010-2

Weng, Y.-X., Jin, Y.-J., Meng, Q.-Y., Wang, L., Zhang, M., & Wang, Y.-Z. (2013). Biodegradation Behavior of Poly(Butylene Adipate-*co*-Terephthalate) (PBAT), Poly(Lactic Acid) (PLA), and Their Blend under Soil Conditions. *Polymer Testing*, *32*(5): 918–926. https://doi.org/10.1016/j.polymertesting.2013.05.001

Wu, C. S. (2009). Antibacterial and Static Dissipating Composites of Poly(Butylene Adipate-*co*-Terephthalate) and Multi-walled Carbon Nanotubes. *Carbon*, *47*(13): 3091–3098. https://doi.org/10.1016/j.carbon.2009.07.023

Wu, S., Zhang, J., Ladani, R. B., Ravindran, A. R., Mouritz, A. P., & Kinloch, A. J. (2017). Novel Electrically-Conductive Porous PDMS/Carbon Nanofibre Composites for Deformable Strain-Sensors and Conductors Novel Electrically Conductive Porous PDMS/Carbon Nanofibre Composites for Deformable StrainSensors and Conductors. *ACS Appl. Mater. Interfaces 9*(16)*: 14207–14215.

Xiang, D., Zhang, X., Li, Y., Harkin-Jones, E., Zheng, Y., Wang, L., Zhao, C., & Wang, P. (2019). Enhanced Performance of 3D Printed Highly Elastic Strain Sensors of Carbon Nanotube/Thermoplastic Polyurethane Nanocomposites *via* Non-covalent Interactions. *Composites Part B: Engineering*, *176*(July): 107250. https://doi.org/10.1016/j.compositesb.2019.107250

Xie, M., Hisano, K., Zhu, M., Toyoshi, T., Pan, M., Okada, S., Tsutsumi, O., Kawamura, S., & Bowen, C. (2019). Flexible Multifunctional Sensors for Wearable and Robotic Applications. *Advanced Materials Technologies*, *4*(3): 1–29. https://doi.org/10.1002/admt.201800626

Xu, C., Zhang, X., Jin, X., Nie, S., & Yang, R. (2019). Study on Mechanical and Thermal Properties of Poly(Lactic acid)/Poly(Butylene Adipate-*co*-Terephthalate)/Office Wastepaper Fiber Biodegradable Composites. *Journal of Polymers and the Environment*, *27*(6): 1273–1284. https://doi.org/10.1007/s10924-019-01428-9

Xu, S., Rezvanian, O., Peters, K., & Zikry, M. A. (2013). The Viability and Limitations of Percolation Theory in Modeling the Electrical Behavior of Carbon Nanotube-polymer Composites. *Nanotechnology*, *24*(15): 155706 https://doi.org/10.1088/0957-4484/24/15/155706

Yang, F., & Qiu, Z. (2011). Preparation, Crystallization, and Properties of Biodegradable Poly(Butylene Adipate-*co*-Terephthalate)/Organomodified Montmorillonite Nanocomposites. *Journal of Applied Polymer Science*, *119*(3): 1426–1434. https://doi.org/10.1002/app.32619

Yee, M. J., Mubarak, N. M., Abdullah, E. C., Khalid, M., Walvekar, R., Karri, R. R., Nizamuddin, S., & Numan, A. (2019). Carbon Nanomaterials Based Films for Strain Sensing Application—A Review. *Nano-Structures and Nano-Objects*, *18***:** 100312. https://doi.org/10.1016/j.nanoso.2019.100312

Yu, T., & Li, Y. (2014). Influence of Poly(Butylenes Adipate-*co*-Terephthalate) on the Properties of the biodegradable Composites Based on Ramie/Poly(Lactic Acid). *Composites Part A: Applied Science and Manufacturing*, *58*: 24–29. https://doi.org/10.1016/j.compositesa.2013.11.013

Yu, X., & Kwon, E. (2009). *A* carbon nanotube / cement composite with piezoresistive properties. *Smart Mater. Struct. 18: 055010 DOI 10.1088/0964-1726/18/5/055010*

Yu, Y., Song, G., & Sun, L. (2010). Determinant Role of Tunneling Resistance in Electrical Conductivity of Polymer Composites Reinforced by Well Dispersed Carbon Nanotubes. *Journal of Applied Physics*, *108*(8): 628. https://doi.org/10.1063/1.3499628

Zhang, R., Deng, H., Valenca, R., Jin, J., Fu, Q., Bilotti, E., & Peijs, T. (2013). Strain Sensing Behaviour of Elastomeric Composite Films Containing Carbon Nanotubes Under Cyclic Loading. *Composites Science and Technology*, *74*: 1–5. https://doi.org/10.1016/j.compscitech.2012.09.016

Zhang, W., Dehghani-Sanij, A. A., & Blackburn, R. S. (2007). Carbon Based Conductive Polymer Composites. *Journal of Materials Science*, *42*(10): 3408–3418. https://doi.org/10.1007/s10853-007-1688-5

Zhang, X., Xiang, H., Li, X., Wen, X., & Lu, C. (2019). Surface Modification of Multi-Walled Carbon Nanotubes Using Acetic Anhydride and its Effects on Poly(butylenesadipate-co-terephthalate) Based Composite. *Polymer Science - Series A*, *61*(6): 897–905. https://doi.org/10.1134/S0965545X19060166

Zhao, J., Wang, G., Yang, R., Lu, X., Cheng, M., He, C., Xie, G., Meng, J., Shi, D., & Zhang, G. (2015). Tunable Piezoresistivity of Nanographene Films for Strain Sensing. *ACS Nano*, *9*(2): 1622–1629. https://doi.org/10.1021/nn506341u

Zhao, S., Li, J., Cao, D., Zhang, G., Li, J., Li, K., Yang, Y., Wang, W., Jin, Y., Sun, R., & Wong, C. P. (2017). Recent Advancements in Flexible and Stretchable Electrodes for Electromechanical Sensors: Strategies, Materials, and Features. *ACS Applied Materials and Interfaces*, *9*(14): 12147–12164. https://doi.org/10.1021/acsami.6b13800

Zhao, Y., Li, Q., Wang, B., Wang, Y., Liu, C., & Shen, C. (2020). Effect of Electron Beam Irradiation Dose on the Properties of Commercial Biodegradable Poly(Lactic Acid), Poly(Butylenes Adipate-*co*-Terephthalate) and Their Blends. *Nuclear Instruments and Methods in Physics Research, Section B: Beam Interactions with Materials and Atoms*, *478*(June): 131–136. https://doi.org/10.1016/j.nimb.2020.06.008

Zheng, S., Deng, J., Yang, L., Ren, D., Huang, S., Yang, W., Liu, Z., & Yang, M. (2014). Investigation on the Piezoresistive Behavior of High-density Polyethylene/Carbon Black Films in the Elastic and Plastic Regimes. *Composites Science and Technology*, *97*: 34–40. https://doi.org/10.1016/j.compscitech.2014.04.001

Zhou, Y., Lei, L., Yang, B., Li, J., & Ren, J. (2018). Preparation and Characterization of Polylactic Acid (PLA) Carbon Nanotube Nanocomposites. *Polymer Testing*, *68*: 34–38. https://doi.org/10.1016/j.polymertesting.2018.03.044